Allosteric Sensitization of Pro-Apoptotic BAX

Allosteric Sensitization of Pro-Apoptotic BAX

A dissertation presented

by

Jonathan R. Pritz

to

The Division of Medical Sciences

in partial fulfillment of the requirements

for the degree of

Doctor of Philosophy

in the subject of

Biological Chemistry and Molecular Pharmacology

Harvard University

Cambridge, Massachusetts

November 2017

Dissertation Advisor: Dr. Loren Walensky Jonathan R. Pritz

Allosteric Sensitization of Pro-Apoptotic BAX

ABSTRACT

BCL-2 family proteins are critical regulators of mitochondrial apoptosis and thus serve as prime targets for therapeutic modulation in diseases of deregulated cell death. Whereas a 20-year effort to inhibit anti-apoptotic proteins has yielded a clinically-approved small molecule inhibitor of BCL-2, drug strategies to directly manipulate pro-apoptotic BCL-2 members, such as BAX, remain underdeveloped. BAX is a critical executioner protein of the apoptotic pathway, transforming from a monomer into a mitochondrial membrane-embedded oligomer in response to stress stimuli. Indeed, the relatively unstable and aggregation-prone nature of recombinant BAX has been a major limitation for conducting large-scale screens for drug discovery. Here, we overcame prior challenges and, to our knowledge, performed the first NMR-based molecular fragment screen of full-length BAX. We identified a class of compounds that sensitizes BH3-mediated direct BAX activation. Applying a series of structure-function analyses, spanning HSQC NMR, hydrogen-deuterium exchange mass spectrometry (HXMS), and correlative biochemical testing, we interrogated both the site of interaction and mechanism of BAX sensitization. Intriguingly, the binding site for this sensitizing molecule localized to a region implicated in BAX inhibition by the cytomegalovirus vMIA protein, rather than to one of the established BH3 activation sites. HXMS studies revealed that BIF-44 induces conformational deprotection of the $\alpha1$–$\alpha2$ loop and BAX BH3 ($\alpha2$), two regions mechanistically linked to the conformational activation of BAX. As these induced structural changes occur at the opposite side of protein from the BIF-44 interaction site, our studies identified a novel allosteric mechanism of BAX sensitization. Taken together, the molecular screening results and structure-function analyses inform fundamental mechanisms for conformational regulation of BAX and provide a new opportunity to reduce the apoptotic threshold for potential therapeutic benefit in cancer and other diseases of pathologic cell survival.

TABLE OF CONTENTS

ABBREVIATIONS

AML	acute myeloid leukemia
APAF1	apoptotic protease activating factor 1
BAM	BAX activator molecule
BIF	BAX-interacting fragment
BCL-2	B-cell lymphoma-2
BAD	BCL-2 antagonist of cell death
BAK	BCL-2 antagonist/killer
BFL1	bovine fetal liver 1
BH	BCL-2 homology motif
BIM	BCL-2 interacting mediator of cell death
BMF	BCL-2 modifying factor
BAX	BCL-2-associated X protein
BID	BH3 interacting domain death agonist
BIK	BCL-2-interacting killer
BOK	BCL-2-related ovarian killer
BTSA1	BAX trigger site activator 1
CPMG	Carr–Purcell–Meiboom–Gill
CEBPα	CCAAT-enhancer binding protein α
CHOP	CEBP homologous protein
CLL	chronic lymphocytic leukemia
DISC	death-inducing signaling complex
FADD	FAS-associated death domain
FP	fluorescence polarization
HRK	harakiri
HSQC	heteronuclear single quantum correlation

HTS	high-throughput screening
HXMS	hydrogen-deuterium exchange mass spectrometry
ITC	isothermal calorimetry
MOMP	mitochondrial outer membrane permeabilization
MCL-1	myeloid cell leukemia 1
MD	molecular dynamics
NMA	normal mode analysis
NMR	nuclear magnetic resonance
PAINS	pan-assay interference compounds
PCA	principle component analysis
PUMA	p53 upregulated modulator of apoptosis
SAHB	stabilized alpha-helix of BCL-2 domain
STD	saturation transfer difference
SMAC	second mitochondria-derived activator of caspases
SAR	structure-activity relationship
TRAIL	tumor necrosis factor (TNF)-related apoptosis-inducing ligand
XIAP	X-linked inhibitor of apoptosis protein

ACKNOWLEDGMENTS

The path to a PhD is long and circuitous. I found myself lost at times, retracing my steps and unsure of which way to turn. Thankfully, there were many people along the way who helped me through this endeavor. There were some who gave me guidance and assurance that I was, indeed, traveling in the right direction; some who encouraged me to keep pushing forward, one step at a time; some who joined me for a section, walking by my side. As I near the end of this journey, I would like to thank these mentors, colleagues, classmates, friends, and family for helping me to realize this goal.

Loren Walensky, for your leadership, optimism, patience, passion, and drive, thank you. Thank you for teaching me to keep an eye on the big picture, even when it seems so far away. Thank you for pushing me dig deeper and to accomplish more. Thank you for fighting for me and for my work. There were times I doubted, but, in the end, you knew what was best.

The members of my dissertation advisory committee, Randy King, Nika Danial, and Nathanael Gray, for project guidance and valuable input. To my dissertation examiners, Randy King, Hari Arthanari, Sara Buhrlage, and Joshua Kritzer, thank you for taking the time to read and review my dissertation.

Our collaborators, who helped make this work possible: Greg Heffron, Paul Coote, and Charlie Sheahan from the Harvard NMR core for running and analyzing the NMR screen, John Engen and Thomas Wales from Northeastern, for providing HXMS support and guidance, and Eric Smith, for many of the beautiful graphics that fill this dissertation.

Walt Massefski, who went above and beyond to help me succeed. Thank you for the NMR lessons, assistance with data interpretation, follow-up ideas, and general mentorship.

The team who made this work possible: Susan Lee, James Luccarelli, Daniel Cohen, and Franziska Wachter. Susan, thank you for your leadership on the HXMS work and for taking time

during your maternity leave to help put together figures. James, thanks for launching the screen, for providing regular feedback on the progress of the project, and for just being you. Daniel, thank you for assisting during that first crazy screening weekend, helping me make sense of strange results, and for being someone to share random observations, findings, or funny stories with. Franzi, thank you for working closely with me to achieve such an ambitious project. Your insight, focus, dedication, and clever solutions were invaluable.

The members of the Walensky lab past and present. Thank you to Liza, Lauren, and Amanda for welcoming me to the lab, teaching me the basics, and serving as early role models. Molly, thanks for being a friendly face from day one in Smith and for helping me to open up. Greg, thanks for providing valuable insight and being open to discuss crazy new ideas. Marina, thanks for the support and continued interest in my well-being. Rida, thanks for the stimulating discussions and late-night debriefings. Silvia, thanks for sharing your advice and general insight, for helping me improve my figures and writing, and for always being open for an afternoon chat. To the rest of the lab, thank you for fostering such a supportive environment. You all have made this a great place to work, learn, and grow.

My classmates, a group of like-minded individuals, thanks for making graduate school a surprisingly vibrant experience. From recruitment, to retreat, to ski trips, to happy hours, there was no shortage of good times.

My close friends, who help to keep my life balanced. Dana, Alli, and Rit, my adventure buddies, thanks for giving me the opportunity to escape to some wild places. Rob and Ayano, thanks for being open to listen, discuss, laugh, and explore the mountains. Murphy and Elsa, thanks for the enthusiastic greetings and the occasional cuddle.

My family, for their unconditional love and encouragement, I am truly fortunate. Words cannot fully express my gratitude.

For my parents,

who taught me the value of perseverance

Your unwavering support made this whole thing possible

CHAPTER 1

Introduction

The stream will cease to flow;
The wind will cease to blow;
The clouds will cease to fleet;
The heart will cease to beat;
For all things must die.

Excerpt from *All Things Will Die*

Alfred Lord Tennyson

BCL-2 Family Regulation of Apoptosis

Overview of Cell Death

Cells grow. Cells divide. Cells, like all things, will die. Cell death is a fundamental and essential aspect of biology. The health of all multicellular organisms relies on a delicate balance between cellular division and death. However, not all manners of death are equivalent. As in humans, the death of a cell can occur by one of four broad classifications: accident, homicide, natural causes, or suicide. Accidental and homicidal cell death are associated with necrotic cell death (from the Greek for “process of death”). Necrosis is caused by acute injury from toxins, extreme temperature, or hypoxia, resulting in cellular and organellar swelling and the physical disruption of the cellular membrane[1,2]. This produces an inflammatory immune response and damage to the surrounding tissue. On the other hand, natural and suicidal cell death are the result of the intracellular process called programmed cell death. This process is invoked to eliminate cells to help promote the health and survival of the organism at large. In contrast to necrosis, programmed cell death is a finely-tuned, genetically-encoded process which results in the death of individual cells. This meticulously-controlled programmed cell death is critical for the removal of cells during organismal development and homeostatic maintenance[1,3,4].

The most common and best characterized form of programmed cell death is called apoptosis. It is a highly conserved process, occurring across the metazoan branch of the evolutionary tree, in all cell types within an organism, and throughout the various stages of the life cycle[5,6]. During development, apoptosis sculpts the limbs through the removal of interdigital webs[7-9] and prunes the cells of the nervous system to ensure proper connections[10-12]. During metamorphosis of amphibians, apoptosis drives the regression of the tadpole tail and gills, and induces intestinal remodeling, allowing for the switch to a carnivorous diet[8,9,13]. In adults, apoptosis regulates homeostatic cell turnover in numerous tissues including the skin, gut, and liver[14-16]. In males, apoptosis is essential for eliminating excess germ cells during spermatogenesis, allowing for proper maturation of the spermatazoa[17,185,16]. In females, apoptosis regulates duct formation and

subsequent involution of the mammary gland during pregnancy[19,20]. Additionally, apoptosis is crucial in all aspects of the immune system including the removal of self-reacting cells in the maturation of immune cells, the cytotoxic killing of infected cells, and the termination of activated immune cells following the clearance of the immunogen[21,22]. Importantly, apoptosis is also responsible for the removal of stressed, damaged (e.g. following exposure to UV radiation[8,9,11]), or infected cells[23].

Hallmarks of Apoptosis

Naturally occurring cell death was first reported in 1842 by Carl Vogt, who, while studying the development of the midwife toad, recognized the destruction of cells in the notochord and surrounding cartilage to be a normal part of development[24,25]. The first observation of what is now considered apoptosis was made in 1885 by Walther Flemming, a pioneering cell biologist better known for his work detailing chromosomal movement in a process he termed mitosis[25,26]. While studying ovarian follicles in the rabbit, Flemming noted the disintegration of the chromatin in dying cells, calling the process chromatolysis. Despite these and other 19th century descriptions of cell death, its importance as a normal biological phenomenon was not recognized until the mid-20th century. In 1951, Alfred Glücksmann assembled dozens of examples of cell death across various tissues and organisms, leading to the conclusion that “there can be no doubt that cell deaths occur regularly at certain developmental stages of all vertebrate embryos”[27]. This work paved the way for the burgeoning field of cell death.

The classification of apoptosis as a distinct form of cell death came from the observable changes in the morphology of a dying cell. In their seminal 1972 paper, Kerr, Wyllie, and Currie, through the careful examination of mammalian tissues, noted a process of cell death morphologically distinct from necrosis[28,29]. This form of cell death was found throughout the body in normal, malignant, and developing tissues. They proceeded to define a common series of steps that led to cullar death (**Figure 1.1**): (1) The dying cell detaches from the surrounding tissue; (2)

The cell shrinks in size and the nucleus compacts and increases in density; (3) The cell breaks up into apoptotic bodies or blebs; (4) The cellular remains are engulfed by immune cells where they are eliminated from the tissue and eventually degraded. These clearly defined hallmarks of apoptosis allow the process to be readily classified microscopically.

Apoptosis was originally termed “shrinkage necrosis” to emphasize the dramatic reduction in cellular size preceding cellular death[29]. However, there are several key differences that make this process distinct to necrosis, thus warranting a distinct name. (1) In apoptosis, the membrane of the dying cell remains intact, thereby preventing an inflammatory immune response and resulting damage to neighboring cells; (2) Whereas necrosis usually occurs in large swaths throughout tissue, apoptosis tends to occur in select individual cells within a tissue; (3) While necrosis is mainly associated with acute injury, apoptosis plays a more widespread biological role, balancing mitosis to maintain homeostasis. Therefore, a new term was coined to accentuate the normalcy and selectivity of this death process. It was called apoptosis, a word which is “used in Greek to describe the ‘dropping off’ or ‘falling off’ of petals from flowers, or leaves from trees”[28]. While Kerr, Wyllie, and Currie clearly defined the gross morphological changes associated with apoptosis, the underlying molecular mechanisms involved in the regulation of this process proved to be a much more challenging puzzle.

Genetic Control of Apoptosis in C. elegans

Apoptosis was first mechanistically characterized in a systematic manner using the nematode model organism, *Caenorhabditis elegans*. Through careful mapping of cell division and cell fate, H. Robert Horvitz and John Sulston traced the lineage of each cell from embryo to the 959 cells that make up the adult worm. Remarkably, 131 cells die along the way in a precise, predictable, and reproducible manner[30,31]. The *C. elegans* model system aided in the dissection of the mechanisms behind the process of programmed cell death. Through selection of mutant worms defective in programmed cell death, the proteins CED-3 and CED-4 were shown to be essential

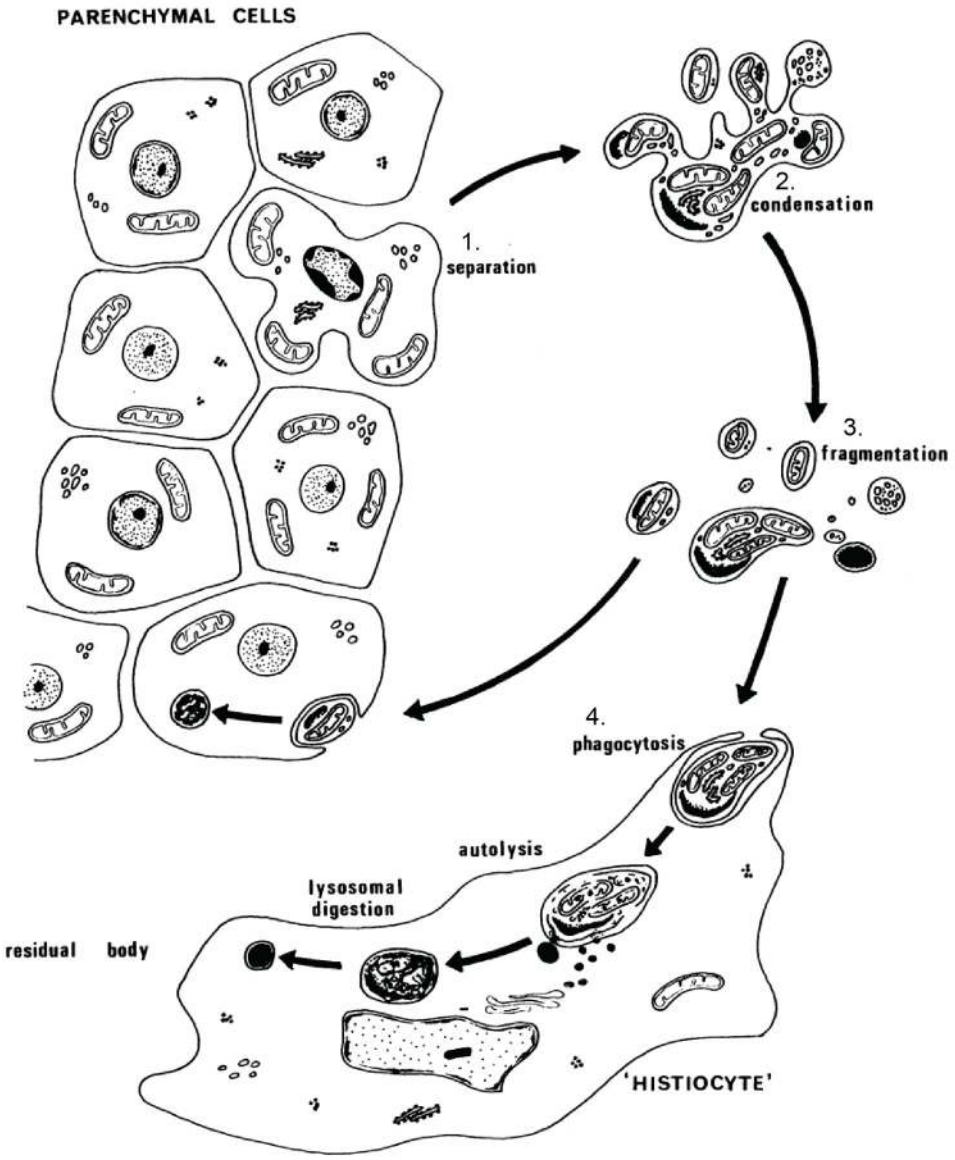

Figure 1.1 *Morphological features of apoptosis.*

The apoptosing cell undergoes a defined series of changes. First, the apoptosing cell separates from the surrounding tissue. The cell then shrinks, forms blebs, and eventually breaks into apoptotic bodies. This involves the condensation of the nuclues and cytoplasm, followed by fragmentation of the nucleus. Finally, these bodies are removed from the tissue by phagocytic cells (histiocytes). Figure from Kerr, Wyllie, and Currie's seminal 1972 paper[28]. Reprinted with permission from Nature Publishing Group.

for the initiation of the process[32]. The protein CED-9 was later shown to block cell death through the inhibition of CED-4[33]. Derepression of this inhibition and the subsequent activation of programmed cell death can be achieved by EGL-1[34]. Together, these discoveries definitively documented that programmed cell death is a carefully regulated genetic program. Furthermore, the CED genes were found to have distinct homologs conserved throughout the metazoan lineage[4], establishing a pathway that carefully regulates the activation of apoptosis across biology. As a result, Horvitz and Sulston, along with their mentor Sydney Brenner, were awarded the 2002 Nobel Prize in Physiology or Medicine, in part, for their discoveries concerning the genetic regulation of programmed cell death.

Apoptotic Cascade in Mammals

In mammals, apoptosis is controlled by a much more elaborate signaling network than that of *C. elegans* (**Figure 1.2**). The rapid, observable cellular changes associated with apoptosis are brought about by a family of cysteine proteases called caspases (cysteine-aspartic proteases)[35]. These enzymes are highly specific, cleaving substrates with a tetrapeptide motif that ends with an aspartic acid residue. Caspases are expressed as zymogens and must be proteolytically cleaved to become enzymatically active. The different members of the caspase family can be classified based on their roles during the apoptotic cascade. Initiator caspases (caspase-8, caspase-9; CED-3 homologs) are the first to be activated and serve to amplify the pro-apoptotic signal. Active initiator caspases cleave the effector or executioner caspases (caspase-3, caspase-6, and caspase-7), which ultimately drive the cellular changes associated with apoptosis by cleaving a diverse array of protein targets throughout the cell [3,35].

Activation of caspases is achieved by one of two distinct pathways, intrinsic or extrinsic apoptosis. Intrinsic, or mitochondrial apoptosis (**Figure 1.2, left**), is initiated by internal stresses such as DNA damage, ER stress, or cytokine deprivation and is characterized by the induction of mitochondrial outer membrane permeabilization (MOMP)[3]. The activation of the pro-apoptotic

proteins BAX (BCL-2-associated X protein) and BAK (BCL-2 antagonist killer) leads to poration of the mitochondrial membrane, directly triggering MOMP[36]. Activation of these toxic pro-death proteins is tightly regulated by other members of the BCL-2 family including the inhibitory anti-apoptotic proteins (CED-9 homologs) and the activating BH3-only proteins (EGL-1 homologs). This BCL-2 family regulation is discussed in detailed in the section below. MOMP causes the release of apoptogenic factors such as cytochrome *c*[37,38] and SMAC (also known as DIABLO) into the cytoplasm[39,40]. In turn, cytochrome *c* can bind to the scaffolding protein APAF1 (CED-4 homolog) to form a protein complex called the apoptosome, which catalyzes the activation of caspase-9, an initiator caspase[41,42]. Moreover, SMAC directly inhibits XIAP, a protein which normally inhibits the activities of caspase-3, -7, and -9 to prevent aberrant caspase cleavage[39,40,43]. Ultimately, the release of these apoptogenic factors from the mitochondria results in the activation of the caspase cascade and the initiation of apoptosis.

The initiation of extrinsic apoptosis (**Figure 1.2, right**) occurs through extracellular ligands such as FAS or TRAIL[3,43]. These ligands bind to specific death receptors (FAS or TRAIL receptors, respectively), which are displayed on the cell surface. The death receptors along with the FADD adapter protein and pro-caspase-8 assemble into the death-inducing signaling complex (DISC)[36,43]. The binding of death ligands to the DISC results in auto-activation of pro-caspase-8 through dimerization-induced self-cleavage[36]. Activated caspase-8 cleaves downstream effector caspases, leading to apoptotic cell death. Additionally, the activation of caspase-8 leads to the cleavage of the BH3 only protein BID to form truncated BID (tBID)[44,45]. This promotes the activation of the intrinsic pathway and an overall amplification of apoptotic signaling in the cell.

Regulation of Apoptosis by the BCL-2 Family

Regulation of intrinsic apoptosis in mammals is achieved by the BCL-2 family of proteins. B-cell lymphoma-2 (BCL-2) is the founding member of this class of structurally homologous proteins. BCL-2 was discovered at the t(14;18) chromosomal breakpoint commonly found in

Figure 1.2 *Overview of the intrinsic and extrinsic apoptotic pathways.*

Activation of intrinsic apoptosis (left) is controlled by the BCL-2 family proteins (boxed). Various cellular stress signals drive an increased expression of BH3-only proteins (BIM, BID, PUMA, etc.). This results in the activation of the pro-apoptotic proteins (BAX, BAK) both by inhibition of the inhibitory anti-apoptotic proteins (BCL-2, BCL-X_L, MCL-1, etc.) and through direct activation of the pro-apoptotic proteins. Activated pro-apoptotic proteins oligomerize to porate the mitochondrial outer membrane (MOMP) and release apoptogenic factors (cytochrome *c*, SMAC) into the cytoplasm. SMAC inhibits the cytoplasmic caspase inhibitor XIAP. Cytochrome *c* binds to APAF-1 leading to the formation of the apoptosome, a protein complex that drives activation (cleavage) of caspase-9. Cleaved caspase-9 subsequently activates effector caspases (caspase-3/6/7), resulting in morphological changes associated with apoptosis. Extrinsic apoptosis (right) is a parallel pathway driven by the binding of extracellular ligands (FAS, TRAIL) to the DISC (complex of death receptor, FADD, and pro-caspase-8) on the cell surface. Death receptor signaling results in the cleavage of pro-caspase 8 which can in turn cleave both downstream effector caspases and BID. Truncated BID or tBID can drive the activation of the intrinsic apoptotic pathway at the mitochondria.

Figure 1.2 (Continued)

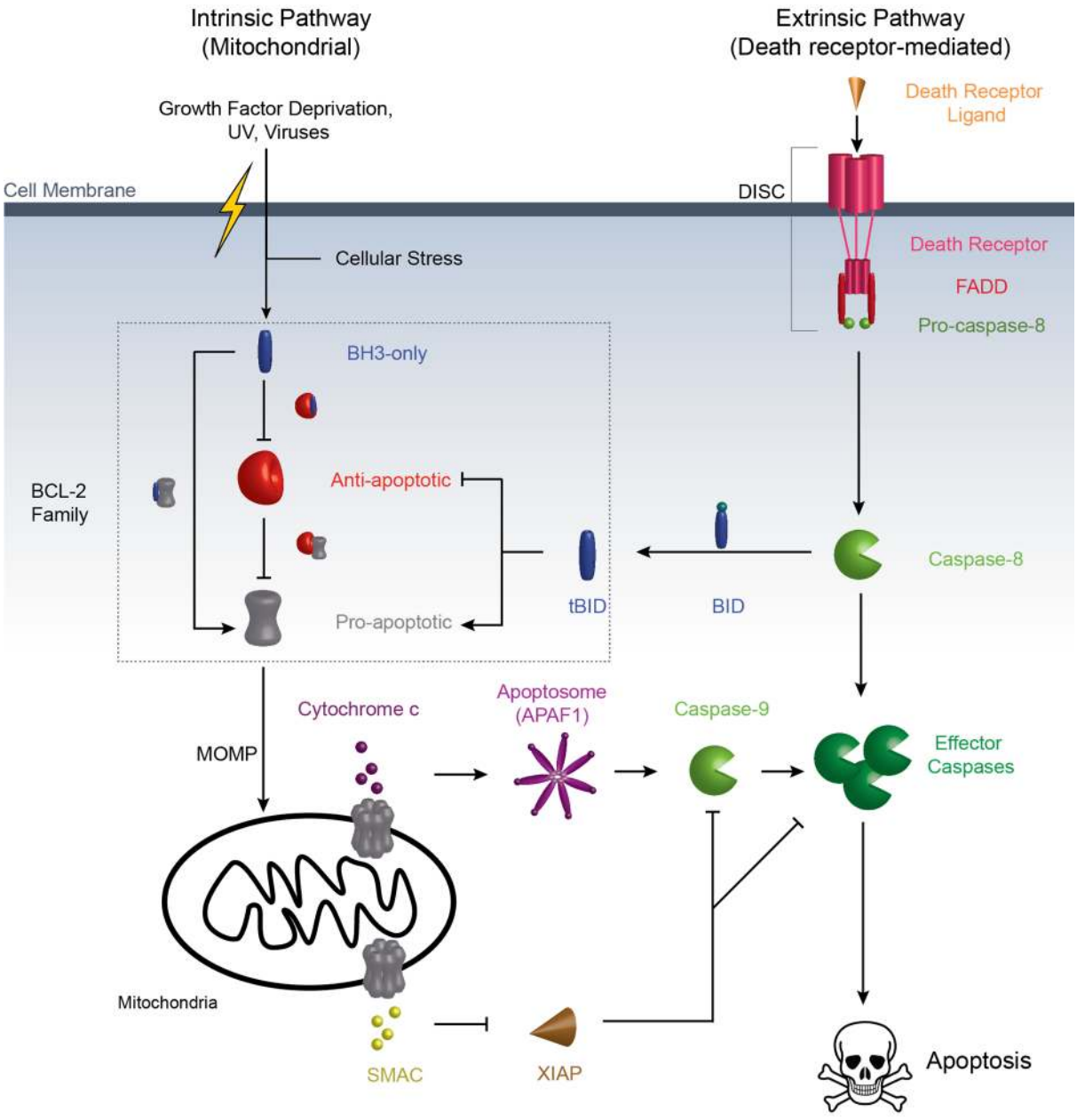

follicular non-Hodgkin B cell lymphoma[46-48]. This genetic rearrangement places the *Bcl-2* locus (found at 18q21) under the same transcriptional regulation as the immunoglobulin heavy chain at 14q32. The functional consequence of this rearrangement is a dramatic overexpression of the BCL-2 transcript[49,50].

Initial efforts to characterize this gene product revealed that, unlike the other known oncogenes at the time, BCL-2 did not promote uncontrolled cellular proliferation. Instead, cells overexpressing BCL-2 failed to die in response to stress from growth factor withdrawal, remaining in a viable, non-proliferative state[51,52]. Furthermore, knocking out BCL-2 in mice led to various defects including apoptotic loss of lymphocytes in the thymus and spleen, polycystic kidney disease, and premature graying of the fur (due to death of hair follicle melanocytes)[53,54]. This experimental evidence strongly linked BCL-2 to the promotion of cell survival. Additionally, it was discovered that BCL-2 shares significant sequence homology with the *C. elegans* CED-9 protein and BCL-2 can rescue the effect of CED-9 loss in worms[55,56]. These findings were revolutionary as they established BCL-2 as a critical regulator of apoptosis in mammals and provided the first evidence that deregulation of this conserved biological pathway can contribute to the pathogenesis of human cancer.

The discovery of BCL-2 as a regulator of apoptosis launched the search for other proteins that could interact with or exhibit a phenotype similar to BCL-2. This effort resulted in the identification of numerous homologs, which are now collectively referred to as the BCL-2 family of proteins. There are three main classes of BCL-2 family proteins that together function as a tripartite regulatory circuit for the control of apoptosis (**Figure 1.3a**).

The pro-apoptotic proteins (**Figure 1.3, gray**) are the key effector proteins in this pathway. When activated, BAX, BAK, and likely BOK function to oligomerize to create a pore in the outer mitochondrial membrane, resulting in MOMP[3,57]. BAX and BAK are the major regulators of apoptosis in most contexts, while the recently characterized protein, BOK, plays a role in sensing ER and proteasomal stress, but may not be regulated by other BCL-2 family members to the

Figure 1.3 *The BCL-2 family interaction network.*

(**a**) BCL-2 family proteins can be subdivided into three groups based on their function. The anti-apoptotic BCL-2 family members (red; represented by BCL-X_L, PDB: 1LXL) block the activation of the pro-apoptotic members (gray; represented by BAX, PDB: 1F16), which serve to permeabilize the mitochondria and initiate apoptosis. The BH3-only proteins (blue; represented by BID, PDB: 2BID) serve as modulators of this network by inhibiting the anti-apoptotic members, resulting in the derepression of BAX/BAK inhibition. A subset of the BH3 only proteins can also directly activate BAX/BAK. The anti-apoptotic proteins and pro-apoptotic proteins share a similar nine-helical bundle fold. (**b**) Sequence alignment of the three BCL-2 family subclasses showing the relative positioning of the BCL-2 homology (BH) motifs, α-helices, and the transmembrane domain within the BCL-2 family member subtypes.

Figure 1.3 (Continued)

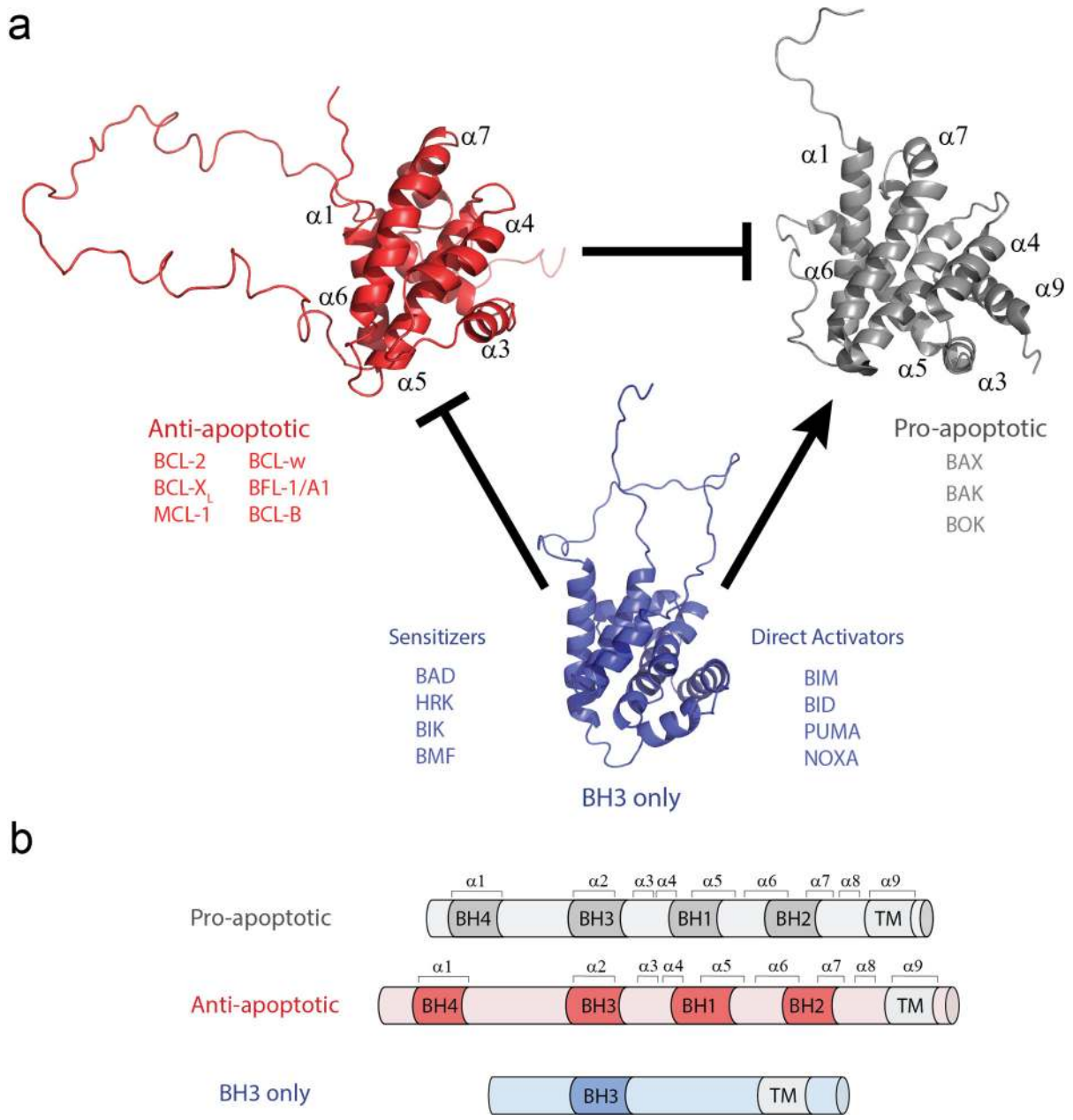

same extent as BAX or BAK[58]. Initial characterization of BAX and BAK revealed that the overexpression of these proteins induces apoptosis and accelerates death by growth factor withdrawal and other stimuli[59,60]. Conversely, loss of BAX in mice leads to hyperplasia of B and T cells and infertility, both due to an inability of precursor cells to die[61]. Additionally, combined loss of both BAX and BAK results in the death of ~90% of mice with the surviving animals displaying numerous defects due to the inability to induce apoptosis, including the accumulation of hematopoietic cells and neurons, persistence of interdigital webs, and an imperforate vaginal canal[62].

The anti-apoptotic proteins of the BCL-2 family (**Figure 1.3, red**) serve to block the induction of apoptosis by inhibiting the activation of the pro-apoptotic proteins. Anti-apoptotic family members bind to BAX/BAK, preventing the activation of apoptosis by physical sequestration. There are several *bona fide* anti-apoptotic proteins including BCL-2 itself, BCL-X_L, MCL-1, BCL-w, BFL1/A1, and BCL-B[3,57,63]. Although these proteins display functional redundancy, spatiotemporal variations in expression results in the differential importance of any particular anti-apoptotic protein in the maintenance of survival.

The third class of proteins in the BCL-2 family consists of the BH3-only members (**Figure 1.3, blue**), which function to drive the activation of BAX/BAK, either indirectly and/or directly. The sensitizer subclass, including BAD, BIK, HRK, and BMF, functions by inhibiting the anti-apoptotic proteins and sensitizing the cell to apoptotic death[3,57,63,64]. In addition to anti-apoptotic inhibition, the direct activators including tBID[65,66], BIM[65-67], PUMA[68,69], and perhaps NOXA[70] can directly activate BAX/BAK to initiate apoptosis. The BH3-only proteins serve as sensors of stress in the cell. They are upregulated in response to various stress stimuli including genotoxic stress, ER stress, and growth factor withdrawal[3]. NOXA and PUMA, for example are transcriptionally upregulated by the tumor suppressor p53 upon DNA damage or hypoxic stress[71-73]. BIM expression is induced by the transcription factor FOXO3a in growth factor withdrawal[74] or by CEBPα or CHOP during ER stress[75]. Posttranslational activation of BID is achieved by caspase-

8 cleavage during death-receptor signaling or by granzyme B cleavage during cytotoxic T-cell killing[76]. A distinct mechanism has been detailed in BAD, whereby dephosphorylation activates the pro-apoptotic protein function of this protein during growth factor deprivation[77].

*S*tructure of BCL-2 Family Proteins

Structurally, both the pro- and anti-apoptotic members adopt a similar globular fold (**Figure 1.3a**). This BCL-2 fold consists of a bundle of nine α-helices (α1–α9) arranged around a central core hairpin (α5–α6)[78]. The pro- and anti-apoptotic BCL-2 family proteins also share four discrete areas of sequence homology called BCL-2 homology (BH) motifs (**Figure 1.3b**). The BH3 motif (defined as LXXXGD) is the most well conserved sequence among the BCL-family members and is the only BH motif that is shared by the BH3-only proteins. The BH3 motif consists of a critical amphipathic helix that serves as the minimal region of pro-apoptotic signaling in BAX/BAK and the BH3-only proteins[63].

The confluence of α2–α5 (BH1–BH3) forms a hydrophobic surface groove, termed the canonical BH3 binding pocket, in anti-apoptotic proteins. This groove is a key interaction interface that bestows the anti-apoptotic proteins with their inhibitory function. Specifically, the canonical BH3-binding pocket sequesters the BH3 helices of BAX/BAK, thereby preventing their activation. This helix-in-groove interface is the result of four hydrophobic interactions, and a salt bridge between the conserved aspartic acid on the BH3 ligand (LXXXG**D**) and an arginine in the BH1 of anti-apoptotic proteins[3]. With the exception of the protein BID[79], the BH3-only proteins are largely structurally divergent from the multi-domain family members. BAD, BMF, and BIM are intrinsically unstructured proteins with the BH3 undergoing binding-induced α-helical folding[80]. In fact, the observed homology in the BH3 region of BH3-only proteins is predicted to have arisen through convergent evolution[81]. Despite the structural diversity of the BH3-only proteins, they all function to inhibit anti-apoptotic proteins by forming stable high affinity complexes at the same surface

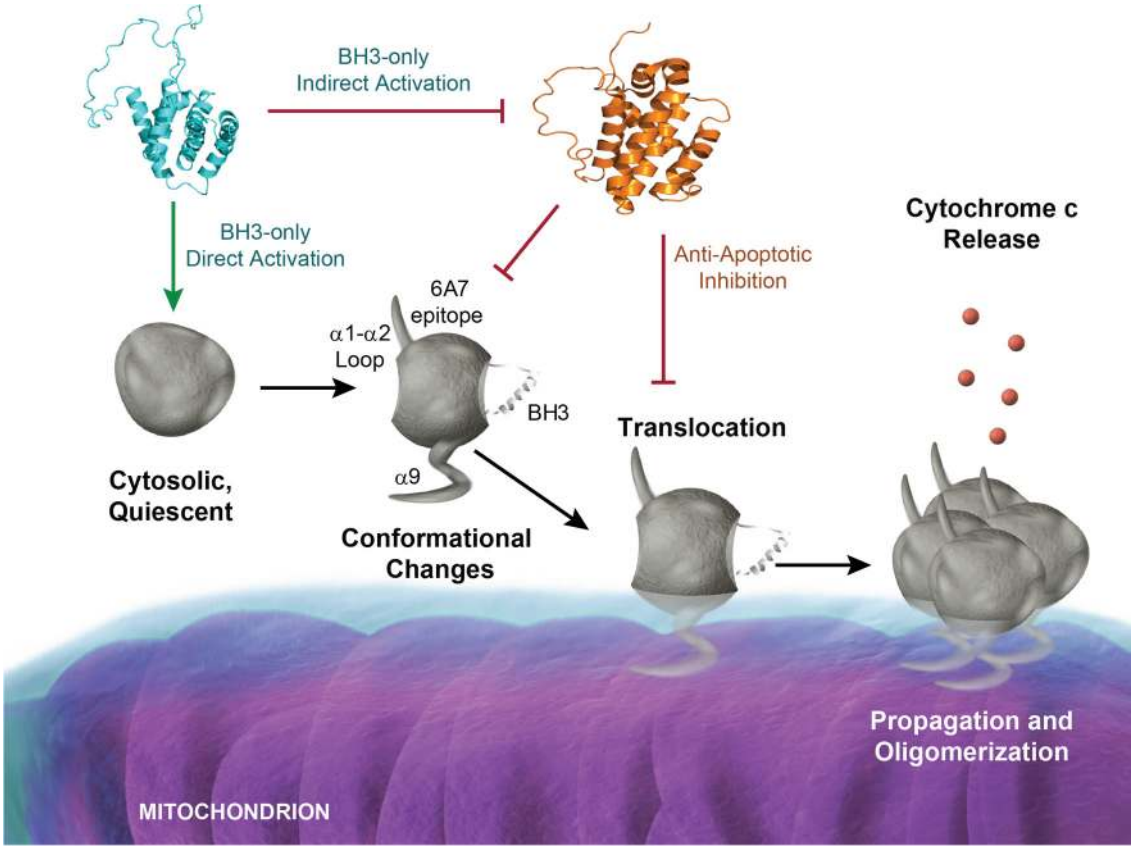

Figure 1.4 *Regulation of BAX-mediated apoptosis.*

BAX (gray) transforms from an inactive cytoplasmic monomer into toxic pores that disrupt the mitochondrial outer membrane. Anti-apoptotic proteins (orange), such as BCL-2 and BCL-X_L, bind and sequester the critical BH3-helix of BAX, preventing apoptosis activation. The upstream BH3-only proteins (cyan) such as BIM, tBID, or PUMA can induce apoptosis by inhibiting the inhibitors or by directly activating BAX. Activated BAX undergoes several conformational changes including the opening of the α1–α2 loop, exposure of the 6A7 activation epitope, mobilization of the BH3 helix, and release of the α9 transmebrane helix. These changes allow for BAX translocation from the cytosol to the mitochondrial outer membrane. At the mitochondria, BAX can oligomerize into a pore that releases cytochrome *c*, thereby driving apoptosis.

groove used by the anti-apoptotics to bind and inhibit BAX. This competition releases the pro-apoptotic BAX and BAK proteins, allowing for their functional activation.

Regulation of BAX and BAK activation

BAX and BAK share significant structural homology with the anti-apoptotic proteins, including a "canonical" groove. Inactive BAK resides at the mitochondria with its C-terminal transmembrane domain inserted into the mitochondrial outer membrane. Binding at the canonical groove by the direct activator BH3-only proteins or the BH3 helix of another unit of BAK mediates activation, which leads to subsequent homo-oligomerization[82,83]. Unlike the stable helix-in-groove interactions observed in anti-apoptotic proteins, BH3-BAK binding interactions are transient, resulting in a "hit-and-run" activation mechanism[84].

In contrast to BAK, the transformation of inactive BAX into the toxic oligomers that porate the mitochondria is a more complex and dynamic process. In healthy cells, inactive BAX primarily resides in the cytoplasm, with its transmembrane domain (α9) tightly bound into the canonical groove of BAX (**Figure 1.3a**)[85]. In response to apoptotic stimuli, BAX translocates to the mitochondria, inserting its transmembrane domain into the mitochondrial outer membrane[86,87] (**Figure 1.4**). These initial conformational changes in BAX are mediated by a distinct site from the canonical groove formed by the intersection of the α1 and α6 helices[88]. Binding at this "trigger" site by BIM[88], BID[89], or PUMA[69] induces several conformational changes in BAX including the opening of the α1-α2 loop, exposure of the 6A7 epitope (conformation-specific antibody epitope that is exposed in activated BAX), mobilization of the BAX BH3, and the release of α9 from the canonical groove[90] (**Figure 1.4**). The catalytic nature of this interaction is further highlighted by the capacity of the exposed BH3 domain of BAX to initiate the activation of another BAX protein by engaging its trigger site[90]. Together, these changes allow for efficient BAX insertion into the mitochondrial outer membrane. Since the α9 is displaced from the canonical groove, membrane-

bound BAX can be further activated by BH3-only proteins, which may bind to its canonical site in a manner similar to that of BAK[91].

In addition to this extra layer of regulation via BH3-induced translocation, recent studies suggest that in normal, unstressed cells BAX may be constitutively targeted to the mitochondria, but then actively cycled back into the cytoplasm[92,93]. Anti-apoptotic proteins, such as BCL-X_L, have been proposed to direct the removal of BAX from the mitochondria through a process called retrotranslocation[92]. Therefore, there are potentially two mechanisms for mitochondrial translocation of BAX, one that is directly induced by BH3-only protein interaction and another, which is the indirect result of a blockade in the retrotranslocation process. In either case, the trigger site-induced exposure of α9 is thought to be critical for the stable insertion of BAX into the mitochondrial membrane.

Given the inherent risk to the cell of wanton BAX activation, several mechanisms can effectively inhibit BAX activation. The best characterized mode of inhibition is through sequestration of the BAX BH3 helix by the groove of an anti-apoptotic protein, as discussed previously. A second mechanism of BAX inhibition occurs through the binding of the anti-apoptotic BH4 helix to a distinct BH4-binding site on BAX[94]. This suggests that anti-apoptotic proteins may inhibit BAX through two distinct, but complementary mechanisms, with the BH4 helix restraining inactive BAX and the groove blocking conformationally active BAX. Additionally, the cytomegalovirus vMIA protein can bind to and inhibit BAX[94-96], a pathway which ensures host cell survival during viral infection and replication[97,98]. The BAX-binding domain of vMIA achieves its inhibitory effect by targeting a discrete pocket on BAX, adjacent to and partially overlapping with the BH4-binding site[95].

Structure of the BAX/BAK pore

Following activation, membrane-bound BAX and BAK oligomerize to form a pore in the mitochondrial outer membrane. The exact mechanism of how BAX/BAK can rearrange into

oligomers and the structural nature of the pore are active areas of study that constitute “the 'holy grail' of apoptosis research”[63]. One challenging aspect is that BAX/BAK form heterogeneous pores of varying diameter that grow over time as more BAX and BAK are recruited[99,100]. These large, dynamic structures are predicted to porate the mitochondrial membrane by inducing membrane curvature stress[99,101-104]. While homology with bacterial pore-forming toxins initially suggested that BAX/BAK may form a well-defined proteinaceous pore[85,105], current data are more consistent with a lipidic (toroidal) pore structure, whereby BAX/BAK induces the formation of a channel lined with the lipid head groups of the mitochondrial membrane. This lipidic structure was validated by a recent study that detected membrane-puncturing ring- and arc-shaped BAX structures using a combination of super-resolution and atomic force microscopy[106,107].

Two main models have been proposed to explain how BAX/BAK may arrange itself within this oligomeric pore. Since the BH3 helix of BAX and BAK has long been recognized as essential to the formation of higher order species[108-110], both models rely on a BH3-in-groove interface to facilitate homo-oligomerization. Beyond that, it is not fully understood how the individual monomers interact within the pore. The first model is the head-to-tail (daisy chain) model in which each BAX/BAK unit is linked onto the end of a growing oligomeric chain[111,112] .This model is based on the structural similarity of BCL-2 family proteins to bacterial toxins that form oligomeric pores in this manner[78]. The trigger site on BAX was proposed as an interface that could mediate such an asymmetric interaction, as a BAX BH3 could then engage the trigger site of another BAX, thereby growing the activated BAX oligomer. In this head-to-tail model, the size of the oligomer would be expected to increase in units of one as the activated monomers are added onto a growing BAX chain. However, a study using single molecule analysis suggested that BAX dimers may be the basic oligomeric unit and that BAX oligomers grow in two-unit intervals[113].

The alternative hypothesis is that BAX/BAK form oligomers comprised of stable symmetric dimers. In this model, the BAX/BAK BH3 inserts into the canonical groove of another unit of BAX/BAK in a reciprocal fashion. These dimers then interact with each other through a secondary

interface to facilitate the formation of a multimer of dimers that porates the membrane[114]. The symmetrical dimer model is supported by crosslinking[109,115], single molecule analysis[113], and crystallographic studies[82,91] that demonstrate the formation of stable, symmetrical dimers following BAX/BAK activation. Furthermore, crystal structures of activated BAX/BAK (notably lacking the C-terminal tail) suggest that the core BH3-binding pocket (α2–α5) separates from the rest of the protein (α6–α8), which forms a latch domain. This core-latch disengagement is proposed to mediate dimerization and has been shown to be a required rearrangement for BAX/BAK activation[91]. However, a recent study demonstrated that the interaction between α9 and the trigger site can lead to an inhibitory BAX dimer[116], suggesting an alternative biological explanation for the observed BAX dimers. Until higher resolution structural information of oligomeric BAX/BAK is obtained, the exact structure of the pore will remain controversial.

Targeting the BCL-2 Family to Treat Disease

BCL-2 Family in Disease

The number of cells in an organism is dependent on a balance between two opposing forces: mitosis, which creates cells, and apoptosis, which removes them. The health of an organism is dependent on the maintenance of this balance and its disruption can lead to diseases of pathologic cell survival or cell death. Improper loss of cells due to deregulated apoptosis can result in conditions of premature cell death. An overabundance of neuronal cell death is characteristic of several neurodegenerative diseases including Alzheimer's, Huntington's and Parkinson's diseases and Amyotrophic Lateral Sclerosis (ALS)[117,118]. Additionally, excessive apoptosis in developing immune cells[21,119,120] or spermatozoa[121,122] can result in immunodeficiency or infertility, respectively. Conversely, the failure to properly activate cell death can lead to conditions of extended cellular survival. Failure to eliminate autoreactive T- and B-cells during lymphocyte maturation can lead to autoimmunity[21,119]. However, the strongest link between

pathologic cell survival and the development of disease is found in cancer.

Deregulation of apoptosis is a critical hallmark of cancer[123,124]. The discovery of BCL-2 at the chromosomal breakpoint in follicular B cell lymphoma led to the hypothesis that the protein acts as an oncogene to promote tumorigenesis. While traditional oncogenes such as MYC, ABL, and RAS promote uncontrolled cell growth and proliferation, BCL-2 prevented the death of the tumor cells[125]. This paradigm-shifting discovery demonstrated that blockade in the natural death pathway is a key driver of oncogenesis.

Since this initial discovery, the connection between the BCL-2 family and cancer has strengthened. Cancer cells utilize a diverse array of mechanisms to increase the expression of anti-apoptotic proteins or inhibit the expression of their pro-apoptotic counterparts[125,126]. Up to 90% of follicular B cell lymphomas display the characteristic t(14;18) chromosomal breakpoint that results in the overexpression of BCL-2. Other anti-apoptotic proteins including MCL-1 and BCL-X_L were shown to be frequently amplified in an analysis of somatic copy number alterations across all tumor types[127]. Another mechanism that results in the overexpression of BCL-2 is loss of microRNA-mediated inhibition. Most cases of chronic lymphocytic leukemia (CLL) display overexpression of BCL-2 through the loss of miR-15a and/or miR-16.1 expression[128]. Similar loss of miRNA regulation can lead to the overexpression of BCL-X_L, MCL-1, and BCL-w in a range of different cancer types[129-131].

In addition to increasing levels of anti-apoptotic proteins, cancer cells also decrease the level of BH3-only and/or pro-apoptotic proteins to prevent induction of apoptosis. Homozygous deletion of BIM is found in approximately 20% of mantle cell lymphomas[132]. Epigenetic silencing of BIM or PUMA expression through promoter hypermethylation has been identified in several cancer types[133,134]. Finally, although rare, a few examples of mutation in BAX have been identified[135,136]. Due to the functional overlap of BAX and BAK, a cancer cell would need to eliminate four alleles to achieve complete loss of apoptotic signaling. Therefore, suppression of BAX and BAK at the protein level is most commonly achieved by modulating the levels of the

upstream regulators, especially the anti-apoptotic suppressors.

Beyond their role in oncogenesis, BCL-2 family proteins play a key role in the response to anti-cancer therapeutics. The killing activity of most chemotherapeutics is mediated by the apoptotic machinery. Therefore, the expression of various BCL-2 family proteins can determine the efficacy of a range of therapeutic treatments[125,126]. For example, BCL-2 overexpressing cells are resistant to gamma-radiation and a variety of chemotherapeutic agents such as etoposide and dexamethasone[137,138]. In addition to mediating resistance to therapy, BH3-only proteins have been shown to be crucial for chemotherapeutic agents to be efficacious. In particular, PUMA is required for killing by etoposide or cyclophosamide[72,73] and BIM expression is required for the efficacy of taxol[139], histone deacetylase inhibitors[140], oncogenic kinase inhibitors[141], and epidermal growth factor receptor (EGFR) inhibitors[142,143]. Therefore, pharmacological strategies to strengthen apoptotic signaling could serve as a synergistic approach to bolster the effect of current treatment regimens.

Reactivating Apoptosis in Cancer: Inhibit the Inhibitors

Given that cells turn off apoptosis to promote their growth and survival and that many chemotherapeutic agents rely on an intact apoptotic network, agents that reactivate apoptosis in cancer cells could serve as highly effective and targeted anti-cancer therapeutics. Because apoptotic pathways in both cancerous and normal cells are homologous, one concern about this therapeutic approach is a potentially narrow therapeutic window. Fortunately, it turns out that, in many cancer contexts, a window does exist due to “apoptotic priming”, a concept first promoted by Tony Letai and colleagues[144]. As BH3-only protein expression drives the messaging for apoptosis induction, the ability to survive any given stress is proportional to the anti-apoptotic reserve that is free to inhibit a surge in BH3-only proteins. When the anti-apoptotic reserve is overwhelmed, BAX and/or BAK become activated and the cell undergoes apoptosis. Oncogenic stress signals push cancer cells toward death, through increased BH3-only protein expression or

deployment. In order to thrive in the face of this death signaling, cancer cells must compensate by increasing the expression of anti-apoptotic proteins and/or suppressing BH3-only signaling to match the level of the anti-apoptotic protein reserve. As a result, in many cancer cells, there is little surplus of free, unbound anti-apoptotic proteins. Therefore, it only takes a small perturbation (in the form of a chemotherapeutic, for example) to disrupt this balance, sending the cell over the ledge and inducing apoptosis. In this way, cancer cells are often considered to be more "primed" to die than their normal counterparts.

Since one or more anti-apoptotic proteins are often upregulated in cancer, one strategy to reactivate apoptosis is to functionally block these proteins (**Figure 1.5a**). This "inhibit the inhibitors" strategy aims to decrease the anti-apoptotic protein load, thereby allowing apoptotic activation pathways to take over unchecked. The first attempt at implementing this strategy was to directly knockdown levels of BCL-2 protein expression using an antisense oligonucleotide. Genta Inc. and Aventis developed oblimersen (Genasense) to treat malignant melanoma, CLL, and acute myeloid leukemia (AML), but, in the early 2000's, it failed to meet its primary endpoints in phase 3 clinical trials [145]. Despite this failure, the antisense studies revealed certain patient subsets that responded well, validating BCL-2 as a promising anticancer drug target.

A distinct approach to inhibiting anti-apoptotic function is to directly inhibit the protein's ability to sequester the pro-apoptotic members by mimicking BH3 binding. Peptides corresponding to the BH3 helix of BAX or BAK were shown to inhibit BCL-2 and BCL- X_L in cell-free systems, suggesting that this naturally bioactive domain could serve as a viable strategy for therapeutic inhibition[146,147]. However, peptides are not ideal drug candidates as they suffer from both poor *in vivo* stability and often lack cell penetrance. The breakthrough needed to design a more drug- like inhibitor came when scientists at Abbott Laboratories solved the nuclear magnetic resonance (NMR) structure of BCL-X_L with and without a BAK BH3 peptide bound[78,148]. These studies revealed the structure of the canonical groove, which was predicted to mediate the inhibition of pro-apoptotic BCL-2 family members by a BH3-in-groove binding interaction (**Figure**

Figure 1.5 *Overview of apoptosis reactivation strategies in cancer.*

(**a**) Pharmacologic reactivation of apoptosis can be achieved by inhibition of the anti-apoptotic proteins, leading to derepression of pro-apoptotic BAX/BAK. Alternatively, the direct activation of pro-apoptotic proteins can lead to initiation of apoptosis. (**b**) Examples of the "inhibit the inhibitor" strategy involve blocking the canonical groove (top; BCL-X_L, PBD: 1MAZ), either through occlusion by a BH3-peptide (middle; BAD BH3: BCL-X_L, PDB: 1G5J) or by a small molecule peptidomimetic (bottom; ABT-737: BCL-X_L, PDB: 2YXJ). (**c**) The canonical groove of inactive, cytosolic BAX is occupied by the α9 helix (top; BAX, PDB: 1F16). Therefore, the best example of the "activate the activator" strategy involves targeting the trigger site on BAX. This can be accomplished either through engagement by a BH3-SAHB (middle; BIM SAHB:BAX, PDB:2K7W) or by a small molecule peptidomimetic (bottom, BAM7:BAX).

Figure 1.5 (Continued)

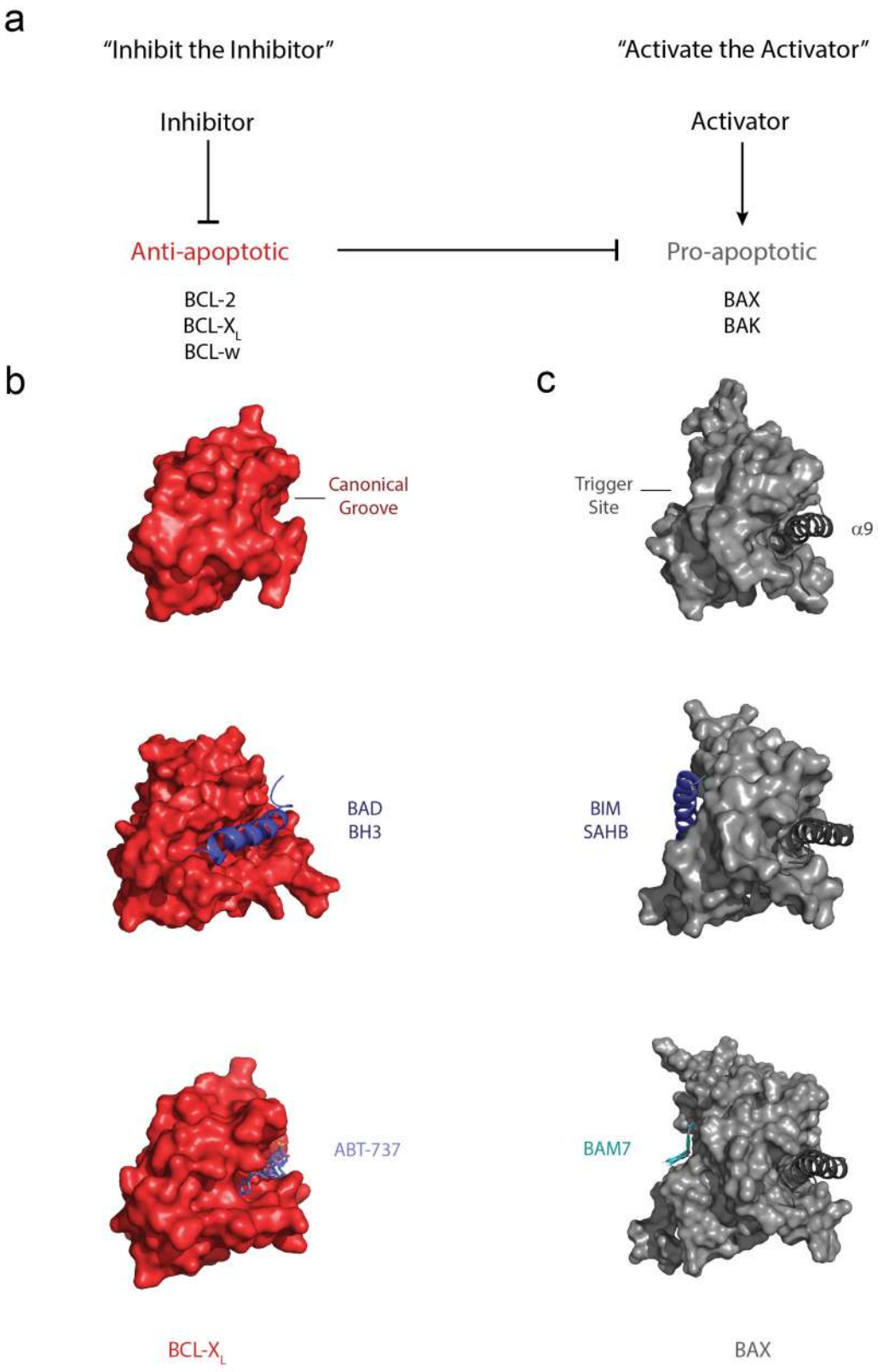

1.5b, top). Several academic groups used these structures, along with the related structure of the BCL-X_L- BAD BH3 complex[149] (**Figure 1.5b, middle**), as starting points for designing compounds that could mimic this protein-protein interaction. Unfortunately, the initial series of compounds lacked the necessary potency to make them clinically useful[150,151].

Steve Fesik and colleagues at Abbott Laboratories were the first to develop a potent, small molecule anti-apoptotic protein inhibitor. The key to their success was the technique called structure-activity relationship (SAR) by NMR, a screening approach pioneered by Fesik[152]. SAR by NMR identifies low molecular weight fragments that bind weakly to the protein of interest. Binding is determined by measuring the change in ^{1}H-^{15}N heteronuclear single quantum correlation (HSQC) NMR spectra upon the addition of the ligand. Weakly binding fragments that bind to adjacent sites of the protein are then chemically linked together, resulting in a high affinity ligand. Utilizing the NMR structure of BCL-X_L/BAK BH3 as a starting point, SAR by NMR was used to screen a 10,000 fragment library for compounds that could bind to the BH3-binding groove[153]. A second round of screening was conducted to identify fragments that bound to an adjacent site. The hits from each site were optimized independently and then chemically linked together to produce a potent lead compound. Continued medicinal chemistry optimization led to a compound with improved solubility and reduced albumin binding. The result was ABT-737, a small molecule peptidomimetic that functionally resembled the BAD BH3 helix (**Figure 1.5b, bottom**), potently and specifically inhibiting BCL-X_L, BCL-2, and BCL-w (with a sub-nanomolar K_i)[154]. Furthermore, ABT-737 was shown to induce cell death in cancer cell lines, patient-derived cells, and in mouse xenograft models[154].

Prior to testing this compound in the clinic, ABT-737 was further optimized to increase its oral bioavailability. The result was the clinical candidate navitoclax (ABT-263), a BCL-2/BCL-X_L/BCL-w selective inhibitor[155]. This compound was shown to have on-target single agent antitumor efficacy in preclinical models. Additionally, it synergized with conventional chemotherapeutic and radiation treatment regimens. The potential of this drug strategy was

confirmed in a phase I/II dose escalation clinical trial where navitoclax displayed single agent efficacy in CLL[156]. However, patients receiving this drug displayed dose-limiting thrombocytopenia, an on-target side effect due to the strong dependency of platelets on BCL-X_L for survival[157,158].

In order to bypass this toxicity in BCL-2-dependent cancers, the potent BCL-2 specific inhibitor venetoclax (ABT-199) was developed[159]. This compound proved to be efficacious as a monotherapy in clinical trials for CLL, mantle cell lymphoma, and Waldenstrom's macroglobulinemia[125]. Venetoclax proved to be especially potent in the treatment of relapsed/refractory CLL, achieving significant response rates (up to 80%)[160]. Further success in treating a chemoresistant subtype of CLL (17p13 deletion) in a phase III clinical trial led to the FDA-approval of venetoclax in 2016. Ongoing clinical trials of venetoclax look to expand on the approved indications. Particularly promising are approaches combining venetoclax with standard of care treatments such as rituximab in CLL or cytarabine in AML[125,126].

Given the clinical success of BCL-2 inhibition, there has been a major academic and pharmaceutical effort to inhibit other anti-apoptotic proteins including BCL-X_L[161,162], MCL-1[163-167] and BFL-1[168], which, have been linked to the pathogenesis of a broad range of hematologic and solid tumors. MCL-1 is a particularly intriguing target as it is one of the most frequently amplified genes across all tumor types[127] and an inhibitor of this protein has the potential to achieve far-reaching anti-tumor efficacy. The compound S63845 (Servier) displays picomolar affinity to MCL-1 and substantial on-target anti-tumor activity in a variety of preclinical models[164]. Future clinical trials with S63845 and the undisclosed MCL-1 inhibitor AMG176 (Amgen) will reveal the efficacy and feasibility of targeting MCL-1 in cancer[169].

Reactivating Apoptosis in Cancer: Activate the Activators

While the "inhibit the inhibitor" strategy has proven to be effective in the clinic, it relies on a tumor's dependency on specific anti-apoptotic proteins for survival. Therefore, the efficacy of this

approach will likely be limited to a subset of cancers. However, deregulation of apoptosis is observed across diverse tumor subtypes. Given that BAX and BAK serve as the critical central regulators of apoptotic initiation, the direct modulation of these pro-apoptotic proteins could serve to reactivate apoptosis in cancer (**Figure 1.5a**). “Activating the activators” could potentially overwhelm and/or bypass anti-apoptotic inhibition and result in the induction of apoptosis across a wide range of cancer types, independently of which particular anti-apoptotic protein subtype the tumor is dependent on. The precedent for this therapeutic strategy comes from the ability of certain BH3-only proteins to directly interact with and activate BAX and BAK. Unlike the formation of a stable protein-inhibitor complex, the interaction between BH3 helices and BAX/BAK is proposed to be a dynamic, “hit-and-run” mechanism. Ligand-activated BAX/BAK can, in turn, lead to BAX/BAK autoactivation, resulting in the rapid, catalytic formation of pores in the mitochondrial outer membrane. Therefore, mimicking this BH3 interaction could yield a novel, apoptosis-reactivating therapeutic.

It was appreciated early on by Stan Korsmeyer and colleagues that certain BH3-only proteins could interact with both anti- and pro-apoptotic proteins. Following the discovery of the protein BID, various mutations in the BH3 helix were found to prevent its binding to anti-apoptotic proteins[170]. However, these same mutations did not abrogate BID’s ability to bind to BAX or to induce BAX-mediated apoptosis. Furthermore, unlike other BH3-only proteins like BIK and BAD, synthetic peptides representing the BH3 sequence of BID and BIM were shown to directly activate BAX in purified mitochondria[66] or in a liposomal system[171]. These experiments supported a model in which a subset of BH3-only proteins is capable of directly activating pro-apoptotic BAX and BAK. However, the validity of this model was challenged due to the inability to measure a direct binding interaction between BAX and BH3 peptides, as well as the high amount of peptide needed to induce activation in these systems[172].

The resolution of this apparent discrepancy came from an improved understanding of the nature of the BH3-only-BAX/BAK interaction. Structural studies revealed that various BH3

peptides interact with the anti-apoptotic proteins via a helix-in-groove interaction[3,57]. Despite the propensity to adopt an α-helical conformation, synthetic BH3 peptides, like most peptides, lack secondary structure in solution[66]. The transformation of unstructured BH3 peptides into α-helical peptides is the result of induced folding caused by interactions with the large BH3-binding surface of the anti-apoptotic groove. The result is the formation of a stable protein-α-helical peptide complex.

To overcome the lack of structure, peptides can be synthetically modified in order to restore their native α-helicity. This is achieved by covalently linking or "stapling" amino acids that are inserted one or two helical turns apart. While several different chemistries for structuring α-helical peptides have been developed[84], the formation of an all-hydrocarbon staple through olefin metathesis was one of the first and, now, the most commonly employed method. In this approach, non-natural amino acids with olefin-containing side chains are inserted into the BH3 sequence at the (*i*, *i*+4) or (*i*, *i*+7) positions. These two side chains are then covalently linked through ruthenium-catalyzed (Grubbs catalyst) olefin metathesis to yield the hydrocarbon staple. In addition to restoring the α-helical secondary structure, these Stabilized Alpha-Helices of BH3 domain (SAHBs) have the additional benefits of being resistant to protease degradation and displaying improved cell uptake, compared to their non-stapled analogs[173].

With these tool compounds in hand, the ability of BH3 peptides to directly activate BAX was clearly demonstrated. Stapled peptides corresponding to the BID BH3 and BIM BH3 were shown to bind and potently activate BAX, both in a reductionist liposomal system and in cells[174,175]. Despite retaining anti-apoptotic protein binding, SAHBs corresponding to the sensitizer BH3-only BAD failed to directly activate BAX. Together, these experiments clearly supported the ability of BID and BIM to directly activate BAX. Given the additional properties of protease resistance and cell permeability, BID and BIM SAHBs were shown to induce apoptosis of cancer cells *in vivo*,

while sparing normal cells[173,175]. The ability of BID and BIM SAHB to activate apoptosis provided a glimpse into the potential therapeutic success of this “activate the activator” strategy.

In order to design a peptidomimetic BAX activator, the activation site on BAX had to first be determined. While BAX shares significant structural homology with the anti-apoptotic proteins, the NMR solution structure of BAX revealed that the α9 transmembrane helix occupied the canonical groove (**Figure 1.5c, top**)[85]. Therefore, this binding site is not accessible in the inactive state, and unlikely to serve as the initial site of activation. Using the BIM SAHB as a tool, a calculated model structure of the BIM SAHB-BAX complex was solved using PRE-NMR, revealing a novel binding interface[88]. BIM SAHB was found to engage a shallow hydrophobic groove on the opposite face of the protein from the canonical BH3-binding groove (**Figure 1.5c, middle**). BH3-engagement at this trigger site causes a variety of conformational changes in BAX and results in activation of the protein (**Figure 1.4)**[90]. The difference in pocket depth between the trigger and canonical sites helped explain why only pre-folded BH3 peptides are capable of binding to full length BAX. Subsequent studies have shown that SAHBs corresponding to the direct activators BID[89] and PUMA[69] can also engage the trigger site on BAX, as can the BAX BH3 helix itself[90].

The discovery of the trigger site revealed a binding interface that can directly control BAX activation and suggested that a small molecule capable of engaging this site could potentially activate BAX therapeutically. The structure of the BIM SAHB-BAX complex was used to conduct an *in silico* screen for small molecules that could mimic the function of the BIM SAHB and directly trigger BAX activity. The result of this screening effort was the small molecule BAM7, the first selective BAX-activating small molecule[176]. BAM7 was shown to bind the trigger site on BAX (**Figure 1.5c, bottom**), promote BAX oligomerization, and induce BAX-dependent apoptosis in cells. Further pharmacological optimization of the BAM7 scaffold led to the development of BTSA1, which displays improved potency for BAX[177]. BTSA1 was shown to readily activate apoptosis in leukemia cell lines and patient-derived samples. Additionally, this compound showed anti-tumor efficacy in xenograft models, with favorable pharmacokinetic properties and oral

bioavailability. In line with the apoptotic priming hypothesis, this molecule was more potent at killing tumor cells over normal cells and did not induce toxicity in normal tissues *in vivo*.

Other small molecule screening efforts against BAX have yielded Compound 106 and SMBA1, hits from two independent *in silico* screens for compounds that could bind in the canonical pocket of BAX[178,179]. Compound 106 was shown to activate BAX and kill cells in a BAX-dependent manner. This compound, however, is a weak activator (~50 μM IC_{50} in cells) and its binding site on BAX is unknown[178] . Similarly, SMBA1 was shown to bind BAX and kill cells in a BAX-dependent manner[179]. Despite an effort to improve the potency of the molecule, confirmation of the binding site and an on-target killing mechanism remains to be demonstrated[180].

The only example of an *in vitro* screen for BAX-activating compounds uncovered a small molecule that activates BAX through a unique mechanism. OICR776A was identified as an activator of BAX in a liposomal screening system[181]. This compound was shown to bind directly to BAX and kill cells in a BAX-dependent manner. Interestingly, the binding to BAX was dependent on the presence of cysteine 126, a residue that is not located in either of the two characterized activation sites on BAX. This suggests that there may be additional mechanisms that can lead to the activation of BAX independently from the characterized BH3-activating modes. Overall, these studies confirmed that direct, pharmacological manipulation of BAX activation could be a viable strategy for treating cancer, prompting our research into the identification and characterization of novel molecular modulators of pro-apoptotic BAX by direct, fragment based-NMR screening.

REFERENCES

1. Hotchkiss, R.S., Strasser, A., McDunn, J.E. & Swanson, P.E. Cell death. *N Engl J Med* **361**, 1570-83 (2009).

2. Kroemer, G. et al. Classification of cell death: recommendations of the Nomenclature Committee on Cell Death 2009. *Cell Death Differ* **16**, 3-11 (2009).

3. Czabotar, P.E., Lessene, G., Strasser, A. & Adams, J.M. Control of apoptosis by the BCL-2 protein family: implications for physiology and therapy. *Nat Rev Mol Cell Biol* **15**, 49-63 (2014).

4. Danial, N.N. & Korsmeyer, S.J. Cell death: critical control points. *Cell* **116**, 205-19 (2004).

5. Zmasek, C.M. & Godzik, A. Evolution of the animal apoptosis network. *Cold Spring Harb Perspect Biol* **5**, a008649 (2013).

6. Oberst, A., Bender, C. & Green, D.R. Living with death: the evolution of the mitochondrial pathway of apoptosis in animals. *Cell Death Differ* **15**, 1139-46 (2008).

7. Meier, P., Finch, A. & Evan, G. Apoptosis in development. *Nature* **407**, 796-801 (2000).

8. Jacobson, M.D., Weil, M. & Raff, M.C. Programmed cell death in animal development. *Cell* **88**, 347-54 (1997).

9. Fuchs, Y. & Steller, H. Programmed cell death in animal development and disease. *Cell* **147**, 742-58 (2011).

10. Oppenheim, R.W. Cell death during development of the nervous system. *Annu Rev Neurosci* **14**, 453-501 (1991).

11. Conradt, B. Genetic control of programmed cell death during animal development. *Annu Rev Genet* **43**, 493-523 (2009).

12. Yuan, J. & Yankner, B.A. Apoptosis in the nervous system. *Nature* **407**, 802-9 (2000).

13. Ishizuya-Oka, A., Hasebe, T. & Shi, Y.B. Apoptosis in amphibian organs during metamorphosis. *Apoptosis* **15**, 350-64 (2010).

14. Raj, D., Brash, D.E. & Grossman, D. Keratinocyte apoptosis in epidermal development and disease. *J Invest Dermatol* **126**, 243-57 (2006).

15. Watson, A.J. & Pritchard, D.M. Lessons from genetically engineered animal models. VII. Apoptosis in intestinal epithelium: lessons from transgenic and knockout mice. *Am J Physiol Gastrointest Liver Physiol* **278**, G1-5 (2000).

16. Jones, B.A. & Gores, G.J. Physiology and pathophysiology of apoptosis in epithelial cells of the liver, pancreas, and intestine. *Am J Physiol* **273**, G1174-88 (1997).

17. Lee, J., Richburg, J.H., Younkin, S.C. & Boekelheide, K. The Fas system is a key regulator of germ cell apoptosis in the testis. *Endocrinology* **138**, 2081-8 (1997).

18. Levy, R. & Seifer-Aknin, I. [Apoptosis during spermatogenesis and in ejaculated spermatozoa: importance for fertilization]. *Ann Biol Clin (Paris)* **59**, 531-45 (2001).

19. Lund, L.R. et al. Two distinct phases of apoptosis in mammary gland involution: proteinase-independent and -dependent pathways. *Development* **122**, 181-93 (1996).

20. Humphreys, R.C. et al. Apoptosis in the terminal endbud of the murine mammary gland: a mechanism of ductal morphogenesis. *Development* **122**, 4013-22 (1996).

21. Opferman, J.T. & Korsmeyer, S.J. Apoptosis in the development and maintenance of the immune system. *Nat Immunol* **4**, 410-5 (2003).

22. Rathmell, J.C. & Thompson, C.B. Pathways of apoptosis in lymphocyte development, homeostasis, and disease. *Cell* **109 Suppl**, S97-107 (2002).

23. Lamkanfi, M. & Dixit, V.M. Manipulation of host cell death pathways during microbial infections. *Cell Host Microbe* **8**, 44-54 (2010).

24. Lockshin, R.A. & Zakeri, Z. Programmed cell death and apoptosis: origins of the theory. *Nat Rev Mol Cell Biol* **2**, 545-50 (2001).

25. Clarke, P.G. & Clarke, S. Nineteenth century research on naturally occurring cell death and related phenomena. *Anat Embryol (Berl)* **193**, 81-99 (1996).

26. Paweletz, N. Walther Flemming: pioneer of mitosis research. *Nat Rev Mol Cell Biol* **2**, 72-5 (2001).

27. Glucksmann, A. Cell deaths in normal vertebrate ontogeny. *Biol Rev Camb Philos Soc* **26**, 59-86 (1951).

28. Kerr, J.F., Wyllie, A.H. & Currie, A.R. Apoptosis: a basic biological phenomenon with wide-ranging implications in tissue kinetics. *Br J Cancer* **26**, 239-57 (1972).

29. Kerr, J.F. Shrinkage necrosis: a distinct mode of cellular death. *J Pathol* **105**, 13-20 (1971).

30. Sulston, J.E. & Horvitz, H.R. Post-embryonic cell lineages of the nematode, Caenorhabditis elegans. *Dev Biol* **56**, 110-56 (1977).

31. Sulston, J.E., Schierenberg, E., White, J.G. & Thomson, J.N. The embryonic cell lineage of the nematode Caenorhabditis elegans. *Dev Biol* **100**, 64-119 (1983).

32. Ellis, H.M. & Horvitz, H.R. Genetic control of programmed cell death in the nematode C. elegans. *Cell* **44**, 817-29 (1986).

33. Hengartner, M.O., Ellis, R.E. & Horvitz, H.R. Caenorhabditis elegans gene ced-9 protects cells from programmed cell death. *Nature* **356**, 494-9 (1992).

34. Conradt, B. & Horvitz, H.R. The C. elegans protein EGL-1 is required for programmed cell death and interacts with the Bcl-2-like protein CED-9. *Cell* **93**, 519-29 (1998).

35. Taylor, R.C., Cullen, S.P. & Martin, S.J. Apoptosis: controlled demolition at the cellular level. *Nat Rev Mol Cell Biol* **9**, 231-41 (2008).

36. Tait, S.W. & Green, D.R. Mitochondria and cell death: outer membrane permeabilization and beyond. *Nat Rev Mol Cell Biol* **11**, 621-32 (2010).

37. Liu, X., Kim, C.N., Yang, J., Jemmerson, R. & Wang, X. Induction of apoptotic program in cell-free extracts: requirement for dATP and cytochrome c. *Cell* **86**, 147-57 (1996).

38. Yang, J. et al. Prevention of apoptosis by Bcl-2: release of cytochrome c from mitochondria blocked. *Science* **275**, 1129-32 (1997).

39. Du, C., Fang, M., Li, Y., Li, L. & Wang, X. Smac, a mitochondrial protein that promotes cytochrome c-dependent caspase activation by eliminating IAP inhibition. *Cell* **102**, 33-42 (2000).

40. Verhagen, A.M. et al. Identification of DIABLO, a mammalian protein that promotes apoptosis by binding to and antagonizing IAP proteins. *Cell* **102**, 43-53 (2000).

41. Kluck, R.M., Bossy-Wetzel, E., Green, D.R. & Newmeyer, D.D. The release of cytochrome c from mitochondria: a primary site for Bcl-2 regulation of apoptosis. *Science* **275**, 1132-6 (1997).

42. Li, P. et al. Cytochrome c and dATP-dependent formation of Apaf-1/caspase-9 complex initiates an apoptotic protease cascade. *Cell* **91**, 479-89 (1997).

43. Kaufmann, T., Strasser, A. & Jost, P.J. Fas death receptor signalling: roles of Bid and XIAP. *Cell Death Differ* **19**, 42-50 (2012).

44. Li, H., Zhu, H., Xu, C.J. & Yuan, J. Cleavage of BID by caspase 8 mediates the mitochondrial damage in the Fas pathway of apoptosis. *Cell* **94**, 491-501 (1998).

45. Luo, X., Budihardjo, I., Zou, H., Slaughter, C. & Wang, X. Bid, a Bcl2 interacting protein, mediates cytochrome c release from mitochondria in response to activation of cell surface death receptors. *Cell* **94**, 481-90 (1998).

46. Bakhshi, A. et al. Cloning the chromosomal breakpoint of t(14;18) human lymphomas: clustering around JH on chromosome 14 and near a transcriptional unit on 18. *Cell* **41**, 899-906 (1985).

47. Cleary, M.L. & Sklar, J. Nucleotide sequence of a t(14;18) chromosomal breakpoint in follicular lymphoma and demonstration of a breakpoint-cluster region near a transcriptionally active locus on chromosome 18. *Proc Natl Acad Sci U S A* **82**, 7439-43 (1985).

48. Tsujimoto, Y., Cossman, J., Jaffe, E. & Croce, C.M. Involvement of the bcl-2 gene in human follicular lymphoma. *Science* **228**, 1440-3 (1985).

49. Graninger, W.B., Seto, M., Boutain, B., Goldman, P. & Korsmeyer, S.J. Expression of Bcl-2 and Bcl-2-Ig fusion transcripts in normal and neoplastic cells. *J Clin Invest* **80**, 1512-5 (1987).

50. Seto, M. et al. Alternative promoters and exons, somatic mutation and deregulation of the Bcl-2-Ig fusion gene in lymphoma. *EMBO J* **7**, 123-31 (1988).

51. Vaux, D.L., Cory, S. & Adams, J.M. Bcl-2 gene promotes haemopoietic cell survival and cooperates with c-myc to immortalize pre-B cells. *Nature* **335**, 440-2 (1988).

52. McDonnell, T.J. et al. bcl-2-immunoglobulin transgenic mice demonstrate extended B cell survival and follicular lymphoproliferation. *Cell* **57**, 79-88 (1989).

53. Nakayama, K. et al. Targeted disruption of Bcl-2 alpha beta in mice: occurrence of gray hair, polycystic kidney disease, and lymphocytopenia. *Proc Natl Acad Sci U S A* **91**, 3700-4 (1994).

54. Veis, D.J., Sorenson, C.M., Shutter, J.R. & Korsmeyer, S.J. Bcl-2-deficient mice demonstrate fulminant lymphoid apoptosis, polycystic kidneys, and hypopigmented hair. *Cell* **75**, 229-40 (1993).

55. Hengartner, M.O. & Horvitz, H.R. C. elegans cell survival gene ced-9 encodes a functional homolog of the mammalian proto-oncogene bcl-2. *Cell* **76**, 665-76 (1994).

56. Vaux, D.L., Weissman, I.L. & Kim, S.K. Prevention of programmed cell death in Caenorhabditis elegans by human bcl-2. *Science* **258**, 1955-7 (1992).

57. Chipuk, J.E., Moldoveanu, T., Llambi, F., Parsons, M.J. & Green, D.R. The BCL-2 family reunion. *Mol Cell* **37**, 299-310 (2010).

58. Llambi, F. et al. BOK Is a Non-canonical BCL-2 Family Effector of Apoptosis Regulated by ER-Associated Degradation. *Cell* **165**, 421-33 (2016).

59. Chittenden, T. et al. Induction of apoptosis by the Bcl-2 homologue Bak. *Nature* **374**, 733-6 (1995).

60. Oltvai, Z.N., Milliman, C.L. & Korsmeyer, S.J. Bcl-2 heterodimerizes in vivo with a conserved homolog, Bax, that accelerates programmed cell death. *Cell* **74**, 609-19 (1993).

61. Knudson, C.M., Tung, K.S., Tourtellotte, W.G., Brown, G.A. & Korsmeyer, S.J. Bax-deficient mice with lymphoid hyperplasia and male germ cell death. *Science* **270**, 96-9 (1995).

62. Lindsten, T. et al. The combined functions of proapoptotic Bcl-2 family members bak and bax are essential for normal development of multiple tissues. *Mol Cell* **6**, 1389-99 (2000).

63. Youle, R.J. & Strasser, A. The BCL-2 protein family: opposing activities that mediate cell death. *Nat Rev Mol Cell Biol* **9**, 47-59 (2008).

64. Kim, H. et al. Hierarchical regulation of mitochondrion-dependent apoptosis by BCL-2 subfamilies. *Nat Cell Biol* **8**, 1348-58 (2006).

65. Llambi, F. et al. A unified model of mammalian BCL-2 protein family interactions at the mitochondria. *Mol Cell* **44**, 517-31 (2011).

66. Letai, A. et al. Distinct BH3 domains either sensitize or activate mitochondrial apoptosis, serving as prototype cancer therapeutics. *Cancer Cell* **2**, 183-92 (2002).

67. Merino, D. et al. The role of BH3-only protein Bim extends beyond inhibiting Bcl-2-like prosurvival proteins. *J Cell Biol* **186**, 355-62 (2009).

68. Dai, H., Pang, Y.P., Ramirez-Alvarado, M. & Kaufmann, S.H. Evaluation of the BH3-only protein Puma as a direct Bak activator. *J Biol Chem* **289**, 89-99 (2014).

69. Edwards, A.L. et al. Multimodal interaction with BCL-2 family proteins underlies the proapoptotic activity of PUMA BH3. *Chem Biol* **20**, 888-902 (2013).

70. Chen, H.C. et al. An interconnected hierarchical model of cell death regulation by the BCL-2 family. *Nat Cell Biol* **17**, 1270-81 (2015).

71. Shibue, T. et al. Integral role of Noxa in p53-mediated apoptotic response. *Genes Dev* **17**, 2233-8 (2003).

72. Jeffers, J.R. et al. Puma is an essential mediator of p53-dependent and -independent apoptotic pathways. *Cancer Cell* **4**, 321-8 (2003).

73. Villunger, A. et al. p53- and drug-induced apoptotic responses mediated by BH3-only proteins puma and noxa. *Science* **302**, 1036-8 (2003).

74. Zhang, X., Tang, N., Hadden, T.J. & Rishi, A.K. Akt, FoxO and regulation of apoptosis. *Biochim Biophys Acta* **1813**, 1978-86 (2011).

75. Puthalakath, H. et al. ER stress triggers apoptosis by activating BH3-only protein Bim. *Cell* **129**, 1337-49 (2007).

76. Barry, M. et al. Granzyme B short-circuits the need for caspase 8 activity during granule-mediated cytotoxic T-lymphocyte killing by directly cleaving Bid. *Mol Cell Biol* **20**, 3781-94 (2000).

77. Downward, J. How BAD phosphorylation is good for survival. *Nat Cell Biol* **1**, E33-5 (1999).

78. Muchmore, S.W. et al. X-ray and NMR structure of human Bcl-xL, an inhibitor of programmed cell death. *Nature* **381**, 335-41 (1996).

79. Chou, J.J., Li, H., Salvesen, G.S., Yuan, J. & Wagner, G. Solution structure of BID, an intracellular amplifier of apoptotic signaling. *Cell* **96**, 615-24 (1999).

80. Hinds, M.G. et al. Bim, Bad and Bmf: intrinsically unstructured BH3-only proteins that undergo a localized conformational change upon binding to prosurvival Bcl-2 targets. *Cell Death Differ* **14**, 128-36 (2007).

81. Aouacheria, A., Brunet, F. & Gouy, M. Phylogenomics of life-or-death switches in multicellular animals: Bcl-2, BH3-Only, and BNip families of apoptotic regulators. *Mol Biol Evol* **22**, 2395-416 (2005).

82. Brouwer, J.M. et al. Bak core and latch domains separate during activation, and freed core domains form symmetric homodimers. *Mol Cell* **55**, 938-46 (2014).

83. Moldoveanu, T. et al. BID-induced structural changes in BAK promote apoptosis. *Nat Struct Mol Biol* **20**, 589-97 (2013).

84. Walensky, L.D. BCL-2 in the crosshairs: tipping the balance of life and death. *Cell Death Differ* **13**, 1339-50 (2006).

85. Suzuki, M., Youle, R.J. & Tjandra, N. Structure of Bax: coregulation of dimer formation and intracellular localization. *Cell* **103**, 645-54 (2000).

86. Nechushtan, A., Smith, C.L., Hsu, Y.T. & Youle, R.J. Conformation of the Bax C-terminus regulates subcellular location and cell death. *EMBO J* **18**, 2330-41 (1999).

87. Wolter, K.G. et al. Movement of Bax from the cytosol to mitochondria during apoptosis. *J Cell Biol* **139**, 1281-92 (1997).

88. Gavathiotis, E. et al. BAX activation is initiated at a novel interaction site. *Nature* **455**, 1076-81 (2008).

89. Leshchiner, E.S., Braun, C.R., Bird, G.H. & Walensky, L.D. Direct activation of full-length proapoptotic BAK. *Proc Natl Acad Sci U S A* **110**, E986-95 (2013).

90. Gavathiotis, E., Reyna, D.E., Davis, M.L., Bird, G.H. & Walensky, L.D. BH3-triggered structural reorganization drives the activation of proapoptotic BAX. *Mol Cell* **40**, 481-92 (2010).

91. Czabotar, P.E. et al. Bax crystal structures reveal how BH3 domains activate Bax and nucleate its oligomerization to induce apoptosis. *Cell* **152**, 519-31 (2013).

92. Edlich, F. et al. Bcl-x(L) retrotranslocates Bax from the mitochondria into the cytosol. *Cell* **145**, 104-16 (2011).

93. Schellenberg, B. et al. Bax exists in a dynamic equilibrium between the cytosol and mitochondria to control apoptotic priming. *Mol Cell* **49**, 959-71 (2013).

94. Barclay, L.A. et al. Inhibition of Pro-apoptotic BAX by a noncanonical interaction mechanism. *Mol Cell* **57**, 873-86 (2015).

95. Ma, J. et al. Structural mechanism of Bax inhibition by cytomegalovirus protein vMIA. *Proc Natl Acad Sci U S A* **109**, 20901-6 (2012).

96. Petros, A.M. et al. Solution structure of the antiapoptotic protein bcl-2. *Proc Natl Acad Sci U S A* **98**, 3012-7 (2001).

97. Arnoult, D. et al. Cytomegalovirus cell death suppressor vMIA blocks Bax- but not Bak-mediated apoptosis by binding and sequestering Bax at mitochondria. *Proc Natl Acad Sci U S A* **101**, 7988-93 (2004).

98. Poncet, D. et al. An anti-apoptotic viral protein that recruits Bax to mitochondria. *J Biol Chem* **279**, 22605-14 (2004).

99. Kuwana, T. et al. Bid, Bax, and lipids cooperate to form supramolecular openings in the outer mitochondrial membrane. *Cell* **111**, 331-42 (2002).

100. Kuwana, T., Olson, N.H., Kiosses, W.B., Peters, B. & Newmeyer, D.D. Pro-apoptotic Bax molecules densely populate the edges of membrane pores. *Sci Rep* **6**, 27299 (2016).

101. Basanez, G. et al. Bax, but not Bcl-xL, decreases the lifetime of planar phospholipid bilayer membranes at subnanomolar concentrations. *Proc Natl Acad Sci U S A* **96**, 5492-7 (1999).

102. Basanez, G. et al. Bax-type apoptotic proteins porate pure lipid bilayers through a mechanism sensitive to intrinsic monolayer curvature. *J Biol Chem* **277**, 49360-5 (2002).

103. Terrones, O. et al. Lipidic pore formation by the concerted action of proapoptotic BAX and tBID. *J Biol Chem* **279**, 30081-91 (2004).

104. Hardwick, J.M. & Polster, B.M. Bax, along with lipid conspirators, allows cytochrome c to escape mitochondria. *Mol Cell* **10**, 963-5 (2002).

105. Schendel, S.L., Montal, M. & Reed, J.C. Bcl-2 family proteins as ion-channels. *Cell Death Differ* **5**, 372-80 (1998).

106. Grosse, L. et al. Bax assembles into large ring-like structures remodeling the mitochondrial outer membrane in apoptosis. *EMBO J* **35**, 402-13 (2016).

107. Salvador-Gallego, R. et al. Bax assembly into rings and arcs in apoptotic mitochondria is linked to membrane pores. *EMBO J* **35**, 389-401 (2016).

108. Wang, K., Gross, A., Waksman, G. & Korsmeyer, S.J. Mutagenesis of the BH3 domain of BAX identifies residues critical for dimerization and killing. *Mol Cell Biol* **18**, 6083-9 (1998).

109. Dewson, G. et al. To trigger apoptosis, Bak exposes its BH3 domain and homodimerizes via BH3:groove interactions. *Mol Cell* **30**, 369-80 (2008).

110. Zha, H., Aime-Sempe, C., Sato, T. & Reed, J.C. Proapoptotic protein Bax heterodimerizes with Bcl-2 and homodimerizes with Bax via a novel domain (BH3) distinct from BH1 and BH2. *J Biol Chem* **271**, 7440-4 (1996).

111. Bogner, C., Leber, B. & Andrews, D.W. Apoptosis: embedded in membranes. *Curr Opin Cell Biol* **22**, 845-51 (2010).

112. Pang, Y.P. et al. Bak Conformational Changes Induced by Ligand Binding: Insight into BH3 Domain Binding and Bak Homo-Oligomerization. *Sci Rep* **2**, 257 (2012).

113. Subburaj, Y. et al. Bax monomers form dimer units in the membrane that further self-assemble into multiple oligomeric species. *Nat Commun* **6**, 8042 (2015).

114. Westphal, D., Dewson, G., Czabotar, P.E. & Kluck, R.M. Molecular biology of Bax and Bak activation and action. *Biochim Biophys Acta* **1813**, 521-31 (2011).

115. Dewson, G. et al. Bax dimerizes via a symmetric BH3:groove interface during apoptosis. *Cell Death Differ* **19**, 661-70 (2012).

116. Garner, T.P. et al. An Autoinhibited Dimeric Form of BAX Regulates the BAX Activation Pathway. *Mol Cell* **63**, 485-97 (2016).

117. Friedlander, R.M. Apoptosis and caspases in neurodegenerative diseases. *N Engl J Med* **348**, 1365-75 (2003).

118. Shacka, J.J. & Roth, K.A. Regulation of neuronal cell death and neurodegeneration by members of the Bcl-2 family: therapeutic implications. *Curr Drug Targets CNS Neurol Disord* **4**, 25-39 (2005).

119. Opferman, J.T. Apoptosis in the development of the immune system. *Cell Death Differ* **15**, 234-42 (2008).

120. Zhang, N., Hartig, H., Dzhagalov, I., Draper, D. & He, Y.W. The role of apoptosis in the development and function of T lymphocytes. *Cell Res* **15**, 749-69 (2005).

121. Aitken, R.J., Findlay, J.K., Hutt, K.J. & Kerr, J.B. Apoptosis in the germ line. *Reproduction* **141**, 139-50 (2011).

122. Hikim, A.P. et al. Spontaneous germ cell apoptosis in humans: evidence for ethnic differences in the susceptibility of germ cells to programmed cell death. *J Clin Endocrinol Metab* **83**, 152-6 (1998).

123. Hanahan, D. & Weinberg, R.A. The hallmarks of cancer. *Cell* **100**, 57-70 (2000).

124. Hanahan, D. & Weinberg, R.A. Hallmarks of cancer: the next generation. *Cell* **144**, 646-74 (2011).

125. Delbridge, A.R., Grabow, S., Strasser, A. & Vaux, D.L. Thirty years of BCL-2: translating cell death discoveries into novel cancer therapies. *Nat Rev Cancer* **16**, 99-109 (2016).

126. Croce, C.M. & Reed, J.C. Finally, An Apoptosis-Targeting Therapeutic for Cancer. *Cancer Res* **76**, 5914-5920 (2016).

127. Beroukhim, R. et al. The landscape of somatic copy-number alteration across human cancers. *Nature* **463**, 899-905 (2010).

128. Cimmino, A. et al. miR-15 and miR-16 induce apoptosis by targeting BCL2. *Proc Natl Acad Sci U S A* **102**, 13944-9 (2005).

129. Chen, J. et al. miR-193b Regulates Mcl-1 in Melanoma. *Am J Pathol* **179**, 2162-8 (2011).

130. Gong, J. et al. MicroRNA-125b promotes apoptosis by regulating the expression of Mcl-1, Bcl-w and IL-6R. *Oncogene* **32**, 3071-9 (2013).

131. Shimizu, S. et al. The let-7 family of microRNAs inhibits Bcl-xL expression and potentiates sorafenib-induced apoptosis in human hepatocellular carcinoma. *J Hepatol* **52**, 698-704 (2010).

132. Tagawa, H. et al. Genome-wide array-based CGH for mantle cell lymphoma: identification of homozygous deletions of the proapoptotic gene BIM. *Oncogene* **24**, 1348-58 (2005).

133. Garrison, S.P. et al. Selection against PUMA gene expression in Myc-driven B-cell lymphomagenesis. *Mol Cell Biol* **28**, 5391-402 (2008).

134. Richter-Larrea, J.A. et al. Reversion of epigenetically mediated BIM silencing overcomes chemoresistance in Burkitt lymphoma. *Blood* **116**, 2531-42 (2010).

135. Rampino, N. et al. Somatic frameshift mutations in the BAX gene in colon cancers of the microsatellite mutator phenotype. *Science* **275**, 967-9 (1997).

136. Meijerink, J.P. et al. Hematopoietic malignancies demonstrate loss-of-function mutations of BAX. *Blood* **91**, 2991-7 (1998).

137. Strasser, A., Harris, A.W. & Cory, S. bcl-2 transgene inhibits T cell death and perturbs thymic self-censorship. *Cell* **67**, 889-99 (1991).

138. Sentman, C.L., Shutter, J.R., Hockenbery, D., Kanagawa, O. & Korsmeyer, S.J. bcl-2 inhibits multiple forms of apoptosis but not negative selection in thymocytes. *Cell* **67**, 879-88 (1991).

139. Bouillet, P. et al. Proapoptotic Bcl-2 relative Bim required for certain apoptotic responses, leukocyte homeostasis, and to preclude autoimmunity. *Science* **286**, 1735-8 (1999).

140. Zhao, Y. et al. Inhibitors of histone deacetylases target the Rb-E2F1 pathway for apoptosis induction through activation of proapoptotic protein Bim. *Proc Natl Acad Sci U S A* **102**, 16090-5 (2005).

141. Kuribara, R. et al. Roles of Bim in apoptosis of normal and Bcr-Abl-expressing hematopoietic progenitors. *Mol Cell Biol* **24**, 6172-83 (2004).

142. Costa, D.B. et al. BIM mediates EGFR tyrosine kinase inhibitor-induced apoptosis in lung cancers with oncogenic EGFR mutations. *PLoS Med* **4**, 1669-79; discussion 1680 (2007).

143. Gong, Y. et al. Induction of BIM is essential for apoptosis triggered by EGFR kinase inhibitors in mutant EGFR-dependent lung adenocarcinomas. *PLoS Med* **4**, e294 (2007).

144. Certo, M. et al. Mitochondria primed by death signals determine cellular addiction to antiapoptotic BCL-2 family members. *Cancer Cell* **9**, 351-65 (2006).

145. Frantz, S. Lessons learnt from Genasense's failure. *Nat Rev Drug Discov* **3**, 542-3 (2004).

146. Holinger, E.P., Chittenden, T. & Lutz, R.J. Bak BH3 peptides antagonize Bcl-xL function and induce apoptosis through cytochrome c-independent activation of caspases. *J Biol Chem* **274**, 13298-304 (1999).

147. Cosulich, S.C., Worrall, V., Hedge, P.J., Green, S. & Clarke, P.R. Regulation of apoptosis by BH3 domains in a cell-free system. *Curr Biol* **7**, 913-20 (1997).

148. Sattler, M. et al. Structure of Bcl-xL-Bak peptide complex: recognition between regulators of apoptosis. *Science* **275**, 983-6 (1997).

149. Petros, A.M. et al. Rationale for Bcl-xL/Bad peptide complex formation from structure, mutagenesis, and biophysical studies. *Protein Sci* **9**, 2528-34 (2000).

150. Wang, J.L. et al. Structure-based discovery of an organic compound that binds Bcl-2 protein and induces apoptosis of tumor cells. *Proc Natl Acad Sci U S A* **97**, 7124-9 (2000).

151. Degterev, A. et al. Identification of small-molecule inhibitors of interaction between the BH3 domain and Bcl-xL. *Nat Cell Biol* **3**, 173-82 (2001).

152. Shuker, S.B., Hajduk, P.J., Meadows, R.P. & Fesik, S.W. Discovering high-affinity ligands for proteins: SAR by NMR. *Science* **274**, 1531-4 (1996).

153. Petros, A.M. et al. Discovery of a potent inhibitor of the antiapoptotic protein Bcl-xL from NMR and parallel synthesis. *J Med Chem* **49**, 656-63 (2006).

154. Oltersdorf, T. et al. An inhibitor of Bcl-2 family proteins induces regression of solid tumours. *Nature* **435**, 677-81 (2005).

155. Tse, C. et al. ABT-263: a potent and orally bioavailable Bcl-2 family inhibitor. *Cancer Res* **68**, 3421-8 (2008).

156. Roberts, A.W. et al. Substantial susceptibility of chronic lymphocytic leukemia to BCL2 inhibition: results of a phase I study of navitoclax in patients with relapsed or refractory disease. *J Clin Oncol* **30**, 488-96 (2012).

157. Mason, K.D. et al. Programmed anuclear cell death delimits platelet life span. *Cell* **128**, 1173-86 (2007).

158. Zhang, H. et al. Bcl-2 family proteins are essential for platelet survival. *Cell Death Differ* **14**, 943-51 (2007).

159. Souers, A.J. et al. ABT-199, a potent and selective BCL-2 inhibitor, achieves antitumor activity while sparing platelets. *Nat Med* **19**, 202-8 (2013).

160. Roberts, A.W. et al. Targeting BCL2 with Venetoclax in Relapsed Chronic Lymphocytic Leukemia. *N Engl J Med* **374**, 311-22 (2016).

161. Tao, Z.F. et al. Discovery of a Potent and Selective BCL-XL Inhibitor with in Vivo Activity. *ACS Med Chem Lett* **5**, 1088-93 (2014).

162. Lessene, G. et al. Structure-guided design of a selective BCL-X(L) inhibitor. *Nat Chem Biol* **9**, 390-7 (2013).

163. Cohen, N.A. et al. A competitive stapled peptide screen identifies a selective small molecule that overcomes MCL-1-dependent leukemia cell survival. *Chem Biol* **19**, 1175-86 (2012).

164. Kotschy, A. et al. The MCL1 inhibitor S63845 is tolerable and effective in diverse cancer models. *Nature* **538**, 477-482 (2016).

165. Bruncko, M. et al. Structure-guided design of a series of MCL-1 inhibitors with high affinity and selectivity. *J Med Chem* **58**, 2180-94 (2015).

166. Pelz, N.F. et al. Discovery of 2-Indole-acylsulfonamide Myeloid Cell Leukemia 1 (Mcl-1) Inhibitors Using Fragment-Based Methods. *J Med Chem* **59**, 2054-66 (2016).

167. Stewart, M.L., Fire, E., Keating, A.E. & Walensky, L.D. The MCL-1 BH3 helix is an exclusive MCL-1 inhibitor and apoptosis sensitizer. *Nat Chem Biol* **6**, 595-601 (2010).

168. Huhn, A.J., Guerra, R.M., Harvey, E.P., Bird, G.H. & Walensky, L.D. Selective Covalent Targeting of Anti-Apoptotic BFL-1 by Cysteine-Reactive Stapled Peptide Inhibitors. *Cell Chem Biol* **23**, 1123-34 (2016).

169. Ashkenazi, A., Fairbrother, W.J., Leverson, J.D. & Souers, A.J. From basic apoptosis discoveries to advanced selective BCL-2 family inhibitors. *Nat Rev Drug Discov* **16**, 273-284 (2017).

170. Wang, K., Yin, X.M., Chao, D.T., Milliman, C.L. & Korsmeyer, S.J. BID: a novel BH3 domain-only death agonist. *Genes Dev* **10**, 2859-69 (1996).

171. Kuwana, T. et al. BH3 domains of BH3-only proteins differentially regulate Bax-mediated mitochondrial membrane permeabilization both directly and indirectly. *Mol Cell* **17**, 525-35 (2005).

172. Chen, L. et al. Differential targeting of prosurvival Bcl-2 proteins by their BH3-only ligands allows complementary apoptotic function. *Mol Cell* **17**, 393-403 (2005).

173. Walensky, L.D. et al. Activation of apoptosis in vivo by a hydrocarbon-stapled BH3 helix. *Science* **305**, 1466-70 (2004).

174. Walensky, L.D. et al. A stapled BID BH3 helix directly binds and activates BAX. *Mol Cell* **24**, 199-210 (2006).

175. LaBelle, J.L. et al. A stapled BIM peptide overcomes apoptotic resistance in hematologic cancers. *J Clin Invest* **122**, 2018-31 (2012).

176. Gavathiotis, E., Reyna, D.E., Bellairs, J.A., Leshchiner, E.S. & Walensky, L.D. Direct and selective small-molecule activation of proapoptotic BAX. *Nat Chem Biol* **8**, 639-45 (2012).

177. Reyna, D.E. et al. Direct Activation of BAX by BTSA1 Overcomes Apoptosis Resistance in Acute Myeloid Leukemia. *Cancer Cell* **32**, 490-505 e10 (2017).

178. Zhao, G. et al. Activation of the proapoptotic Bcl-2 protein Bax by a small molecule induces tumor cell apoptosis. *Mol Cell Biol* **34**, 1198-207 (2014).

179. Xin, M. et al. Small-molecule Bax agonists for cancer therapy. *Nat Commun* **5**, 4935 (2014).

180. Li, R. et al. Modulation of Bax and mTOR for Cancer Therapeutics. *Cancer Res* **77**, 3001-3012 (2017).

181. Brahmbhatt, H., Uehling, D., Al-Awar, R., Leber, B. & Andrews, D. Small molecules reveal an alternative mechanism of Bax activation. *Biochem J* **473**, 1073-83 (2016).

Chapter 2

NMR-based Fragment Screening Identifies BIF-44 as a Sensitizer of BAX Activation

This is, for the future, the most interesting and challenging task:
to further explore, in order to reach a more refined manner
to induce cell death in cancer cells.

—Jan-Åke Gustafsson

Introduction to the Nobel Lectures in Medicine, 2002

ABSTRACT

BCL-2-associated X protein (BAX) is a critical apoptotic regulator that can be transformed from a cytosolic monomer into a lethal mitochondrial oligomer. Drug strategies to modulate BAX are relatively underdeveloped due to longstanding difficulties in conducting screens on this aggregation-prone protein. Here, we overcame prior challenges and, to our knowledge, performed the first NMR-based fragment screen of full-length human BAX. We identified 53 BAX-interacting fragments (BIFs) that were subsequently counterscreened for BAX-modulating activity. Intriguingly, one compound, BIF-44, demonstrated a robust BAX sensitization profile in the presence of the activator BIM $SAHB_{A2}$. Validation of small molecule binding by CPMG NMR and ITC confirmed that BIF-44 directly engages BAX. Select structural changes to the BIF-44 core abrogated its functional effect, suggesting a compound-specific effect. Furthermore, BIF-44 displayed no signs of aggregation in solution as verified by a series of orthogonal analyses. Thus, BIF-44 represents a novel approach sensitizing BAX to BH3-mediated activation and warranted further exploration as a pharmacologic mechanism to induce the apoptosis of cancer cells.

ATTRIBUTIONS

Portions of this chapter were published in the following manuscript: Pritz, J.R. et al. Allosteric sensitization of proapoptotic BAX. *Nat Chem Biol* **13**, 961-967 (2017).

Contributions to the work described in this chapter were made by Jonathan R. Pritz, Franziska Wachter, James Luccarelli, Daniel T. Cohen, Paul W. Coote, Gregory J. Heffron, Walter Massefski, and Loren D. Walensky

J.R.P., F.W., J.L., G.J.H., W.M., and L.D.W. designed the study. J.R.P., F.W., and D.T.C. generated BAX protein; J.R.P. conducted NMR experiments under the guidance of G.J.H., W.M., J.L., and L.D.W.; G.J.H, P.W.C., and W.M. analyzed screening results utilizing software developed by P.W.C.; J.R.P. and F.W. performed biochemical assays.

Additionally, we thank C. Sheahan for operational assistance with the NMR screen, G. Bird and T. Oo for peptide production, M. Ericsson and Z. Hauseman for technical assistance with electron microscopy, H.-S. Seo and S. Dhe-Paganon for ITC experiments.

INTRODUCTION

The BCL-2 family plays a central role in the regulation of apoptosis during health and disease. Inhibition of apoptosis is one of key hallmarks of cancer, where sequestration and inactivation of pro-apoptotic members drives cellular immortality[1,2]. Therefore, a major pharmaceutical effort has been underway to disarm anti-apoptotic proteins in cancer. The primary goal has been to block the mechanism by which anti-apoptotic proteins such as BCL-2 deploy a surface groove to trap the apoptosis-triggering BCL-2 homology 3 (BH3) helices of pro-apoptotic proteins. This 20-year effort has culminated in the FDA-approval of a selective BCL-2 pocket inhibitor, venetoclax[3,4]. This "inhibit the inhibitor" therapeutic strategy is now being applied to develop drugs against the broad spectrum of anti-apoptotic targets implicated in cancer, including BCL-X_L[5-7], MCL-1[8-13], and BFL-1/A1[14].

The discovery of an α1/α6 trigger site for direct BAX activation by pro-apoptotic BH3 domains has motivated the exploration of an "activate the activators" strategy to drive cancer cell death[15,16]. This effort was initiated with an *in silico* screening approach because, in contrast to the highly stable anti-apoptotic targets, the production of BAX for direct, experimental screening was hampered by the challenge of expressing sufficient quantities of recombinant BAX and the general instability of BAX in solution, especially when exposed to potential activators. Biochemical and cellular validation efforts yielded the first class of direct and selective BAX activator molecules (BAMs)[17]. Other groups have also applied *in silico* screening to identify putative canonical site BAX activators[18-20]. However, given the difficulties associated with recombinant BAX outlined above, an unbiased screening approach has not been attempted.

The purpose of any small molecule screen is to identify chemical matter that can interact with the protein of interest and elicit a biological response[21]. Traditional high-throughput screening (HTS) methods seek to identify molecules that bind to or alter the function of the protein of interest by sifting through a large library of diverse, "drug-like" compounds[22,23]. The compounds in these HTS libraries typically obey the "Lipinski's rule of five", a guideline for the properties of orally

bioavailable compounds, including molecular weight less than 500 Da, no more than five hydrogen bond donors, no more than 10 hydrogen bond acceptors, and a calculated octanol-water partition coefficient (clogP; measure of hydrophilicity) not greater than five[24]. While the HTS technique has succeeded in identifying lead compounds for many protein targets, the overall screening process is inherently inefficient. The larger the small molecule, the more possible interactions (both favorable and unfavorable) that molecule can have with the protein. As near perfect complementarity is needed to engage the protein of interest, an increasingly large library (10^5-10^7 compounds) must be screened to find the relatively few compounds that exhibit a high degree of binding[21,25]. Furthermore, HTS can fail to generate hits against more complex "undruggable" targets[26] and is plagued by a high rate of false positives[25], especially from pan-assay interference compounds (PAINS)[27] and non-specifically aggregating compounds[28,29].

In contrast, fragment-based screening utilizes the power of small, low complexity compounds (<300 Da) to efficiently sample the chemical interaction space using a much smaller (10^3-10^4) library of molecules[21,23]. Fragment-based screening approaches have successfully produced leads for pharmacological targeting of a number of challenging targets, including the BRAF inhibitor vemurafenib[30] and the BCL-2/BCL-X_L inhibitor ABT-737[31,32]. Since fragments have simpler chemical structures, they engage a greater number of binding sites and thus yield higher hit rates[25]. Despite these advantages, fragments usually have weak affinity for their target and sensitive biophysical methods such a nuclear magnetic resonance (NMR) must be used to detect target engagement. Beyond drug discovery, fragment screening can identify new ways to alter protein behavior and provide a platform to explore the biology of the protein target[25].

The use of fragment-based screening was popularized by Steve Fesik and colleagues, who developed an approach to enhance screening efforts called structure activity relationship (SAR) by NMR[33]. This technique uses two dimensional-NMR to screen for fragments that shift the protein amide crosspeaks. In this manner, information on both target engagement and location of the putative binding site for each ligand in the library can be collected simultaneously during the

screen. This approach can be an efficient starting point to identify chemical matter that binds to a protein of interest. In fact, this technique was successfully implemented by Abbott Laboratories in the development of ABT-737[31,32].

Here, we sought to expand the repertoire of BAX-activating compounds[18,19,34,35] for potential clinical development by use of an NMR-based fragment screen. Indeed, by employing this approach we successfully identified 53 BAX interacting fragments (BIFs). Intriguingly, one of these hits, BIF-44, strongly sensitized BAX to BH3-mediated direct activation, revealing a previously undescribed biochemical phenomenon.

METHODS

Small Molecules

The Ro3 diversity fragment library used for screening by NMR was purchased from Maybridge. All BIFs were repurchased for biochemical characterization from Maybridge, with documented purities of ≥95%. BIF-44 (4-phenoxyphenol) was also ordered from Alfa Aesar (99% purity). ANA-BIF-1 (3-phenoxyphenol) was purchased from Alfa Aesar (98% purity), ANA-BIF-2 (4-benzylphenol), ANA-BIF-3 (4-phenoxyaniline), and ANA-BIF-5 (4-phenoxybenzoic acid) from Sigma-Aldrich (purities of 99%, 97%, and 97%, respectively), and ANA-BIF-4 (4,4'-oxydiphenol) from MP Biomedicals (≥95% purity). 4-ADPA (4-aminodiphenylamine) and I4PTH (3',3'',5',5''-tetraiodophenolphthalein) were purchased from TCI (>98% and >95% purity, respectively).

Peptide Synthesis

Solid-state peptide synthesis using Fmoc chemistry was performed as previously described[36]. BIM $SAHB_{A2}$ (^{145}EIWIAQELRXIGDXFNAYYA^{164}-$CONH_2$)[16] peptide (X, (*S*)-*N*-2-(4′-pentenyl) alanine) was N-terminally derivatized with either an acetyl group or fluorescein isothiocyanate (FITC)-β-alanine for the indicated applications in NMR and biochemical experiments. Peptides were purified by LC-MS to >95% purity (**Appendix: Figure S.1**) and quantified by amino acid analysis. Lyophilized peptides were reconstituted in 100% DMSO or DMSO-d_6 and diluted into the indicated aqueous buffers for experimental use.

Expression and Purification of Full-length BAX

Recombinant, full-length BAX was expressed in BL21 (DE3) *E. coli* using the pTYB1 vector[16,37]. Cell pellets were resuspended in 20 mM Tris, 250 mM NaCl, pH 7.2 and lysed by two passes through a microfluidizer (Microfluidics) chilled to 4°C. The lysate was clarified by centrifugation at 20,000 rpm. BAX was purified by batch affinity binding at 4°C using chitin resin (New England Biolabs), followed by loading onto gravity flow columns for washing and elution. The intein-chitin

binding domain tag was cleaved by 36 hour incubation in 50 mM dithiothreitol at 4°C. Pure protein was isolated by size exclusion chromatography (Superdex 75 10/300; 20 mM HEPES, 150 mM KCl, pH 7.2 or 20 mM potassium phosphate, pH 6.2) using an FPLC system (GE Healthcare Life Sciences).

Fragment Screening by STD NMR

Molecular fragments (Ro3 diversity library, Maybridge) were characterized by ^{1}H-NMR and then pooled in groups of 10 to minimize spectral overlap using in-house software. During the process of library curation, ^{1}H-NMR spectra were collected at a concentration of 500 μM in phosphate buffered saline (pH 7.4) and fragments exhibiting poor solubility, aggregation, or whose NMR spectra were inconsistent with the chemical structure (total of 40), were removed prior to pooling. Fragment pools were added to a 5 μM solution of unlabeled, full-length human BAX in 20 mM potassium phosphate buffer, pH 6.2 in 10% (v/v) D_2O, resulting in a final compound concentration of 300 μM. The mixing and loading of samples into a 5-mm NMR tube was performed using a liquid handling robot (Gilson). STD NMR measurements were acquired at 25°C on a Varian Inova 500-MHz spectrometer equipped with a helium-cooled cryoprobe. Low power saturation of the protein was achieved with a series of 50 ms Gaussian pulses for a total of 3 seconds; on-resonance irradiation was performed at 0.8 ppm, and off-resonance irradiation at 30 ppm. Standard excitation sculpting was used for solvent suppression. Each experiment was run for 14 min. The results were initially analyzed by comparing the on and off resonance STD spectra for each pool to determine the presence of binders. Subsequently, each pool was analyzed to identify individual binders using in-house analysis and display software, which allowed for precise alignment of on- and off-resonance spectra. Fragments in pools that yielded a positive STD signal were then subdivided into groups of three for retesting. Those fragments that exhibited STD in both experiments were reordered from Maybridge and tested both as single compounds and in competitive binding experiments.

Liposomal Release Assay

Large unilamellar vesicles (LUVs) with a lipid composition similar to the outer mitochondrial membrane were formed by liposome extrusion as previously described[38]. Briefly, a lipid mixture containing a 48:28:10:10:4 molar ratio of phosphatidylcholine, phosphatidylethanolamine, phosphatidylinositol, dioleoyl phosphatidylserine, and tetraoleolyl cardiolipin (Avanti Polar Lipids) was generated in chloroform. Lipid films were formed by evaporation of solvent, initially under nitrogen gas and then by overnight vacuum, followed by storage at –80 °C under nitrogen. Lipid films were hydrated in 1 mL assay buffer (10 mM HEPES, 200 mM KCl, 1 mM $MgCl_2$, pH 7.0) and mixed with the fluorophore and quencher pair, 8-aminonaphthalene-1,3,6-trisulfonic acid (ANTS, 12.5 mM) and p-xylene-bis-pyridinium bromide (DPX, 45 mM). Liposomes were formed by 5 freeze/thaw cycles followed by extrusion through a 100 nm polycarbonate membrane and purified using a Sepharose CL-2B size-exclusion column. For measurement of BAX activation, BAX (750 nM) was added to the indicated concentration of molecular fragment in the presence of liposomes, followed by the activator BIM $SAHB_{A2}$ at the indicated time points. The assay was carried out in black opaque 384 well plates (30 µl per well). ANTS/DPX release was monitored over time at room temperature in a spectrofluorometer (Tecan Infinite M1000) using an excitation wavelength of 355 nm, an emission wavelength of 540 nm, and a bandwidth of 20 nm. Maximal release was determined by the addition of Triton X-100 to a final concentration of 0.2% (v/v). Percent release was calculated as $((F-F_0)/(F_{100}-F_0)) \times 100$, where F is the observed fluorescence at a given time, and F_0 and F_{100} represent baseline and maximal fluorescence, respectively.

CPMG NMR

CPMG experiments were performed using standard methods[39]. NMR analyses employed BIF-44 at a concentration of 300 µM, with or without added BAX (5 µM), in a 20 mM potassium phosphate buffer, pH 6.2. A 0.5 millisecond tau delay (1 ms per CPMG echo cycle) was applied, with the

number of echo cycles corresponding to 500 ms. Excitation sculpting was used for solvent suppression, as reported[40].

Isothermal titration calorimetry (ITC)

Binding affinity was measured by adding 0.15 mM recombinant BAX protein to the cell and injecting 2.0 µL of 1.0 mM ligand by syringe for a total of 30 injections using an Affinity ITC (TA instruments) at 25°C. BAX and BIF-44 solutions were prepared in 20 mM potassium phosphate buffer (pH 6.2), with a final concentration of 2% (v/v) DMSO. The samples were centrifuged for 15 min at 4°C before titration. ITC experiments were performed in duplicate and the data analyzed with the NanoAnalyze software package (TA instruments) using a single binding site model and thermodynamic parameters calculated as follows: $\Delta G = \Delta H - T\Delta S = -RT\ln K_{B,}$ where ΔG, ΔH and ΔS are the changes in free energy, enthalpy and entropy of binding, respectively.

NMR-based Detection of Small Molecule Aggregators

To detect line broadening, standard ^{1}H-NMR spectra were acquired. T2 decay curves were generated by measuring the CPMG NMR spectra of the molecules, performed as described above. The number of echo cycles corresponds to the decay time. The intensity of the aromatic peaks at the indicated decay times were measured and normalized to a maximum intensity of 1 at the 10 ms decay time. The curves were fitted to a one phase decay model using Prism software (Graphpad). Excitation sculpting was used for solvent suppression. Samples for both analyses were prepared in 20 mM potassium phosphate buffer, pH 6.2, 10% (v/v) D_2O.

Dynamic Light Scattering (DLS)

The indicated molecules were diluted from a 100 mM stock into 20 mM potassium phosphate buffer, pH 6.2, with a final DMSO concentration of 1%. Samples were analyzed at room

temperature on a DynaPro-99 instrument equipped with a 90° detector angle using a 10 second acquisition time per measurement.

Negative Stain Electron Microscopy

Small molecules were diluted from 100 mM DMSO stocks into 20 mM Tris-HCl, pH 7.2 to 100 μM for I4PTH, and 300 μM for 4-ADPA and BIF-44. Samples were then applied to a glow discharged carbon-coated grid (Electron Microscopy Sciences) for 60 seconds. The grid was blotted to remove excess solution, washed once in water, and stained with 1% (w/v) uranyl formate for 20 seconds. Images were acquired using a JEOL JEM1200 EX transmission electron microscope (Harvard Medical School Electron Microscopy Facility).

RESULTS

NMR Screen Identifies BAX Interacting Fragments (BIFs)

To generate recombinant, full-length, monomeric BAX of sufficient quantity and stability to execute a molecular fragment screen, we scaled up our production method to an overall culture volume of 48 liters, and then performed sequential lysis of bacterial pellets at 4°C using a microfluidizer, followed by batch binding of the lysate to chitin affinity resin, dithiothreitol (DTT) cleavage, and purification by size exclusion chromatography (**Figure 2.1a–b**). Using this approach, we were able to generate 22 mg of BAX protein at a concentration of 0.6 mg/mL for initial screening, representing an overall yield of 0.5 mg of pure, full-length protein per liter of bacterial culture. We further confirmed by ^{15}N-HSQC NMR analysis that our preparation of recombinant, full-length BAX monomer was stable for days at room temperature, enabling us to embark on a small molecule screening effort (**Figure. 2.1c**).

Given the relatively low yield of recombinant BAX and induction of protein aggregation upon exposure to a potential activator, the traditional protein-detected NMR methods like those used in SAR by NMR are not feasible for BAX. In contrast, ligand-based methods require a much lower amount of protein (typically around 5 μM) and the protein does not need to be isotopically labeled[25,41]. Additionally, the rapid acquisition time, relative ease of analysis, and the ability to pool compounds with non-overlapping ^{1}H-NMR spectra make ligand-detected NMR screening a tractable platform for advancing a fragment-based screen of pro-apoptotic BAX[41,42]. Specifically, we employed fragment screening by saturation transfer difference (STD) NMR to identify molecules that interact with BAX. STD NMR allows for the sensitive detection of ligand binding (up to millimolar K_D) by measuring the change in the ^{1}H-NMR signal of a ligand following the selective saturation of resonances in the target protein (0.5-1.0 ppm, protons on methyl sidechains)[23,43]. Transfer of this magnetization from the protein to any bound ligand causes a decrease in signal that is reflective of a ligand-protein binding interaction. When this “on” resonance spectrum is subtracted from that of the same sample exposed to “off” resonance

Figure 2.1 *Expression, purification, and stability of full-length monomeric BAX.*

(**a**) Size exclusion chromatography (SEC) demonstrates that BAX is produced and isolated in monomeric (e.g. fractions B12–B9, rightward peak) and oligomeric forms (left). Conditions are optimized to afford maximal yield of monomeric protein. BAX protein is identified and tracked in SEC fractions by western analysis (right). Of note, preparation of monomeric BAX for SDS PAGE (e.g. boiling, detergent) can induce low-level dimerization, which can be detected by western blot. (**b**) SEC traces of the BAX preparations used for each step of STD NMR screening (left), with an exemplary coomassie stain of the isolated fractions of purified monomeric BAX (right). (**c**) Stability of purified, recombinant, and monomeric full-length BAX, as demonstrated by ^{15}N-HSQC NMR analysis of the same ^{15}N-BAX (50 μM) sample after 24 (blue) and 48 (red) hours at room temperature.

Figure 2.1 (Continued)

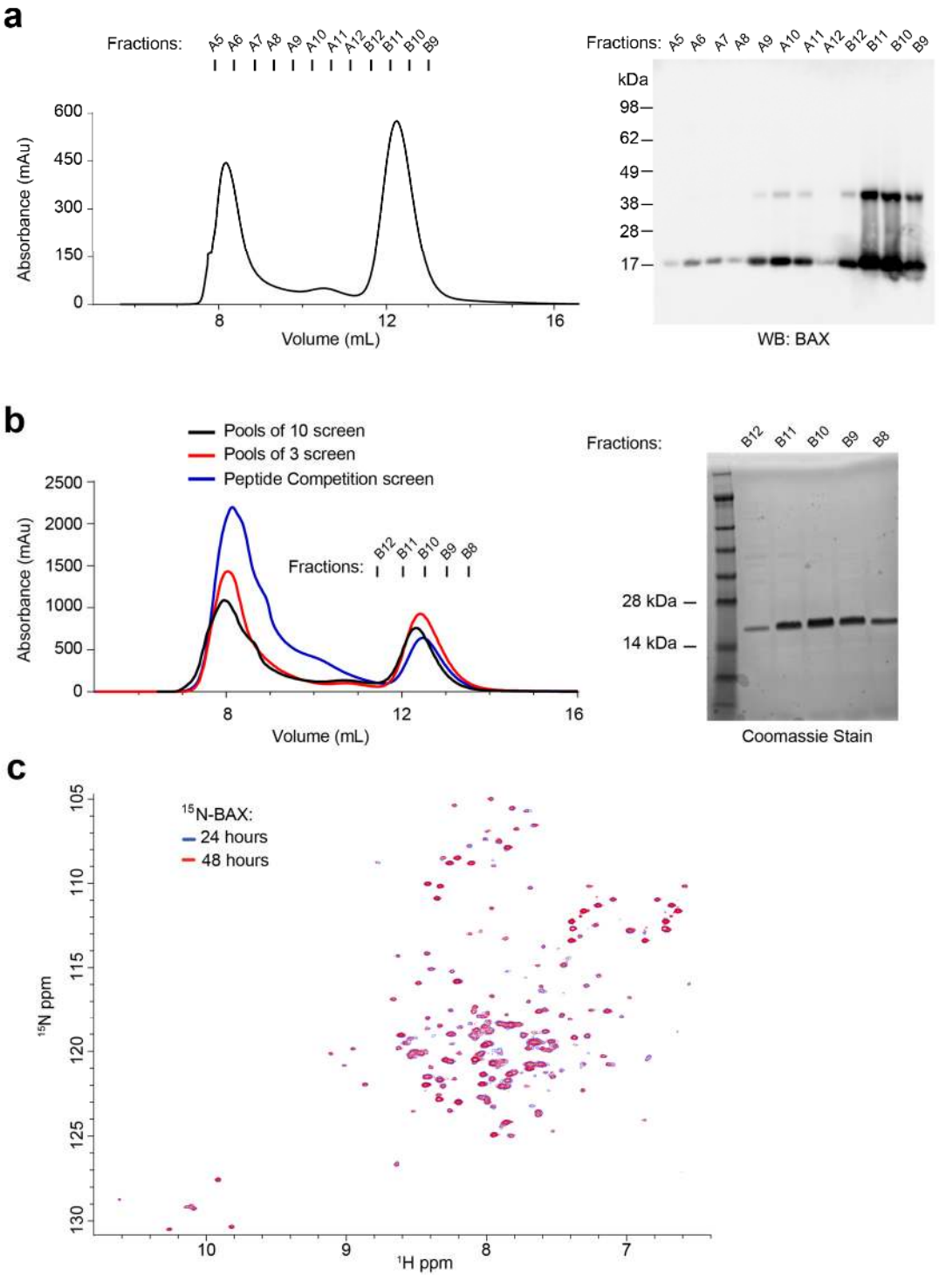

Table 2.1 *Overview of fragment screen*

Category	Parameter	Description
Assay	Type of assay	*In vitro*
	Target	BAX
	Primary measurement	Saturation-Transfer Difference (STD) NMR
	Key reagents	Recombinant Human BAX protein
	Assay protocol	Molecular fragments were pooled in groups of 10 to minimize spectral overlap and added to a solution of BAX in 20 mM potassium phosphate buffer, pH 6.2 in 10% (v/v) D_2O. STD NMR measurements were acquired at 25°C. Low power saturation of the protein was achieved with a series of 50 ms Gaussian pulses for a total of 3 seconds; on-resonance irradiation was performed at 0.8 ppm, and off-resonance irradiation at 30 ppm. Standard excitation sculpting was used for solvent suppression.
Library	Library size	960 fragments
	Library composition	Rule of Three (Ro3) compliant fragments
	Source	Maybridge Ro3 Diversity Fragment Library
	Library curation	^{1}H-NMR spectra for each fragment were collected at a concentration of 500 μM in phosphate buffered saline (pH 7.4). Fragments exhibiting poor solubility, aggregation, or whose NMR spectra were inconsistent with the chemical structure (total of 40) were removed prior to screening.
Screen	Format	5 mm NMR tubes
	Concentration(s) tested	5 μM BAX 300 μM compound 3% DMSO
	Controls	DMSO
	Reagent/compound dispensing system	Liquid handling robot (Gilson) was used for mixing and loading of samples into NMR tubes.
	Detection instrument	Varian Inova 500-MHz spectrometer equipped with a helium-cooled cryoprobe
Post-screen analysis	Hit criteria	Each pool was analyzed to identify individual binders using in-house analysis and display software, which allowed for precise alignment of on- and off-resonance spectra. Fragments that displayed a positive STD signal were considered hits.
	Hit rate	56/960 (5.8%) after both rounds of screening
	Additional assay(s)	Initial hits were subdivided into groups of three and retested by STD.
	Confirmation of hit purity and structure	Hits from the first two rounds of screening were repurchased from Maybridge and screened for binding by STD NMR as singletons

irradiation (outside proton frequency range), the result is a difference spectra (STD). Since peaks that do not change following irradiation subtract to zero, ligand binding is indicated by the appearance of peaks in the difference spectrum.

We performed the BAX screen using the Maybridge Rule of Three (Ro3) fragment library. The “rule of three”, similar to the rule of five, is a guideline for designing fragment libraries based on the properties of compounds that frequently score in a screen[44]. Ro3 fragments have a molecular weight of <300 Da, ≤3 hydrogen bond donors/acceptors, and a calculated logP ≤3. In addition to being Ro3 compliant, the members of the library represent a diverse set of pharmacophores, further curated to remove reactive functional groups. The 1000 molecular fragments were first subjected to a quality control workflow to eliminate any fragments that exhibited poor solubility, aggregation below 500 μM, or whose NMR spectra were not consistent with the chemical structure. The 960 compounds that passed this quality control step were characterized by ^{1}H-NMR and STD NMR in the absence of protein to ensure the specificity of any observed hit in the screen. Using custom, in-house software, the compounds were then pooled in groups of ten such that spectral overlap of the members of each pool was minimized.

The on- and off-resonance STD spectra for each pool of fragments was collected and carefully aligned, using in-house display and analysis software. The data interpretation was a binary “yes or no” answer based on the appearance of peaks in the difference spectrum. Deconvolution of the pools was achieved by comparing each STD difference spectrum with the ^{1}H-spectra of the constituents of the pool. Of the 96 pools analyzed, we detected a positive STD signal in 37, which represented 86 individual hits. To confirm the screening results, the compounds were then rescreened using similar conditions in pools of three, ultimately yielding 56 confirmed interactors (**Table 2.1**, **Figure. 2.2a**). Fifty-three commercially available fragments were ordered, retested by STD as singletons, and confirmed as BAX-Interacting Fragments (BIFs) (**Appendix: Table S.1**). While the hits are diverse, nearly half of the identified BIFs were composed of linked or fused five and six-membered rings (**Appendix: Table S.2**).

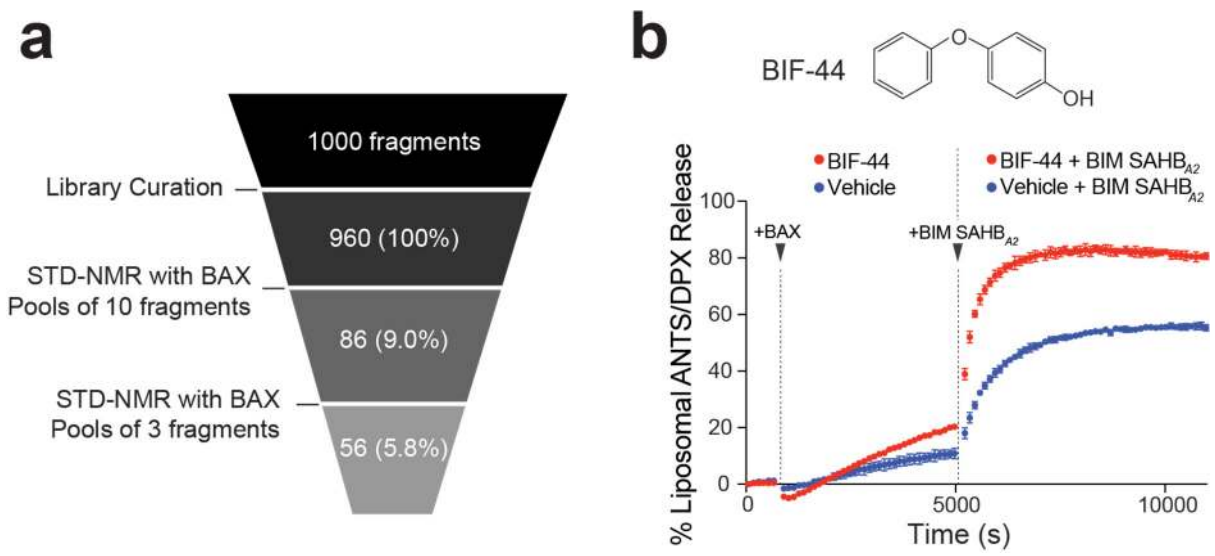

Figure 2.2 *STD NMR-based identification of BAX-interacting fragments that modulate BH3-mediated BAX activation.*

(a) Identification of BAX-interacting fragments (BIFs) by sequential rounds of STD NMR screening in pools of 10, 3, and then singlet, yielding 56 candidate BIFs. BAX, 5 μM; Molecules, 300 μM (**b**) BIF-44 has no independent effect on the liposomes (red, left), minimal direct BAX activation activity (red, middle), but notably enhances the kinetics and quantity of liposomal release upon addition of BIM SAHB$_{A2}$ (red, right), exceeding the maximal level of release achieved by the BIM SAHB$_{A2}$ and BAX combination alone (blue, right). Error bars are mean ± SD for experiments performed in technical triplicate, and repeated twice more with similar results using independent liposomal and protein preparations. BAX, 0.75 μM; BIM SAHB$_{A2}$, 0.75 μM; BIF-44, 113 μM (150x)

BIF-44 Specifically Sensitizes BAX Activation

To determine if any of the identified BIFs influenced the function of BAX, we screened the 53 BIFs in a liposomal release assay. This technique measures the ability of BAX to permeabilize fluorophore/quencher-packed large, unilamellar vesicles (LUVs) with a lipid composition mimicking that of the outer mitochondrial membrane. This assay was designed to identify both (1) direct BAX activators and (2) sensitizers or inhibitors of direct BAX activation induced by a stapled BIM BH3 helix, BIM SAHB$_{A2}$ (aa 145–164)[16]. First, baseline fluorescence with liposomes and compound alone was read, followed by the addition of BAX to evaluate for direct activation; then, BIM SAHB$_{A2}$ was added to this mixture and the effect of the combination monitored, and compared with the triggering activity of BIM SAHB$_{A2}$ and BAX in the absence of compound. Using this assay format, we identified 4 direct activators of BAX-mediated liposomal release and 8 sensitizers of BIM SAHB$_{A2}$-triggered, BAX activation (**Appendix: Table S.1**). The direct activator profile is exemplified by the positive control BIM SAHB$_{A2}$ peptide, which induces time-responsive liposomal release in the presence of BAX (**Figure. 2.2b, Appendix: Table S.2**). A novel sensitizer profile was most strikingly reflected by the activity of BIF-44, which had a minimal effect on BAX when incubated as a single agent, but when combined with BIM SAHB$_{A2}$ enhanced both the kinetics and maximal amount of BAX-mediated release as compared to treatment with BIM SAHB$_{A2}$ alone (**Figure 2.2b**).

Given these intriguing results, we subjected BIF-44 to a rigorous workflow of validation studies. First, we confirmed the screening results by demonstrating that the BIF-44 STD signal is dependent on BAX and not a non-specific result of the experimental setup (**Figure. 2.3a**). The off-resonance condition shows no effect on the aromatic region of BIF-44 in the presence or absence of BAX (**Figure. 2.3a, top**). An STD signal (STD = off resonance minus on resonance) for BIF-44 is only detected in the presence of BAX, reflective of ligand-protein interaction (**Figure. 2.3a, middle**).

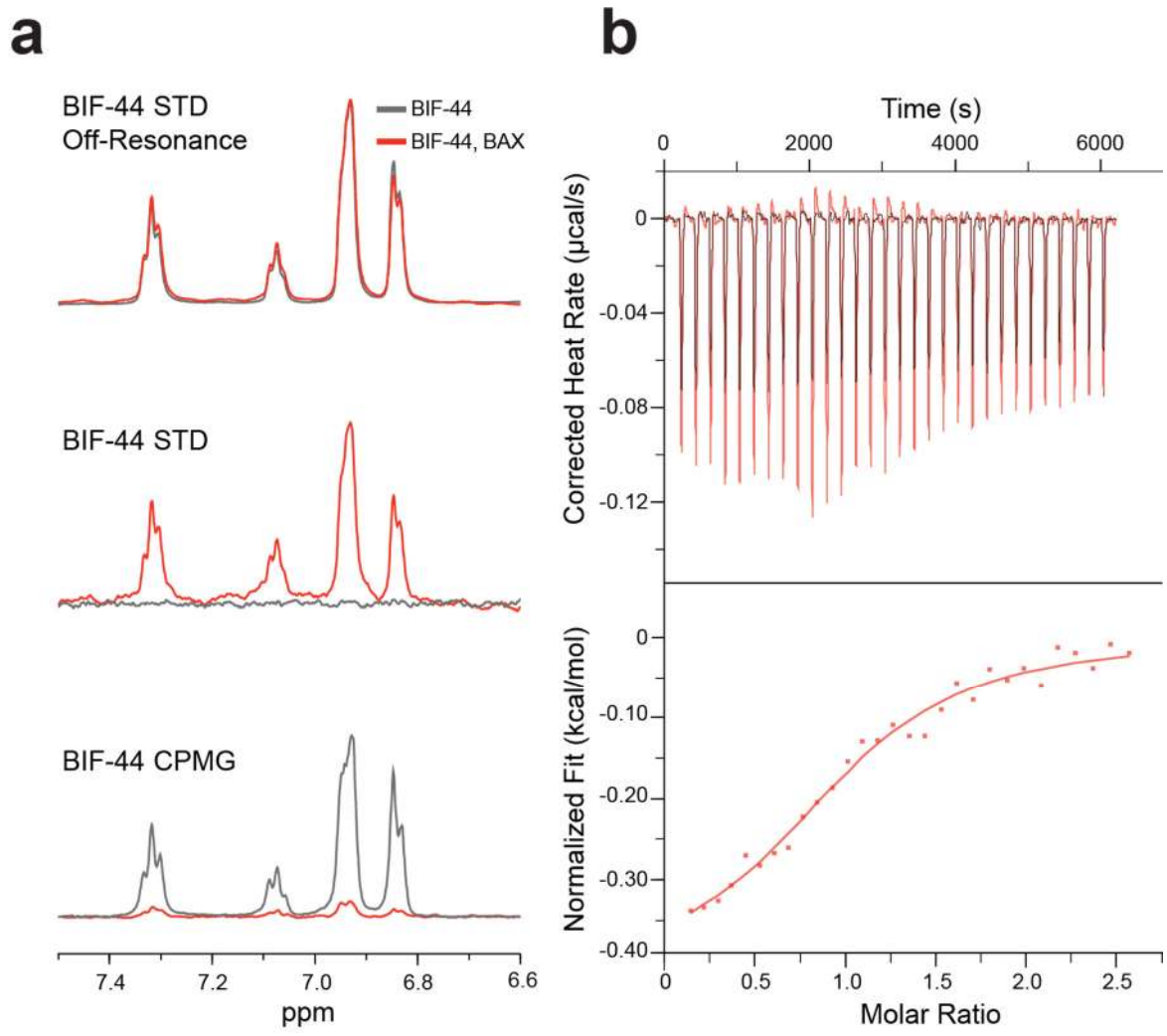

Figure 2.3 *Validation of BIF-44 as a BAX binder*.

(**a**) ^{1}H NMR spectrum of BIF-44 in the presence (red) and absence (gray) of BAX protein: STD off resonance (top), STD (middle), CPMG (500 ms) (bottom). BAX, 5 µM; BIF-44, 300 µM (**b**) Isothermal titration calorimetry analysis of the BIF-44/BAX interaction. ITC was performed in duplicate with a representative analysis shown (single binding site model; BAX, 150 µM; K_d, 37 ± 12 µM).

Next, we sought to corroborate our BIF-44/BAX interaction findings with an orthogonal NMR measure. We applied Carr–Purcell–Meiboom–Gill (CPMG)-NMR to monitor for a potential change in BIF-44 signal upon incubation with BAX[42]. This method measures the change in the T2 relaxation time of the ligand due to the formation of a protein-ligand complex. As the protein has a much faster relaxation time compared to the small ligand, interactions with the protein results in a measurable decrease in ^{1}H-NMR signal. In the presence of BAX, we indeed observed a sharp reduction in signal, indicative of BIF-44 binding (**Figure. 2.3a, bottom**).

We then quantified the BIF-44/BAX interaction by isothermal calorimetry (ITC), which revealed a K_d of 37 ± 12 μM (**Figure. 2.3b**). This double-digit micromolar affinity is both consistent with expectations for a small molecule fragment and the capacity of low affinity interactions to activate BAX. Indeed, in contrast to the nanomolar and subnanomolar affinities required for BH3-only protein and BH3-mimetic inhibition of anti-apoptotic targets, BAX activation occurs by a transient "hit-and-run" mechanism in which ligand-induced $\alpha1$–$\alpha2$ loop mobilization and BAX BH3 domain exposure catalyzes signal propagation through subsequent BAX autoactivation[15,45,46].

To evaluate the structure-based reproducibility and selectivity of the observed BIF-44 activity, we evaluated the binding and functional properties of a series of BIF-44 analogs. Importantly, we find that BIF-44-like diaryl ethers that either shift the hydroxyl from the *para* to the *meta* position (ANA-BIF-1), replace the ether linkage with a methylene group (ANA-BIF-2), or replace the hydroxyl group with an amine or methoxy in the same position (ANA-BIF-3; BIF-27), all retain BAX-binding activity as assessed by STD NMR, and demonstrate BAX-sensitization activity (**Figure. 2.4a–c, Appendix: Table S.1**). In contrast, diaryl ethers that bear a *para*-hydroxyl group in each aromatic ring (ANA-BIF-4), or that replace the BIF-44 hydroxyl with a carboxyl group (ANA-BIF-5), manifest little to no BAX-binding or sensitization activity (**Figure. 2.4d–e**). These data provide evidence for a structure-activity relationship that supports the specificity of action of BIF-44 in binding to BAX and sensitizing BH3-mediated BAX activation.

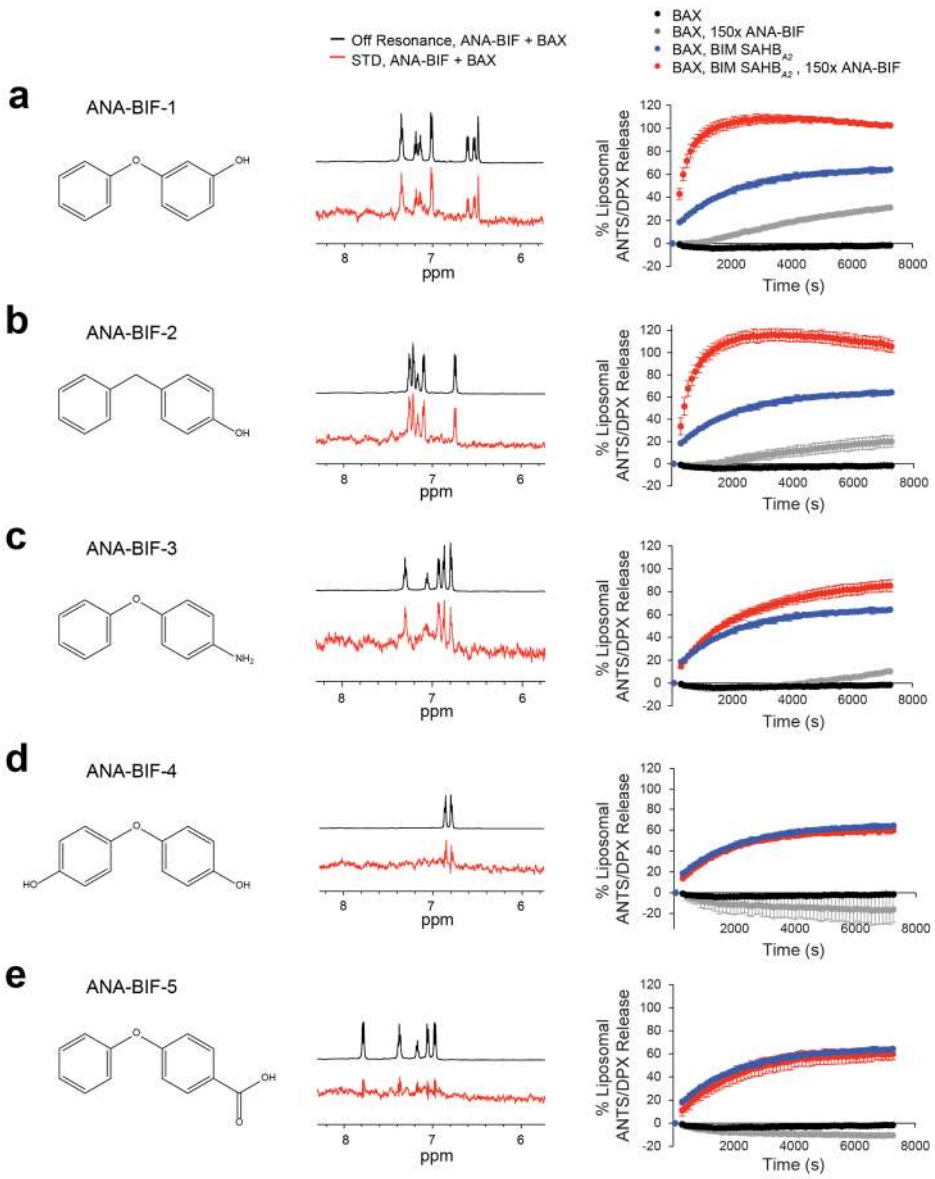

Figure 2.4 *Structure-activity relationships of BIF-44 analogs.*

(**a–e**) Chemical structures (left), STD binding (red) profiles (middle), and BAX-mediated liposomal release sensitization activity (right) of BIF-44 analogs (ANA-BIFs, compounds **2-5**). Error bars are mean ± SD for experiments performed in technical triplicate and repeated twice more with similar results using independent liposomal and protein preparations. For STD NMR, BAX 5 μM; ANA-BIFs 300 μM. For liposomal release assays, BAX 0.75 μM; BIM SAHB$_{A2}$, 0.75 μM; ANA-BIFs, 113 μM (150x).

Finally, before advancing the BIF-44/BAX interaction to more rigorous structural and mechanistic analyses, we sought to rule out non-specific activity that could derive from aggregation of the small molecule fragment. In addition to passing our initial quality control testing performed on the Maybridge Ro3 library, we evaluated BIF-44 in a series of aggregation assays alongside positive control aggregator compounds[28]. First, we queried an aggregator web tool (http://advisor.bkslab.org/)[29], which found no structural similarities between BIF-44 and other aggregator compounds in the database. The presence of broad ^{1}H NMR spectra can be a sign of aggregation[47]. In stark contrast to the small molecule aggregators 4-aminodiphenylamine (4-ADPA)[29] and tetraiodophenolphthalein (I4PTH)[28], BIF-44 showed no NMR line broadening at the highest micromolar dosing (300 μM) used in our studies (**Figure. 2.5a–b**). Whereas 4-ADPA demonstrated rapid NMR signal decay over time at 300 μM dosing, the BIF-44 signal was stable at this dose (**Figure. 2.5c**), and showed little to no difference in decay between 25 and 300 μM dosing when evaluated at even longer time points (**Figure. 2.5d**).

We then compared BIF-44, 4-ADPA, and I4PTH in dynamic light scattering experiments across a broad dose range. Whereas 4-ADPA and I4PTH show evidence of light scattering at 300 μM and 10 μM, respectively, BIF-44 showed no such effect even at 1 mM concentration (**Figure. 2.5e**). Finally, small molecule formation of structured aggregates has also been shown to cause spurious effects on protein targets[28,48]. To rule out this possibility, we compared the morphology of micromolar solutions of I4PTH, a robust aggregator compound, to that of BIF-44 by negative stain electron microscopy. Whereas I4PTH produced prominent, structured aggregates, as previously reported[28], BIF-44 showed no such effect (**Figure. 2.5f**). In addition, neither small molecule aggregator, 4-ADPA or I4PTH, had any effect on BIM SAHB$_{A2}$-triggered, BAX-mediated liposomal release (**Figure. 2.5g–h**). Thus, we find by a series of orthogonal measures that BIF-44 demonstrates no evidence of small molecule aggregation even at very high concentrations and induces a specific sensitizing effect on BAX activation and poration.

Figure 2.5 *BIF-44 does not form aggregates in solution.*

(**a**) Chemical structures of BIF-44 (top), 4-ADPA (middle), and I4PTH (bottom). (**b**) ^{1}H NMR spectra of BIF-44 (300 μM), 4-ADPA (300 μM), and I4PTH (100 μM). (**c**) T2 decay curves of BIF-44 (300 μM) and 4-ADPA (300 μM). Data are mean ± SD for the decay of three peaks per spectrum. (**d**) T2 decay curves of BIF-44 at the indicated concentrations. Data are mean ± SD for the decay of three peaks per spectrum. (**e**) Dynamic light scattering intensities of BIF-44, 4-ADPA, and I4PTH at the indicated concentrations. Data are mean ± SD for 10 runs per sample and repeated with similar results using independent compound dilutions. (**f**) Negative stain electron microscopy of I4TPH (top left, top right magnification), 4-ADPA (bottom left), and BIF-44 (bottom right). Bars: top left, 2 μm; top right, 0.4 μm; bottom left, 2 μm; bottom right, 2 μm. (**g–h**) The addition of aggregator molecules 4-ADPA (**g**) or I4PTH (**h**) have no sensitizing effect on BIM SAHB$_{A2}$-triggered, BAX-mediated liposomal release. Error bars are mean ± SD for experiments performed in technical triplicate and repeated twice more with similar results using independent liposomal and protein preparations. BAX, 0.75 μM; BIM SAHB$_{A2}$, 0.75 μM; ADPA or I4PTH, 113 μM (150x).

Figure 2.5 (Continued)

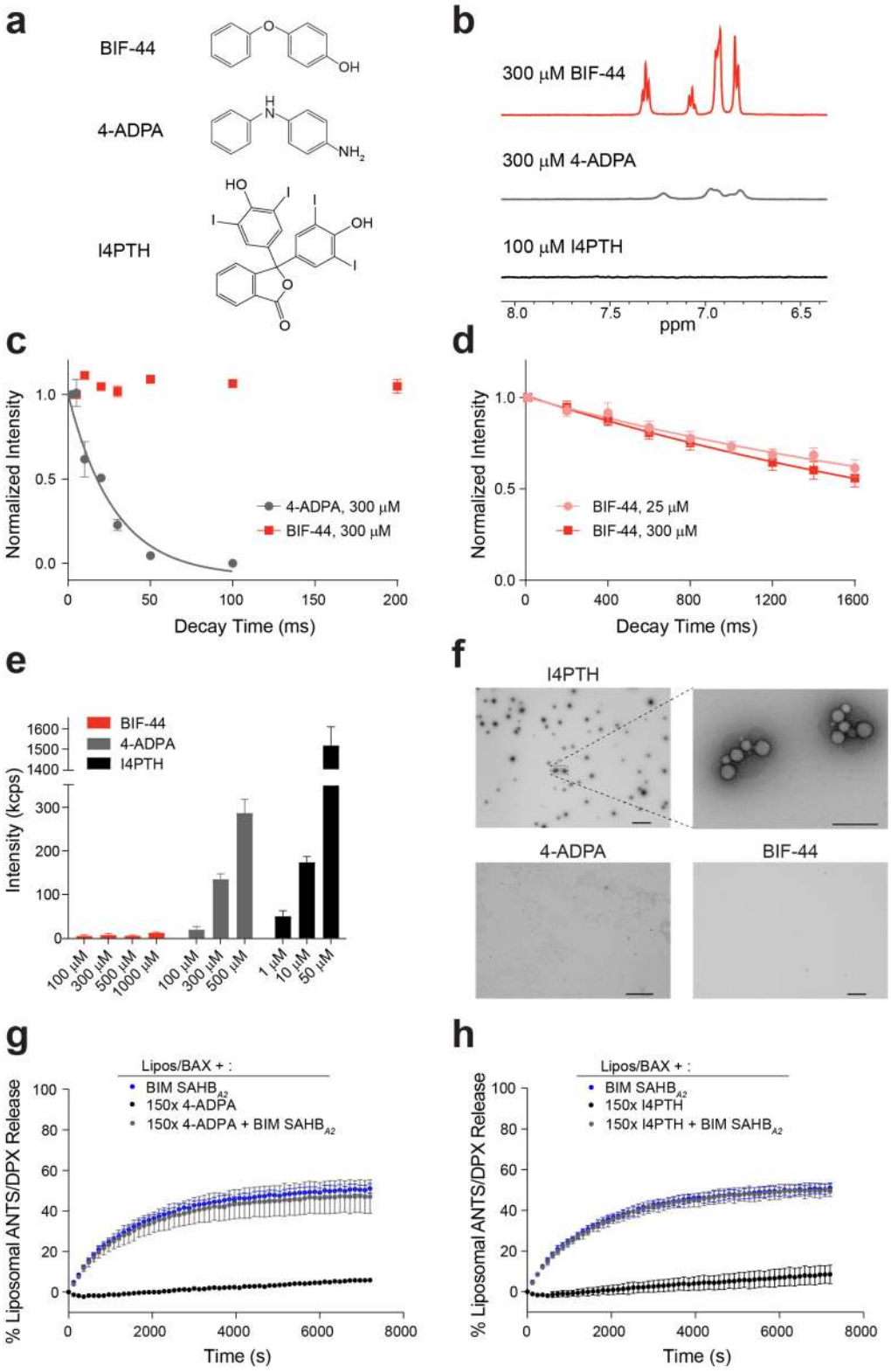

DISCUSSION

BCL-2 family proteins tightly control the initiation of apoptosis. In particular, BAX activation represents a critical regulatory step of the apoptotic cascade. Activated BAX forms pores in the mitochondria, and thereby induces mitochondrial outer membrane permeabilization (MOMP), the point of no return for apoptotic cell death. Given their central role in apoptosis regulation, BCL-2 family proteins have been longstanding targets for pharmacologic development. Whereas drug discovery efforts reported over a decade ago for an anti-apoptotic BCL-2 family member have now led to the first, selective small molecule inhibitor of BCL-2, venetoclax[3,31], an analogous drug development strategy has remained out of reach for BAX.

A major limitation in pursuing BAX-modulating compounds has been the inability to generate pure, full-length BAX in sufficient yields to perform a small molecule screen. As a result, previous studies have relied on *in silico* methods to identify potential BAX-binding compounds[17-19]. By using a pooled STD NMR screening strategy, we greatly reduced the protein requirements to conduct an unbiased screen. In addition, we were able to purify the requisite amounts of full length BAX with sufficient stability for screening by optimizing our protein production and handling methodologies. Thus, we were able to conduct what is, to our knowledge, the first NMR-based small molecule screen of full-length BAX in solution. Through successive rounds of fragment screening by STD NMR, we identified 53 BAX-interacting fragments (BIFs) that displayed reproducible binding to BAX. To determine if these 53 BIFs could modulate BAX activity, the molecules were tested in a functional liposomal release assay designed to rapidly screen for BAX activation, inhibition, or sensitization. From this secondary screen, we identified a molecular fragment, BIF-44, with a unique BAX sensitization activity that manifested upon co-incubation of the compound with BAX and a triggering BH3 ligand in a membrane environment.

As non-specific protein modulators can register as hits across a variety of screening methods, a critical step in the characterization of a hit from a small molecule library is to validate the specificity of activity. The so-called “PAINS” compounds have several distinct mechanisms

that can lead to a false positive result, including small molecule aggregation[28,29], detection assay interference [27], covalent crosslinking[27], and effects of compound impurities[49]. While the Maybridge Ro3 fragment library was designed to avoid these “bad actors”, it is critical to rigorously validate any hits experimentally. Therefore, we conducted three orthogonal binding assays including STD NMR, CPMG NMR, and ITC to confirm that BIF-44 directly binds to BAX. Additionally, BIF-44 was ordered from two different vendors at high purity to rule out the presence of an interfering impurity. To ensure the specificity of the BIF-44-BAX interaction, we tested several structurally-related analogs of BIF-44 (ANA-BIFs) to demonstrate a clear SAR. Some, but not all of the ANA-BIF compounds, lost the BAX sensitizing effect, suggesting that BIF-44 induces a specific effect on BAX.

Small molecule aggregators are notorious for foiling screening efforts, producing artefactual modulation of protein activity[28,29]. At high concentrations, these aggregating molecules organize into large colloidal particles[50] or fibrils[51] that can interact with proteins and influence their function. Given the difficulty of accurately predicting aggregator compounds, the prevalence of these compounds in screening libraries can be quite high. Therefore, any small molecule screening hit should be tested experimentally for aggregation in solution. We conducted a suite of experiments that explicitly tested for BIF-44 aggregation. Using two NMR methods, DLS, and electron microscopy, we found no evidence of BIF-44 aggregation. Furthermore, two compounds that do form aggregates did not affect BAX activation. Taken together, these data validated BIF-44 as a novel molecular fragment capable of directly binding to BAX and sensitizing BH3-triggered BAX activation and poration. This work stimulated our efforts to pursue both the BIF-44 binding site and its explicit mechanism of action.

REFERENCES

1. Hanahan, D. & Weinberg, R.A. The hallmarks of cancer. *Cell* **100**, 57-70 (2000).

2. Hanahan, D. & Weinberg, R.A. Hallmarks of cancer: the next generation. *Cell* **144**, 646-74 (2011).

3. Souers, A.J. et al. ABT-199, a potent and selective BCL-2 inhibitor, achieves antitumor activity while sparing platelets. *Nat Med* **19**, 202-8 (2013).

4. Sattler, M. et al. Structure of Bcl-xL-Bak peptide complex: recognition between regulators of apoptosis. *Science* **275**, 983-6 (1997).

5. Lessene, G. et al. Structure-guided design of a selective BCL-X(L) inhibitor. *Nat Chem Biol* **9**, 390-7 (2013).

6. Tao, Z.F. et al. Discovery of a Potent and Selective BCL-XL Inhibitor with in Vivo Activity. *ACS Med Chem Lett* **5**, 1088-93 (2014).

7. Tse, C. et al. ABT-263: a potent and orally bioavailable Bcl-2 family inhibitor. *Cancer Res* **68**, 3421-8 (2008).

8. Bruncko, M. et al. Structure-guided design of a series of MCL-1 inhibitors with high affinity and selectivity. *J Med Chem* **58**, 2180-94 (2015).

9. Cohen, N.A. et al. A competitive stapled peptide screen identifies a selective small molecule that overcomes MCL-1-dependent leukemia cell survival. *Chem Biol* **19**, 1175-86 (2012).

10. Kotschy, A. et al. The MCL1 inhibitor S63845 is tolerable and effective in diverse cancer models. *Nature* **538**, 477-482 (2016).

11. Leverson, J.D. et al. Potent and selective small-molecule MCL-1 inhibitors demonstrate on-target cancer cell killing activity as single agents and in combination with ABT-263 (navitoclax). *Cell Death Dis* **6**, e1590 (2015).

12. Pelz, N.F. et al. Discovery of 2-Indole-acylsulfonamide Myeloid Cell Leukemia 1 (Mcl-1) Inhibitors Using Fragment-Based Methods. *J Med Chem* **59**, 2054-66 (2016).

13. Stewart, M.L., Fire, E., Keating, A.E. & Walensky, L.D. The MCL-1 BH3 helix is an exclusive MCL-1 inhibitor and apoptosis sensitizer. *Nat Chem Biol* **6**, 595-601 (2010).

14. Huhn, A.J., Guerra, R.M., Harvey, E.P., Bird, G.H. & Walensky, L.D. Selective Covalent Targeting of Anti-Apoptotic BFL-1 by Cysteine-Reactive Stapled Peptide Inhibitors. *Cell Chem Biol* **23**, 1123-34 (2016).

15. Gavathiotis, E., Reyna, D.E., Davis, M.L., Bird, G.H. & Walensky, L.D. BH3-triggered structural reorganization drives the activation of proapoptotic BAX. *Mol Cell* **40**, 481-92 (2010).

16. Gavathiotis, E. et al. BAX activation is initiated at a novel interaction site. *Nature* **455**, 1076-81 (2008).

17. Gavathiotis, E., Reyna, D.E., Bellairs, J.A., Leshchiner, E.S. & Walensky, L.D. Direct and selective small-molecule activation of proapoptotic BAX. *Nat Chem Biol* **8**, 639-45 (2012).

18. Zhao, G. et al. Activation of the proapoptotic Bcl-2 protein Bax by a small molecule induces tumor cell apoptosis. *Mol Cell Biol* **34**, 1198-207 (2014).

19. Xin, M. et al. Small-molecule Bax agonists for cancer therapy. *Nat Commun* **5**, 4935 (2014).

20. Li, R. et al. Modulation of Bax and mTOR for Cancer Therapeutics. *Cancer Res* **77**, 3001-3012 (2017).

21. Dias, D.M. & Ciulli, A. NMR approaches in structure-based lead discovery: recent developments and new frontiers for targeting multi-protein complexes. *Prog Biophys Mol Biol* **116**, 101-12 (2014).

22. Murray, C.W. & Rees, D.C. The rise of fragment-based drug discovery. *Nat Chem* **1**, 187-92 (2009).

23. Scott, D.E., Coyne, A.G., Hudson, S.A. & Abell, C. Fragment-based approaches in drug discovery and chemical biology. *Biochemistry* **51**, 4990-5003 (2012).

24. Lipinski, C.A., Lombardo, F., Dominy, B.W. & Feeney, P.J. Experimental and computational approaches to estimate solubility and permeability in drug discovery and development settings. *Adv Drug Deliv Rev* **46**, 3-26 (2001).

25. Erlanson, D.A., Fesik, S.W., Hubbard, R.E., Jahnke, W. & Jhoti, H. Twenty years on: the impact of fragments on drug discovery. *Nat Rev Drug Discov* **15**, 605-19 (2016).

26. Barker, A., Kettle, J.G., Nowak, T. & Pease, J.E. Expanding medicinal chemistry space. *Drug Discov Today* **18**, 298-304 (2013).

27. Baell, J. & Walters, M.A. Chemistry: Chemical con artists foil drug discovery. *Nature* **513**, 481-3 (2014).

28. McGovern, S.L., Helfand, B.T., Feng, B. & Shoichet, B.K. A specific mechanism of nonspecific inhibition. *J Med Chem* **46**, 4265-72 (2003).

29. Irwin, J.J. et al. An Aggregation Advisor for Ligand Discovery. *J Med Chem* **58**, 7076-87 (2015).

30. Tsai, J. et al. Discovery of a selective inhibitor of oncogenic B-Raf kinase with potent antimelanoma activity. *Proc Natl Acad Sci U S A* **105**, 3041-6 (2008).

31. Oltersdorf, T. et al. An inhibitor of Bcl-2 family proteins induces regression of solid tumours. *Nature* **435**, 677-81 (2005).

32. Petros, A.M. et al. Discovery of a potent inhibitor of the antiapoptotic protein Bcl-xL from NMR and parallel synthesis. *J Med Chem* **49**, 656-63 (2006).

33. Shuker, S.B., Hajduk, P.J., Meadows, R.P. & Fesik, S.W. Discovering high-affinity ligands for proteins: SAR by NMR. *Science* **274**, 1531-4 (1996).

34. Brahmbhatt, H., Uehling, D., Al-Awar, R., Leber, B. & Andrews, D. Small molecules reveal an alternative mechanism of Bax activation. *Biochem J* **473**, 1073-83 (2016).

35. LaBelle, J.L. et al. A stapled BIM peptide overcomes apoptotic resistance in hematologic cancers. *J Clin Invest* **122**, 2018-31 (2012).

36. Bird, G.H., Crannell, W.C. & Walensky, L.D. Chemical synthesis of hydrocarbon-stapled peptides for protein interaction research and therapeutic targeting. *Curr Protoc Chem Biol* **3**, 99-117 (2011).

37. Suzuki, M., Youle, R.J. & Tjandra, N. Structure of Bax: coregulation of dimer formation and intracellular localization. *Cell* **103**, 645-54 (2000).

38. Pitter, K., Bernal, F., Labelle, J. & Walensky, L.D. Dissection of the BCL-2 family signaling network with stabilized alpha-helices of BCL-2 domains. *Methods Enzymol* **446**, 387-408 (2008).

39. Hajduk, P.J., Olejniczak, E.T. & Fesik, S.W. One-Dimensional Relaxation- and Diffusion-Edited NMR Methods for Screening Compounds That Bind to Macromolecules. *J Am Chem Soc* **119**, 12257-12261 (1997).

40. Hwang, T. & Shaka, A.J. Water Suppression That Works. Excitation Sculpting Using Arbitrary Waveforms and Pulsed Field Gradients. *J Magn Reson A* **112**, 275-279 (1995).

41. Śledź, P., Abell, C. & Ciulli, A. Ligand-Observed NMR in Fragment-Based Approaches. in *NMR of Biomolecules* 264-280 (Wiley-VCH Verlag GmbH & Co. KGaA, 2012).

42. Stockman, B.J. & Dalvit, C. NMR screening techniques in drug discovery and drug design. *Progress in Nuclear Magnetic Resonance Spectroscopy* **41**, 187-231 (2002).

43. Mayer, M. & Meyer, B. Characterization of Ligand Binding by Saturation Transfer Difference NMR Spectroscopy. *Angewandte Chemie International Edition* **38**, 1784-1788 (1999).

44. Congreve, M., Carr, R., Murray, C. & Jhoti, H. A 'rule of three' for fragment-based lead discovery? *Drug Discov Today* **8**, 876-7 (2003).

45. Tan, C. et al. Auto-activation of the apoptosis protein Bax increases mitochondrial membrane permeability and is inhibited by Bcl-2. *J Biol Chem* **281**, 14764-75 (2006).

46. Wei, M.C. et al. tBID, a membrane-targeted death ligand, oligomerizes BAK to release cytochrome c. *Genes Dev* **14**, 2060-71 (2000).

47. LaPlante, S.R. et al. Compound aggregation in drug discovery: implementing a practical NMR assay for medicinal chemists. *J Med Chem* **56**, 5142-50 (2013).

48. Julien, O. et al. Unraveling the mechanism of cell death induced by chemical fibrils. *Nat Chem Biol* **10**, 969-76 (2014).

49. Morreale, F.E. et al. Mind the Metal: A Fragment Library-Derived Zinc Impurity Binds the E2 Ubiquitin-Conjugating Enzyme Ube2T and Induces Structural Rearrangements. *J Med Chem* (2017).

50. Blevitt, J.M. et al. Structural Basis of Small-Molecule Aggregate Induced Inhibition of a Protein-Protein Interaction. *J Med Chem* **60**, 3511-3517 (2017).

51. Zorn, J.A., Wille, H., Wolan, D.W. & Wells, J.A. Self-assembling small molecules form nanofibrils that bind procaspase-3 to promote activation. *J Am Chem Soc* **133**, 19630-3 (2011).

Chapter 3

Biochemical and Biophysical
Characterization of the BIF-44–BAX Interaction

“Location, Location, Location!”

ABSTRACT

Having identified BIF-44 in a fragment-based screen and validated this compound as a sensitizer of BAX activation (Chapter 2), we sought to further characterize the nature of this interaction. Using BAX-mediated liposomal release as a functional assay, we determined that BIF-44 dose-responsively sensitizes the activation of BAX by BIM $SAHB_{A2}$ and exhibits a similar sensitization effect with a variety of other BAX-activating stimuli. Furthermore, BIF-44 sensitized BAX activation in a mitochondrial release assay, which reflects the physiologic context for BAX activity. Leveraging peptide ligands with known BAX binding sites, we unexpectedly detected competition for BIF-44 binding by the inhibitory vMIA/BH4 peptides. We localized the BIF-44 binding site by HSQC NMR, which revealed prominent chemical shift changes of residues that form a pocket at the junction of the α3–α4 and α5–α6 hairpins, the very same region occupied by the vMIA peptide. Thus, this discrete location on BAX was identified as a critical regulatory center where BIF-44 binding can sensitize BAX, but occlusion by vMIA/BH4 helices can prevent BAX activation.

ATTRIBUTIONS

Portions of this chapter were published in the following manuscript: Pritz, J.R. et al. Allosteric sensitization of proapoptotic BAX. *Nat Chem Biol* **13**, 961-967 (2017).

Contributions to the work described in this chapter were made by Jonathan R. Pritz, Franziska Wachter, Walter Massefski, and Loren D. Walensky

J.R.P., F.W., W.M., and L.D.W. designed the study. J.R.P. and F.W.. generated BAX protein; J.R.P. conducted NMR experiments under the guidance of W.M., and L.D.W.; J.R.P. and F.W. performed biochemical assays.

Additionally, we thank G. Bird and T. Oo for peptide production, M. Godes for assistance with mitochondrial preparation, and D. Andrews and K. Sarosiek for providing BIM_L plasmid and protein, respectively.

INTRODUCTION

BCL-2-associated X protein (BAX) is a 21 kDa globular protein composed of nine α-helices and functions as a critical effector of the BCL-2 family-regulated mitochondrial apoptotic pathway. An α5–α6 hairpin forms the protein's hydrophobic core, the juxtaposition of α-helices 1 and 6 creates a ligand-interaction surface that regulates the initiation of BAX activation, and, at the opposite face of the protein, the auto-inhibitory α9 helix resides in a hydrophobic groove, with portions of α-helices 2, 3 and 4 defining the pocket[1]. BAX's central role in apoptosis induction derives from its capacity to undergo a major conformational change that results in irreversible mitochondrial translocation, intramembrane homo-oligomerization, and mitochondrial outer membrane poration[2]. For such a small protein, a surprisingly large series of regulatory surfaces and complex conformational changes have been defined (**Figure 3.1**). Indeed, the inherent risk to the cell of renegade BAX activation may underlie the mechanistic basis for its multifaceted regulation.

In its conformationally inactive state, BAX is predominantly cytosolic, but in response to stress, BH3-only direct activator proteins, such as BIM, BID, and PUMA, can directly engage an α1/α6 binding site, which triggers the initiating conformational changes of BAX activation[3-6] (**Figure 3.1, orange**). BAM7, the first described BAX-activating compound, mimics the effect of BH3 binding at the trigger site[7]. This first, dynamic activation step may be followed by transient BH3-interactions with the canonical hydrophobic groove to propagate BAX homo-oligomerization[8] **(Figure 3.1, cyan**). Other BAX-activating compounds such as SMBA1 and Compound 106 have been suggested to target the canonical site to induce apoptosis[9,10].

Conversely, there are several mechanisms that inhibit BAX and prevent its activation. The canonical mechanism involves the sequestration of the BAX BH3 α-helix by the surface groove of anti-apoptotic BCL-2 family members. In addition, the BCL-2 BH4 α-helix has been shown to bind BAX at a distinct region defined by the α1, α1–α2 loop, and α2–α3 and α5–α6 hairpins of BAX (**Figure 3.1, yellow**)[11]. The BH4 helix preserves the inactive state of BAX by preventing its

conformational activation by BH3 helices. The third mechanism of inhibition is exemplified by the cytomegalovirus viral mitochondria-localized inhibitor of apoptosis (vMIA). The vMIA protein was identified based on its ability to block cytochrome c release, thereby preventing cell death in infected host cells[12]. It was later shown that vMIA mediates this anti-apoptotic function by directly binding to BAX and, paradoxically, recruiting BAX to the mitochondria[13,14]. Despite sharing functional roles, vMIA has no homology with the BCL-2 family and does not utilize a surface groove to sequester BAX. Instead, the BAX-binding domain of vMIA forms a partially α-helical ligand, which engages BAX at a discrete regulatory site[15] (**Figure 3.1, purple**). This interaction allows vMIA to inhibit BAX by stabilizing an inactive conformation at the mitochondrial outer membrane, thereby preventing further activation and oligomerization.

As detailed in Chapter 2, a fragment-based screen and subsequent validation studies identified BIF-44 as a BAX-sensitizing compound. Given this novel molecular functionality, we sought to further characterize the BIF-44 interaction and specifically determine its site of BAX engagement.

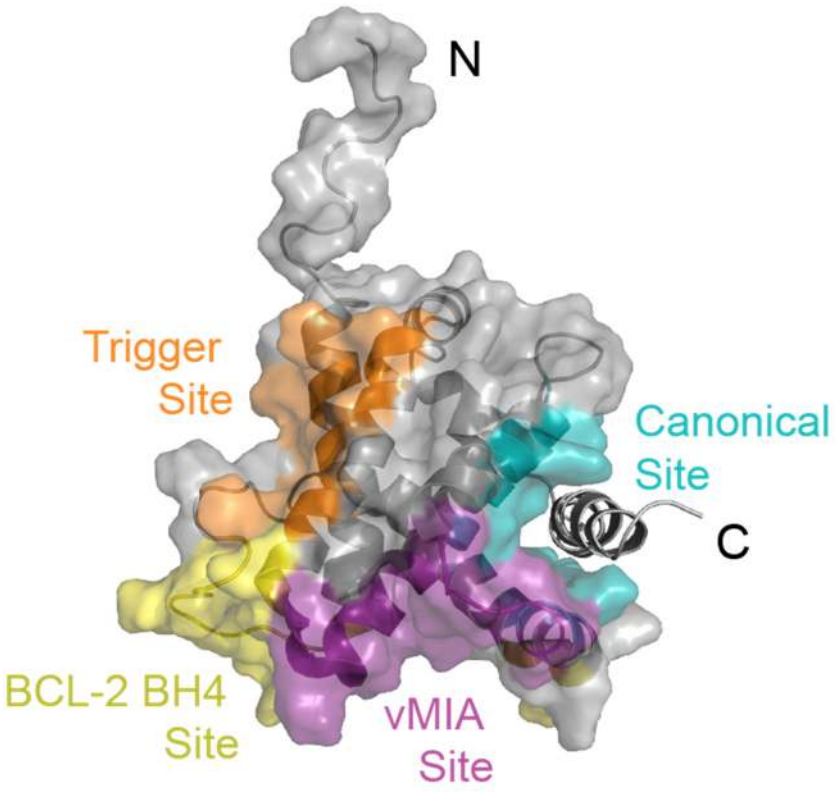

Figure 3.1 *BAX contains a series of surface grooves that regulate its pro-apoptotic activity*. BH3 interactions at the trigger (orange) and canonical (cyan) sites initiate and propagate BAX activation, respectively, whereas engagement at the BCL-2 BH4 domain (yellow) and vMIA (purple) sites inhibit BAX activation. PDB:1F16

METHODS

Peptide Synthesis

Solid-state peptide synthesis using Fmoc chemistry was performed as previously described[16]. The vMIA (^{131}EALKKALRRHRFLWQRRQRA^{150}-$CONH_2$)[15], BCL-2 BH4 $SAHB_A$ (^{13}EIVBKYIHYKL SXRGYXWDA^{32}-$CONH_2$)[11], BIM $SAHB_{A2}$ (^{145}EIWIAQELRXIGDXFNAYY A^{164}-$CONH_2$)[5], PUMA $SAHB_A$ (^{132}EEQWAREIGAQLRXBADXLNAQYERR^{155}-$CONH_2$)[3], and BAX $SAHB_A$ (^{56}TKKLSECL KXIGDXLDSNBE^{75}-$CONH_2$)[4] peptides (X, (*S*)-*N*-2-(4′-pentenyl)alanine; B, norleucine) were N-terminally derivatized with either an acetyl group or fluorescein isothiocyanate (FITC)-β-alanine for the indicated applications in NMR and biochemical experiments. Peptides were purified by LC-MS to >95% purity and quantified by amino acid analysis. Lyophilized peptides were reconstituted in 100% DMSO or DMSO-d_6 and diluted into the indicated aqueous buffers for experimental use.

Expression and Purification of Full-length BAX.

Recombinant, full-length BAX was expressed in BL21 (DE3) *E. coli* using the pTYB1 vector[1,5]. Cell pellets were resuspended in 20 mM Tris, 250 mM NaCl, pH 7.2 and lysed by two passes through a microfluidizer (Microfluidics) chilled to 4°C. The lysate was clarified by centrifugation at 20,000 rpm. BAX was purified by batch affinity binding at 4°C using chitin resin (New England Biolabs), followed by loading onto gravity flow columns for washing and elution. The intein-chitin binding domain tag was cleaved by 36 hour incubation in 50 mM dithiothreitol at 4°C. Pure protein was isolated by size exclusion chromatography (Superdex 75 10/300; 20 mM HEPES, 150 mM KCl, pH 7.2 or 20 mM potassium phosphate, pH 6.2) using an FPLC system (GE Healthcare Life Sciences).

Liposomal Release Assay

Large unilamellar vesicles (LUVs) were formed by liposome extrusion[6,17]. Briefly, a lipid mixture containing a 48:28:10:10:4 molar ratio of phosphatidylcholine, phosphatidylethanolamine,

phosphatidylinositol, dioleoyl phosphatidylserine, and tetraoleolyl cardiolipin (Avanti Polar Lipids) was generated in chloroform. Lipid films were formed by evaporation, initially under nitrogen gas and then by overnight vacuum. Lipid films were hydrated in 1 mL assay buffer (10 mM HEPES, 200 mM KCl, 1 mM $MgCl_2$, pH 7.0) and mixed with the fluorophore/quencher pair, 8-aminonaphthalene-1,3,6-trisulfonic acid (ANTS, 12.5 mM) and p-xylene-bis-pyridinium bromide (DPX, 45 mM). Liposomes were formed by 5 freeze/thaw cycles followed by extrusion through a 100 nm polycarbonate membrane and purified using a Sepharose CL-2B size-exclusion column. For measurement of BAX activation, BAX (750 nM) was added to the indicated concentration of BIF-44 in the presence of liposomes, followed by the specified BAX-triggering condition. BIF-44 (4-phenoxyphenol) was ordered commercially (Alfa Aesar, 99% purity). ANTS/DPX release was monitored over time at room temperature in a spectrofluorometer (Tecan Infinite M1000) using an excitation wavelength of 355 nm, an emission wavelength of 540 nm, and a bandwidth of 20 nm. Maximal release was determined by the addition of Triton X-100 to a final concentration of 0.2% (v/v). Percent release was calculated as $((F-F_0)/(F_{100}-F_0)) \times 100$, where F is the observed fluorescence at a given time, and F_0 and F_{100} represent baseline and maximal fluorescence, respectively.

Mitochondrial Cytochrome c Release Assay

Liver mitochondria from *Alb*^{Cre}*Bax*$^{f/f}$*Bak*$^{-/-}$ mice were isolated and release assays performed as described[18]. Briefly, mitochondria (0.5 mg/mL) were incubated with 100 nM BAX, 250 nM BIM $SAHB_{A2}$ and/or the indicated concentrations of BIF-44 (Alfa-Aesar, 99% purity) for 45 min at room temperature in experimental buffer (200 mM mannitol, 68 mM sucrose, 10 mM HEPES-KOH [pH 7.4], 110 mM KCl, 1 mM EDTA, protease inhibitor)[19]. The pellet and supernatant fractions were isolated by centrifugation, and cytochrome c was quantitated using a colorimetric ELISA assay (R&D Systems). Percent cytochrome c released into the supernatant (%cyto *c* release) was calculated according to the following equation: %cyto *c* release = [cyto c_{sup}]/ [cyto c_{max}]*100, where

cyto c_{sup} and cyto c_{max} represent the amount of cytochrome *c* detected in the supernatant of compound- or 1% (v/v) Triton X-100-treated samples, respectively.

Competition STD NMR

Individual fragments (final compound concentration of 300 μM) were added to 5 μM unlabeled, full-length human BAX with or without 5 μM competitor peptide in 20 mM potassium phosphate buffer, pH 6.2 in 10% (v/v) D_2O. STD NMR measurements were acquired at 25°C on a Varian Inova 500-MHz spectrometer equipped with a helium-cooled cryoprobe. Low power saturation of the protein was achieved with a series of 50 ms Gaussian pulses for a total of 3 seconds; on-resonance irradiation was performed at 0.8 ppm, and off-resonance irradiation at 30 ppm. Standard excitation sculpting was used for solvent suppression. Fragments that were competed by peptide showed a decrease in STD difference spectra intensity in the presence of peptide, relative to no peptide.

Fluorescence Polarization Assay

FITC-peptide (25 nM) was incubated with a serial dilution of recombinant, full-length BAX in binding buffer (20 mM potassium phosphate, pH 6.2). For competitive FP, FITC-peptide (25 nM) was mixed with a fixed concentration of BAX (250 nM) and incubated with a serial dilution of acetylated peptide or molecular fragment. Fluorescence polarization was measured at equilibrium using a SpectraMax M5 microplate reader. Nonlinear regression analysis of dose-response curves was performed using Prism software 7 (GraphPad).

HSQC NMR

Uniformly ^{15}N-labeled recombinant BAX (50 μM) was generated as previously described[1,5]. Protein samples with the indicated molar ratio of fragment were prepared in 25 mM sodium phosphate, 50 mM NaCl solution at pH 6.0 in 10% (v/v) D_2O. Correlation ^{1}H-^{15}N HSQC spectra

were acquired at 25°C on a Bruker 600 MHz NMR spectrometer equipped with a cryogenic probe, processed in Topspin (Bruker) and analyzed using CcpNmr Analysis[20]. The weighted average chemical shift difference was calculated as $\Delta=\sqrt{1/2 \times ((\Delta H)^2 + (\Delta N/5)^2)}$ [21], where ΔH and ΔN are the respective changes in p.p.m. of ^{1}H or ^{15}N chemical shift for the indicated crosspeak. The absence of a bar indicates no chemical shift difference, or the presence of a proline or residue that is overlapped or not assigned. BAX cross-peak assignments were applied as previously reported[1]. The significance threshold for the chemical shift changes was calculated based on the average chemical shift across all residues plus the standard deviation, in accordance with standard methods[4,5].

Binding Site Analysis

The FTsite and FTdyn web servers (ftsite.bu.edu; ftdyn.bu.edu) were used for binding site prediction and dynamic ensemble mapping, respectively[22]. All site prediction analyses were run using default parameters.

RESULTS

BIF-44 Dose-responsively Sensitizes BAX Activation by Multiple Stimuli

The functional effect of BIF-44 on BAX was identified in a single-dose functional screen. To further confirm the sensitization activity, we tested BIF-44 across a broad range of concentrations from 10–175:1 molar ratio of BIF-44 to BAX. While BIF-44 demonstrated little to no independent triggering effect on BAX-mediated liposomal release (**Figure. 3.2a**), in the presence of BIM $SAHB_{A2}$, BIF-44 dose-responsively enhanced both the kinetics and maximum level of BAX-mediated liposomal release (**Figure. 3.2b, Appendix: Table S.3**). We also found that the maximum level of liposomal release achieved upon BIF-44 sensitization was independent of the order of addition of the BIF-44 and BIM $SAHB_{A2}$ ligands (**Figure. 3.3**). This suggests that BIF-44 can cooperate with BIM $SAHB_{A2}$ and support the activation a population of BAX that cannot be readily triggered by BIM $SAHB_{A2}$ alone.

To determine if the observed sensitization effect is generalizable and not specific to BIM $SAHB_{A2}$-induced activation, we tested the ability of BIF-44 to sensitize other BAX-activation stimuli. Stapled peptides corresponding to the BH3 helix of the direct activator PUMA (PUMA $SAHB_A$)[3] and BAX itself (BAX $SAHB_A$)[4] can trigger BAX activation in an analogous manner to BIM $SAHB_{A2}$. When BIF-44 is added to these SAHBs, both the rate and maximal amount of liposomal release increase (**Figure. 3.4 a,b**). Beyond BH3-based activators, BIF-44 sensitized BAX to activation by heat[23] and recombinant BIM_L protein[24] (**Figure. 3.4, c,d**). These experiments demonstrated that BIF-44 can bolster the effect of a wide range of BAX activators, suggesting that BIF-44 acts by directly modulating BAX and rendering it more sensitive to activation. Finally, to link these findings to a physiologic context, we tested the capacity of BIF-44 to sensitize BAX-mediated release of cytochrome *c* from mitochondria. Purified mouse liver mitochondria were treated with BIF-44 and BIM $SAHB_{A2}$, both singly and in combination, and the level cytochrome c in the supernatant was quantified using a sandwich ELISA assay. BIF-44 alone had no effect on the release of cytochrome *c*. However, consistent with the synergy in observed in liposomal

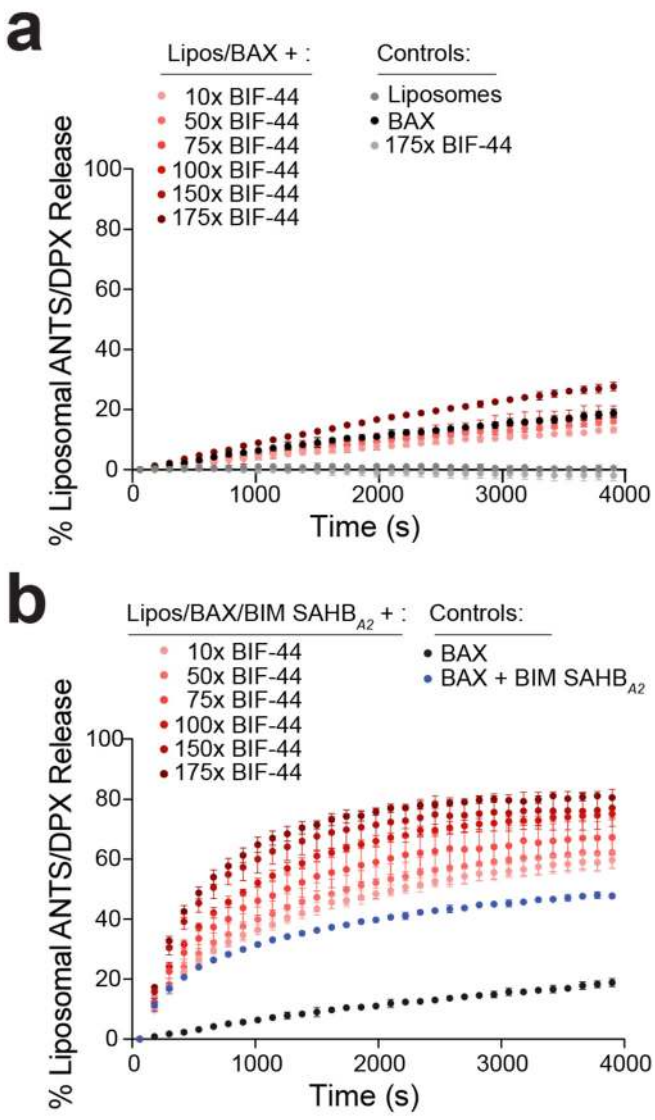

Figure 3.2 *BIF-44 dose-responsively sensitizes BAX activation.*

(**a**) Liposomal release assays demonstrate little to no direct, BAX-activating effect of BIF-44 across a broad dose range, but dose-responsively sensitizes BH3-triggered direct BAX activation upon co-incubation with BIM SAHB$_{A2}$ (**b**). Error bars are mean ± SD for experiments performed in technical triplicate and repeated twice more with similar results using independent liposomal and protein preparations. BAX, 0.75 μM; BIM SAHB$_{A2}$ 0.75 μM; BIF-44, 7.5 μM–131 μM (10x–175x)

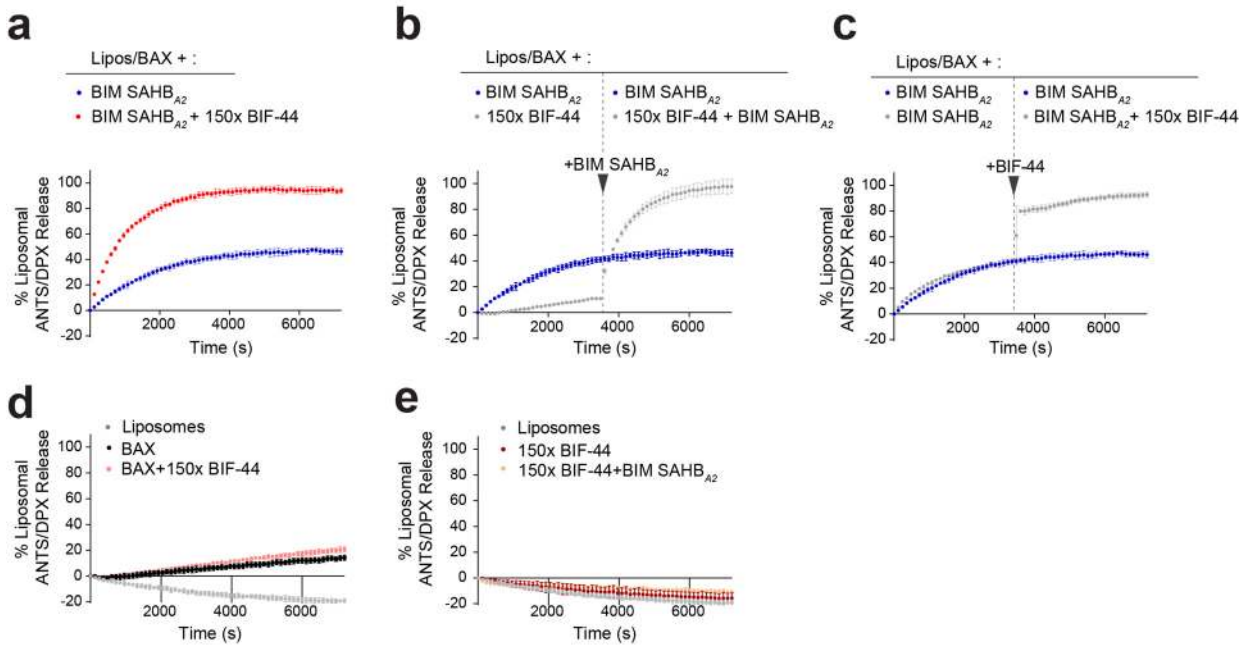

Figure 3.3 *BIF-44 sensitization of BAX is independent of the order of addition.*

In the BAX-mediated liposomal release assay induced by BIF-44 and BIM SAHB$_{A2}$, the same maximal level of release is achieved whether BIF-44 is added simultaneously (**a**), before (**b**) or after (**c**) the addition of BIM SAHB$_{A2}$. Control conditions are shown in (**d–e**). BAX, 0.75 μM; BIM SAHB$_{A2}$ 0.75 μM; BIF-44, 113 μM (150x). Error bars for are mean ± SD for experiments performed in technical triplicate and repeated with similar results using independent liposomal and protein preparations.

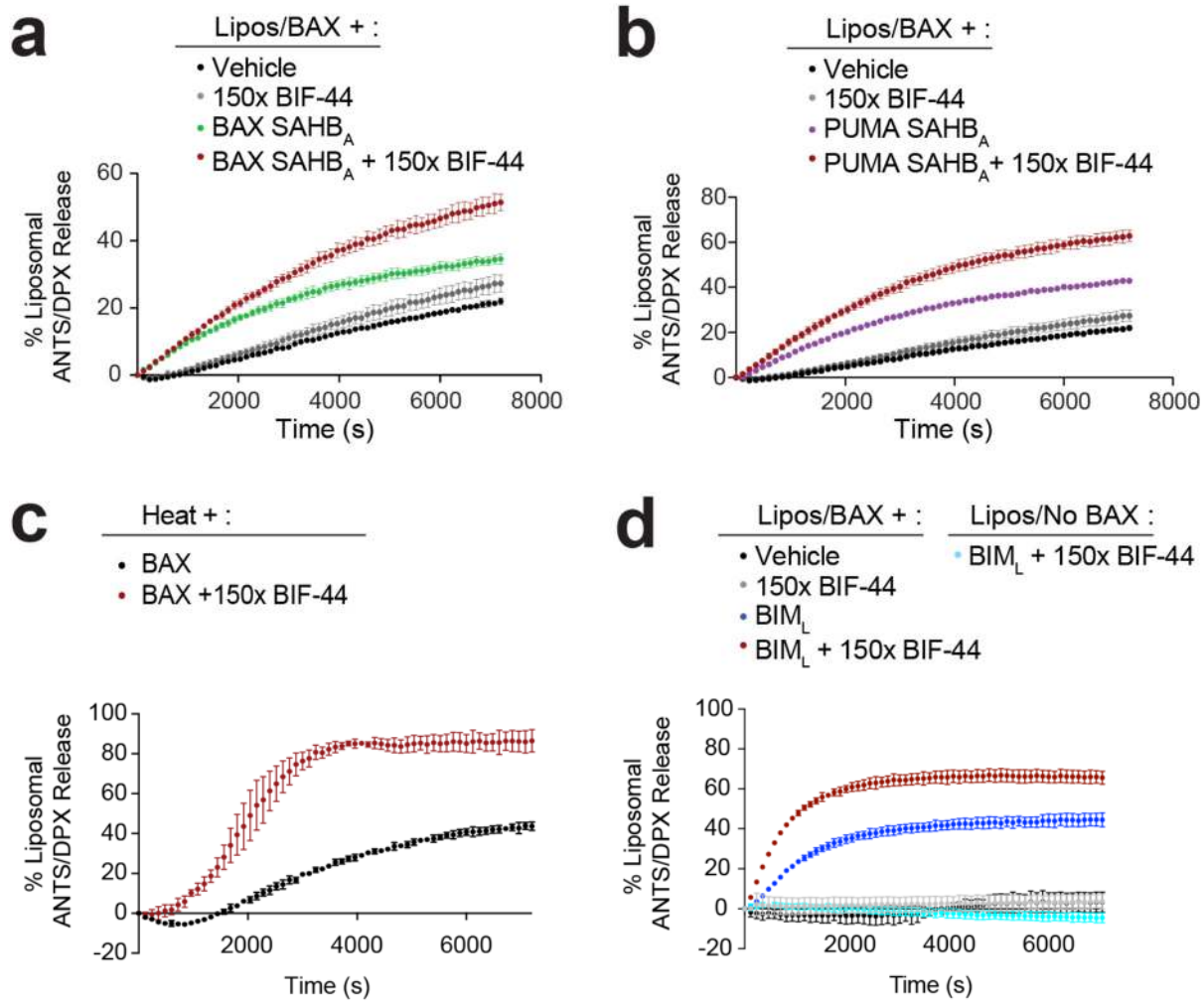

Figure 3.4 *BIF-44 sensitizes BAX activation in response to diverse stimuli.*

BIF-44 sensitizes BAX-mediated liposomal release to the indicated BAX activation stimulus (**a**) BAX SAHB$_A$, 0.75 μM (1x) (**b**) PUMA SAHB$_A$ 1.5 μM (2x) (**c**) heat, 37°C (**d**) BIM$_L$, 20 nM (0.03x) (**d–e**) BAX, 0.75 μM; BIF-44, 113 μM (150x). Error bars are mean ± SD for experiments performed in technical triplicate and repeated with similar results using independent liposomal and protein preparations.

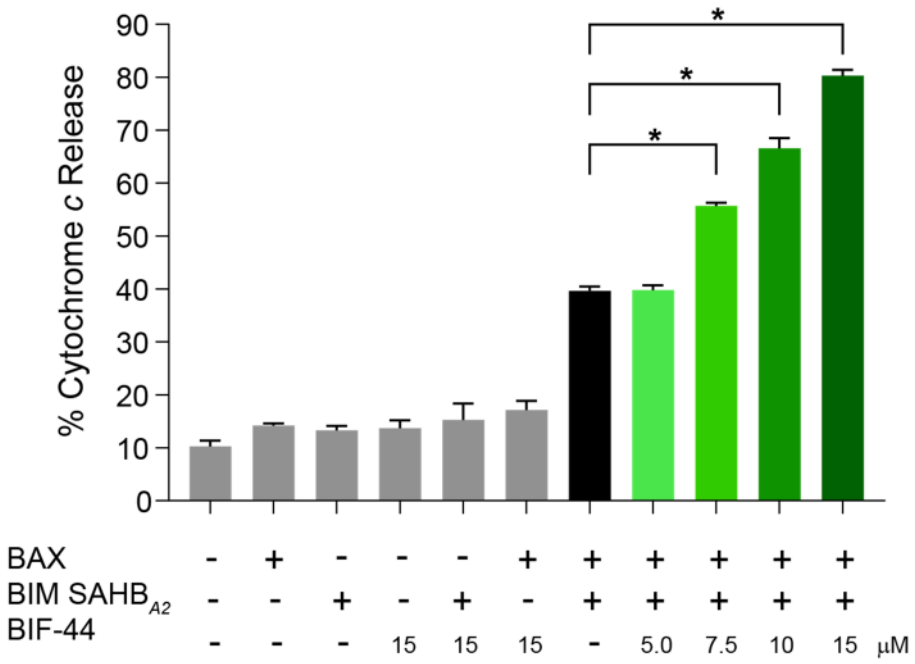

Figure 3.5 *BIF-44 sensitizes BIM SAHB$_{A2}$-triggered cytochrome c release.*

BIF-44 dose-responsively sensitizes BIM SAHB$_{A2}$-triggered, BAX-mediated cytochrome *c* release from isolated *Alb*^{Cre}*Bax*$^{f/f}$*Bak*$^{-/-}$ mouse liver mitochondria. Levels of cytochrome *c* in the supernatant were quantified by sandwich ELISA. Error bars are mean ± SD for experiments performed in technical triplicate, and repeated twice more with similar results using independent preparations and treatments of mitochondria. 100 nM BAX, 250 nM BIM SAHB$_{A2}$, BIF-44, 5–15 μM; *, $p < 0.001$, as calculated by one-way ANOVA analysis.

assays, BIF-44 dose-responsively sensitized BIM SAHB$_{A2}$-induced triggering of BAX-mediated cytochrome *c* release from mitochondria (**Figure 3.5**).

Identification of the BIF-44 Binding Site on BAX

In the characterizing the direct BAX activator molecules (BAMs), BAMs were shown to directly compete with BIM SAHB$_{A2}$ for binding at the BH3-trigger site of BAX[7]. To further evaluate the newly-identified BAX-sensitization activity, we sought to determine the BIF-44 binding site on BAX. We first tested whether BIM SAHB$_{A2}$ could compete with BIF-44 for BAX ineraction using a competitive STD NMR approach. If the addition of a competitive peptide binds to the same site and displaces BIF-44, this appears as a decrease in the magnitude of the peak STD difference spectrum[25]. Surprisingly, we found that BIM SAHB$_{A2}$ had no effect on the STD signal of BIF-44 (**Figure 3.6**). We confirmed the absence of BIM SAHB$_{A2}$ competition for BIF-44 engagement of BAX using the alternative method of competitive fluorescence polarization assay. For this experiment, we employed the direct interaction between fluorescein isothiocyanate (FITC)-BIM SAHB$_{A2}$ and BAX (**Figure 3.7a**) as the basis for comparative competition by N-terminal acetylated BIM SAHB$_{A2}$ and BIF-44. Whereas Ac-BIM SAHB$_{A2}$ dose-responsively competed with FITC-BIM SAHB$_{A2}$ for BAX binding, BIF-44 had little to no effect (**Figure 3.7b**). These data raised the intriguing possibility of an alternative mechanism, beyond engagement of the BH3 trigger site, for BIF-44-mediated sensitization of BAX.

As part of our workflow to screen for compounds that might bind to and inhibit BAX, we also tested whether the identified BIFs could compete with the inhibitory vMIA peptide for BAX interaction. vMIA is a cytomegalovirus protein implicated in blocking BAX-mediated apoptosis, which ensures host cell survival during viral infection and replication[13,14]. Mutational analysis revealed a BAX-binding domain within the vMIA protein and this region is essential to modulate the vMIA-BAX binding interaction and its inhibitory function[13,14]. A synthetic peptide corresponding to this domain was shown to bind BAX at a discrete pocket formed by the flexible loops between

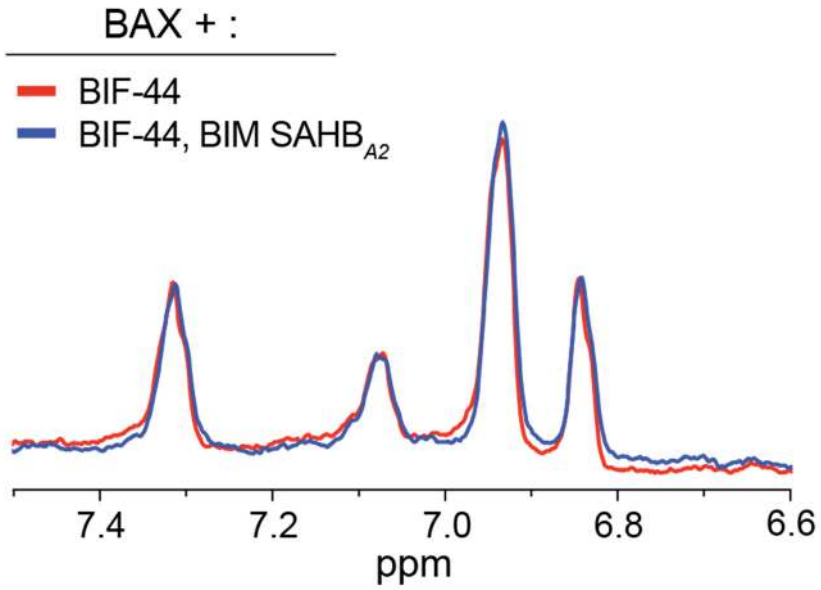

Figure 3.6 *BIF-44 does not compete with BIM SAHB$_{A2}$ by competitive STD NMR*.

STD NMR difference spectra of BIF-44/BAX in the presence (**blue**) or absence (**red**) BIM SAHB$_{A2}$. NMR data are representative of two independent experiments; BAX, 5 μM; BIM SAHB$_{A2}$, 5 μM; BIF-44, 300 μM.

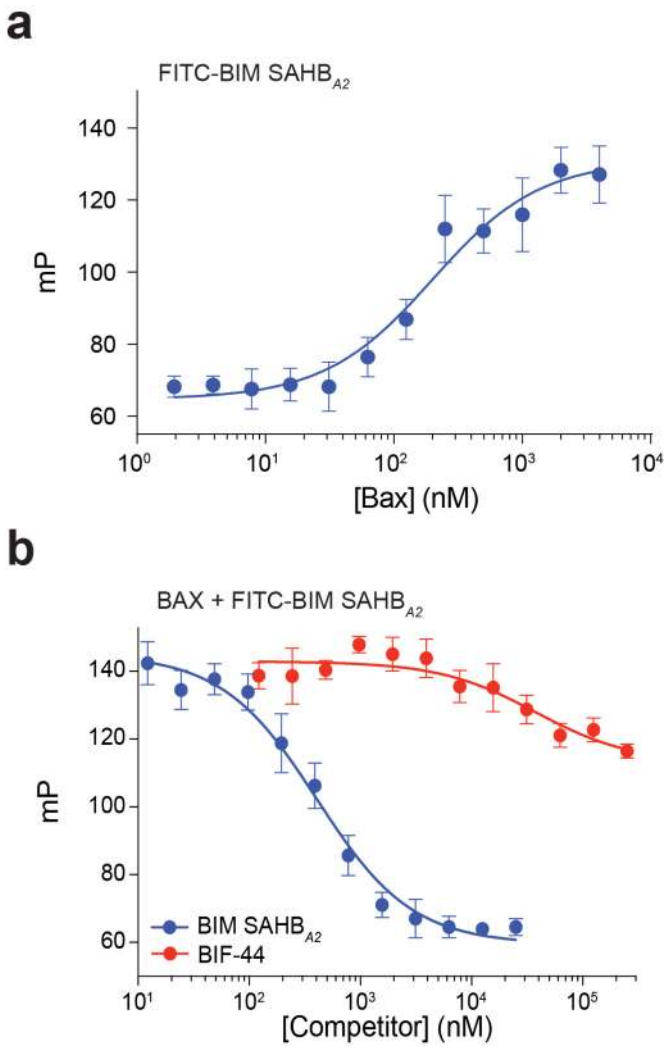

Figure 3.7 *BIF-44 does not compete with BIM SAHB$_{A2}$ by competitive FP*.

(**a**) Fluorescence polarization (FP) assay demonstrates direct interaction between BAX and the FITC-BIM SAHB$_{A2}$ (**b**) Competitive FP analysis of the FITC-BIM SAHB$_{A2}$/BAX interaction in the presence of Ac-BIM SAHB$_{A2}$ (blue) or BIF-44 (red). Error bars are mean ± SD for experiments performed in technical quadruplicate and repeated with similar results using independent reagent preparations. FITC- BIM SAHB$_{A2}$, 25 nM; BAX, 250 nM.

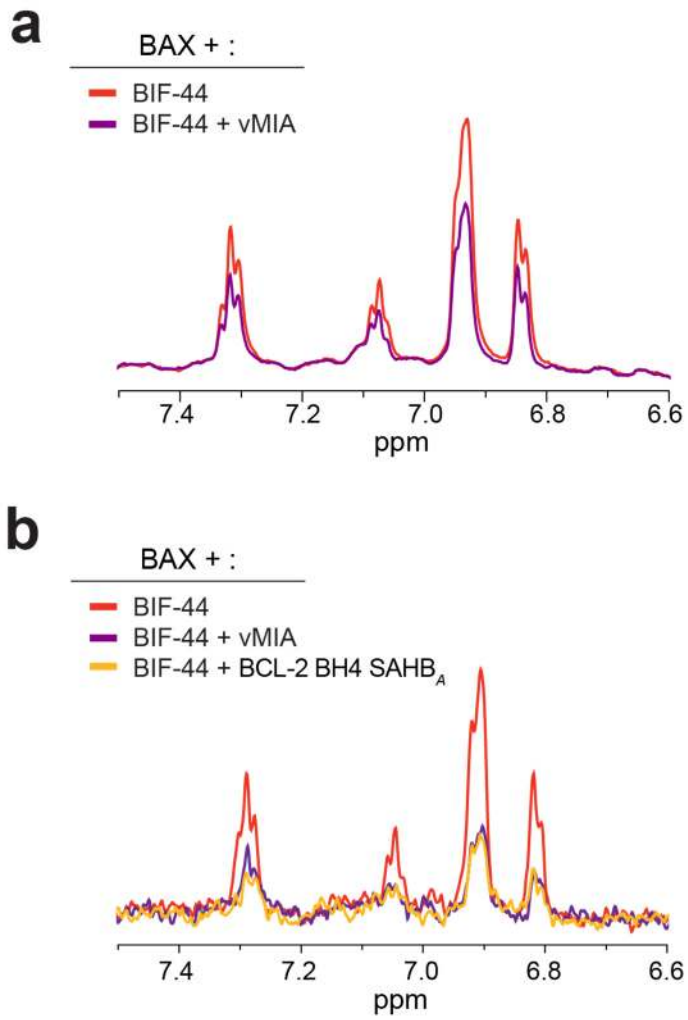

Figure 3.8 *BIF-44 competes with vMIA and BCL-2 BH4 by competitive STD NMR.*

Competitive STD NMR demonstrates a decreased BIF-44 STD signal in the presence of (**a**) vMIA peptide or (**b**) BCL-2 BH4 SAHB$_{A.}$ (**a-b**) STD NMR difference spectra of BIF-44/BAX in the presence of vMIA peptide (purple) or BCL-2 BH4 SAHB$_A$ (yellow). or absence of either competitor (red). BAX, 5 μM; vMIA or BCL-2 BH4 SAHB$_A$, 5 μM; BIF-44, 300 μM.

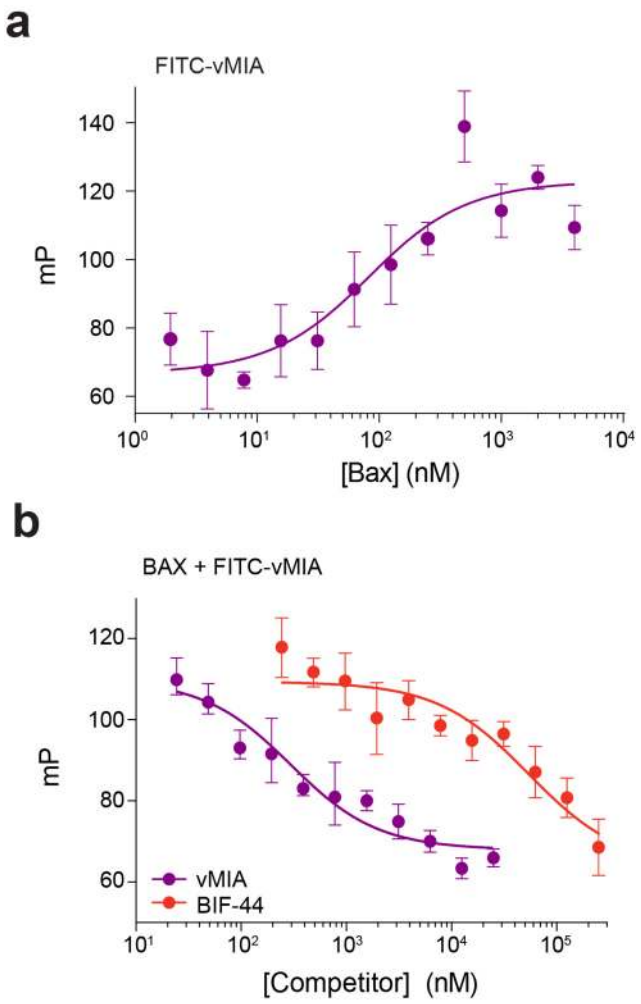

Figure 3.9 *BIF-44 competes with vMIA by competitive FP.*

a) Fluorescence polarization (FP) assay demonstrates direct interaction between BAX and the FITC-vMIA peptide (**b**) Competitive FP analysis of the FITC-BIM SAHB$_{A2}$/BAX interaction in the presence of Ac-vMIA peptide (purple) or BIF-44 (red). Error bars are mean ± SD for experiments performed in technical quadruplicate and repeated with similar results using independent reagent preparations. FITC-vMIA, 25 nM; BAX, 250 nM.

helices α1/α2, α3/α4, and α5/α6 and a portion of the C-terminal α9 helix (**Figure 3.1**)[15]. By stabilizing the α3–α4 and α5–α6 hairpins, vMIA prevents BAX-activating conformational changes from occurring[15]. Much to our surprise, we observed a reduction in the BIF-44 STD signal upon co-incubation with vMIA peptide (**Figure 3.8a**). A BCL-2 BH4 domain helix, which suppresses BAX activation by engaging a groove formed by α1, α1–α2 loop, and α2–α3 and α5–α6 hairpins in the immediate vicinity of the vMIA binding site[11] (**Figure 3.1**), also competes with BIF-44 for BAX interaction, as assessed by STD NMR (**Figure 3.8b**). To confirm that the vMIA peptide competes with BIF-44 for BAX binding, we applied the competitive fluorescence polarization assay, which revealed the dose-responsive displacement of the FITC-vMIA/BAX interaction by BIF-44 (**Figure 3.9**).

As the vMIA binding site had not been previously characterized to bind small molecules, we wanted to test the likelihood of any small molecule binding at this location. Binding sites can be predicted computationally by docking a panel of small organic molecules with different shapes and polarity[22]. The clustering of these probes in the same region of the protein can be used to identify protein “hot-spots”, regions that significantly contribute to the ligand binding free energy[26]. Overall, this method reveals the most important binding surfaces on a protein and can determine the relative “druggability” of any given site. Intriguingly, the vMIA binding pocket emerges as a ligand-binding “hot spot” based on analyses of the BAX structure (PDB ID 1F16) using the FTsite and FTdyn algorithms[22] (**Figure 3.10)**. This analysis further supports the plausibility of BIF-44 binding to a site that overlaps with that of vMIA.

Given the surprising finding that BIF-44, a BAX sensitizer, engages an “inhibitory” binding site, we sought to more definitively define the BIF-44 interaction site on BAX. One powerful technique for binding site identification is ^{1}H-^{15}N heteronuclear single quantum coherence (HSQC) NMR spectroscopy. Since ligand engagement alters the local chemical environment, changes in amide chemical shift can be measured and then mapped back to the structure of the protein. We

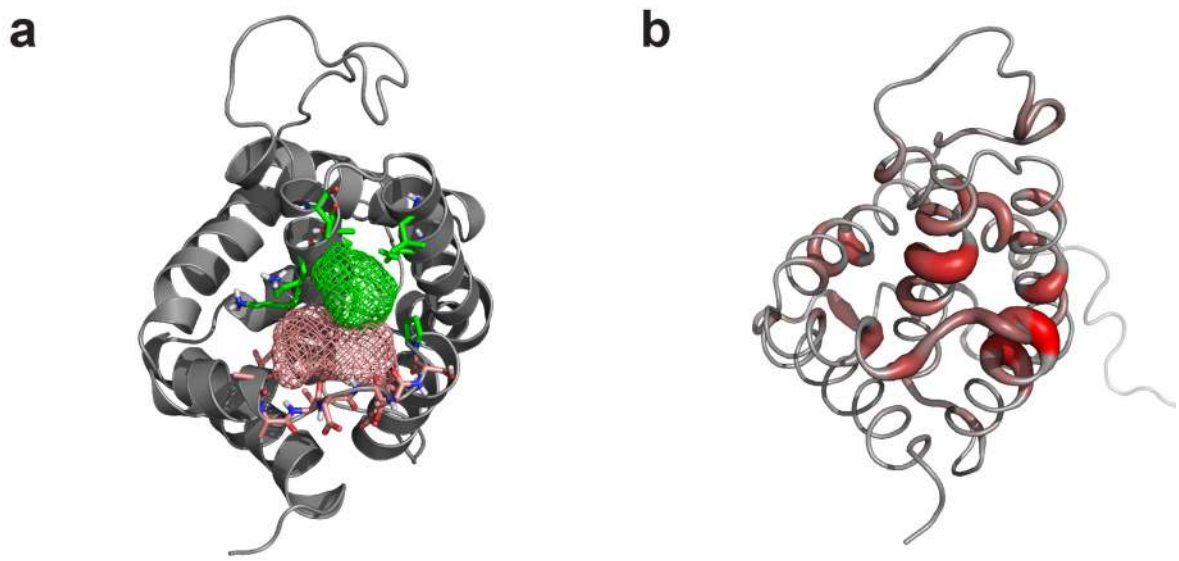

Figure 3.10 *BIF-44 binding site coincides with ligand binding "hot spot" on BAX.*

(**a**) The region of the predicted BIF-44 binding site was identified as a ligand binding "hot spot" (green, pink) using the FTsite algorithm. (**b**) Dynamic ensemble mapping (FTdyn), which incorporates all twenty structures of the BAX ensemble (PDB ID 1F16), identified this same region as a likely ligand-binding site. The color gradient (red) and thickness of the ribbon structure are proportional to the average number of interactions for each amino acid residue with the small molecule probes used in the analysis.

performed HSQC NMR of ^{15}N-BAX upon BIF-44 titration and identified a series of focal, dose-responsive chemical shift changes that colocalized to the vMIA binding site on BAX (**Figure 3.11**, **Figure 3.12**). The most prominent changes (2 SD) localized to the junction of the α3–α4 and α5–α6 hairpins, which juxtapose to form a binding interface (**Figure 3.11**). Especially intriguing are more subtle changes (1 SD) that become amplified with increasing BIF-44 dosage and localize both to the internal helical regions of α5 and α6 (BAX's hydrophobic core), and the neighboring internal interaction surfaces between α1 and α2 (**Figure 3.11** and **Figure 3.12**), the latter helix being the critical BH3 motif that must become exposed for BAX activation and oligomerization to ensue. Thus, these NMR data not only corroborated our STD and FP data with respect to BIF-44 competition with vMIA at a strikingly similar interaction site, but also suggested that BIF-44 interaction induces structural changes transmitted through the α5–α6 hydrophobic core to the internal surfaces of α1 and α2, a region implicated in BIM BH3-mediated direct activation of BAX at its N-terminal surface[4,5].

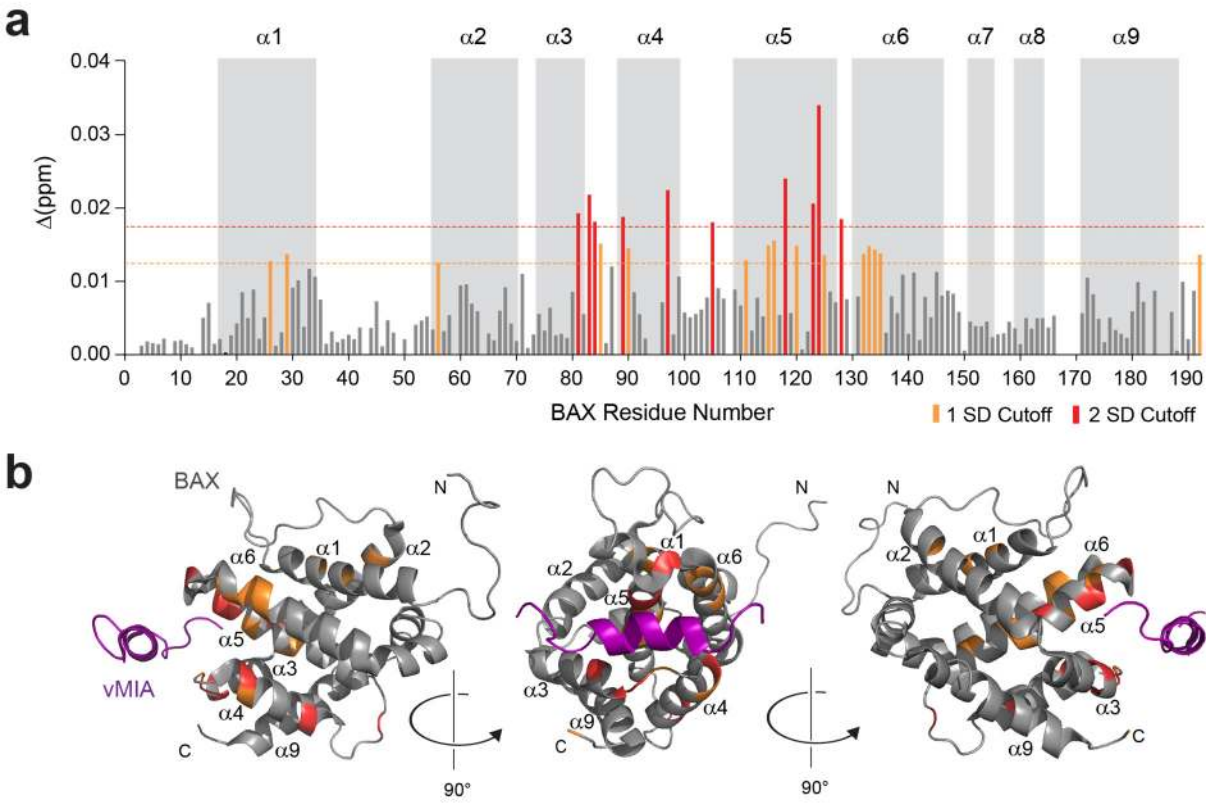

Figure 3.11 *BIF-44 targets the vMIA-binding region of BAX.*

(**a**) Measured chemical shift changes of ^{15}N-BAX (50 μM) upon addition of BIF-44 (6:1, BIF:BAX), plotted as a function of BAX residue number. Chemical shift changes above the 2 SD cutoff (≥ 0.018 ppm significance threshold) are colored red and localize to the junction of the α3/α4 and α5/α6 hairpins. Significant changes at the 1 SD cutoff (≥ 0.012 ppm significance threshold) are colored orange and encompass internal residues of the α5 and α6 core and discrete, juxtaposed residues of α1 and α2. (**b**) Residues represented as red and orange bars in (**a**) are mapped onto the ribbon diagrams of BAX (PDB ID 2LR1).

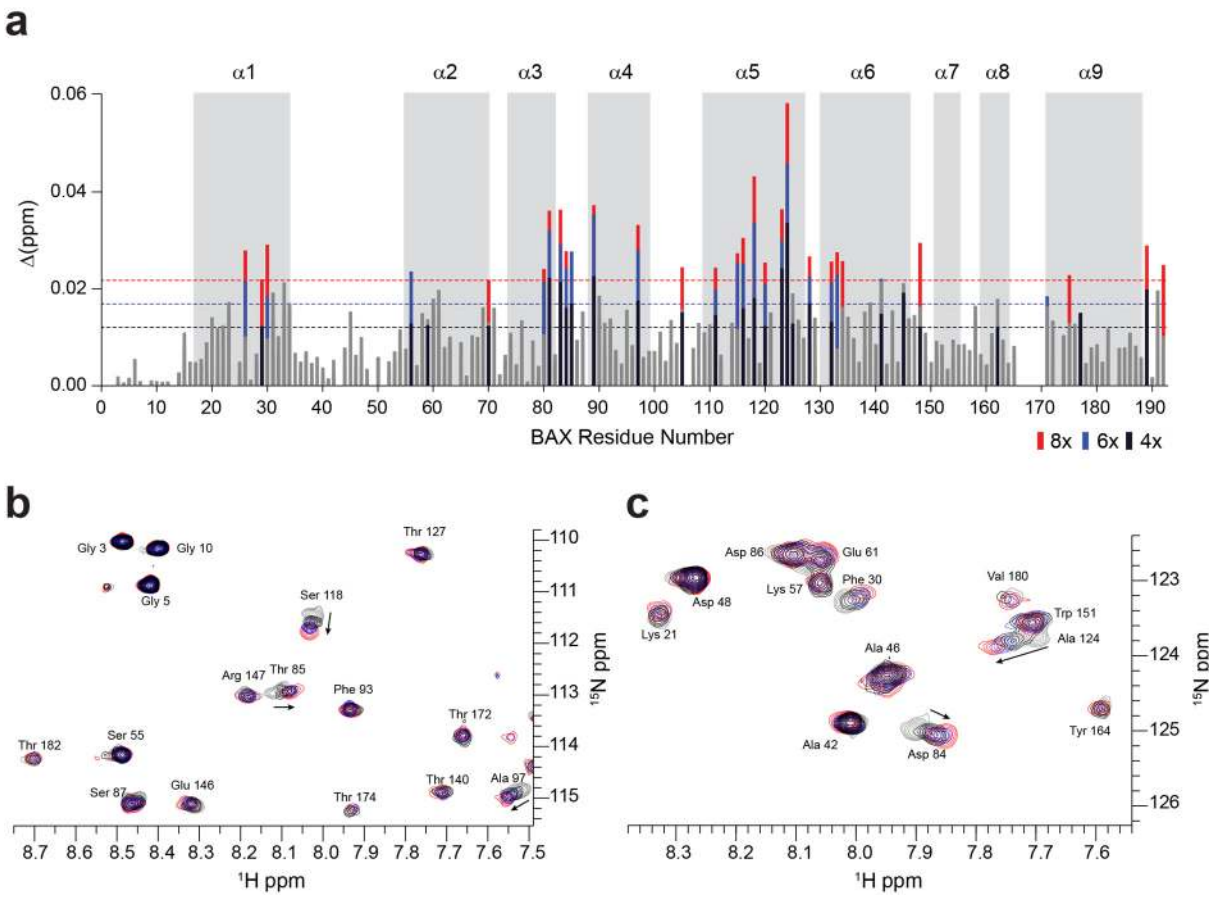

Figure 3.12 *HSQC analysis of ^{15}N-BAX upon BIF-44 titration.*

(**a**) Measured chemical shift changes of ^{15}N-BAX upon addition of BIF-44 at ratios of 4:1, 6:1, and 8:1 (BIF:BAX), plotted as a function of BAX residue number. Significant changes at a 1 SD cutoff threshold for each dosing ratio (≥ 0.012, 0.018, and 0.022 ppm significance thresholds) are colored black, blue, and red, respectively. (**b–c**) Two exemplary regions of the HSQC spectra showing specific, dose-dependent peak shifts. The direction of significant shifts is indicated by a black arrow.

DISCUSSION

The discovery by Gavathiotis *et al.* that small molecules, such as BAM7, can bind to BAX and trigger its activation, suggested that BAX is amenable to targeting by small molecules[7]. Using an NMR-based fragment screening approach, we identified BIF-44 as a molecule that can bind to BAX and sensitize BH3-mediated activation (Chapter 2). Using dose-responsive liposomal and mitochondrial release assays, we confirmed a robust, reproducible BAX sensitization effect that is independent of the order of component addition. Furthermore, this effect extended to activation by other stimuli including PUMA $SAHB_A$, BAX $SAHB_A$, BIM_L protein, and heat. Together, these results suggested that BIF-44 induces changes in BAX binding that render it more amenable to activation by a variety of stimuli.

A critical step in the characterization of a small molecule is the identification of its binding site on the protein target. BAX has four regulatory binding sites that have been identified to date. As small molecule sensitization of BAX has not been previously described, we sought to determine if any of these sites could be the location of BIF-44 interaction. To localize the binding site, we employed a series of assays, including competitive STD NMR, competitive FP, and ^{1}H-^{15}N HSQC NMR. Paradoxically, the binding site for this molecule was not at one of the established BH3 interaction sites[5,6], but instead at a discrete region previously reported to mediate BAX inhibition by the cytomegalovirus vMIA protein[15]. NMR analysis suggested that this molecular interaction transmitted chemical shift changes through the protein core to the N-terminal region of the protein that includes the BH3 helix, suggesting a possible allosteric effect.

The process of BAX activation is dynamic, requiring dramatic structural rearrangements that transform inactive, cytosolic BAX into a homo-oligomeric mitochondrial pore. The results presented here suggest that the BIF-44 binding region could be a site of structural vulnerability for BAX. A distinct BAX activator molecule, OICR766A, was recently identified by a liposomal release assay screen[27]. While the exact binding site is unknown, the BAX binding and activating activity of OICR766A are dependent on cysteine 126, a residue located within the $\alpha5$–$\alpha6$ hairpin.

This suggests that OICR766A may engage BAX at a site proximal to that of BIF-44. Thus, molecule-induced perturbations in this region may be especially capable of promoting BAX sensitization or activation.

To avoid renegade BAX activation and oligomerization in cells, several mechanisms have arisen to prevent or block BAX-activating conformational changes. The most established mechanism is that of the entrapment of the activated, BH3-exposed form of BAX by the canonical surface groove of anti-apoptotic BCL-2 family proteins. By engaging BAX at the confluence of the α3–α4 and α5–α6 hairpins, vMIA can stabilize BAX in a conformation at the mitochondria that prevents its terminal activation[15]. BCL-2 BH4 engages BAX at an adjacent, yet distinct binding site (defined by the α1, α1–α2 loop, and α2–α3 and α5–α6 hairpins) and preserves the inactive state of BAX by preventing the N-terminal rearrangements linked to BH3 initiation of BAX activation. These three mechanisms represent a spectrum of BAX inhibition based on the conformational state of the protein at the point of interdiction. Interestingly, it is the occlusion of the BIF-44 site by the BAX-inhibitory BCL-2 BH4 domain or cytomegalovirus vMIA peptide that specifically prevents the sensitization effect of BIF-44 on BH3-mediated BAX activation.

During tumorigenesis, cancer cells must develop mechanisms to evade apoptotic cell death signaling and ensure survival[28,29]. Frequently, an apoptotic blockade is achieved by upregulating anti-apoptotic proteins. Strategies that remove this blockade by inhibiting anti-apoptotic proteins have proven effective at reactivating apoptosis for therapeutic benefit in patients[30]. An emerging alternative strategy is to overwhelm the anti-apoptotic reserve or bypass the blockade through the direct activation of BAX[7,9,10,27,31]. A potential risk of activating BAX, either directly or indirectly, is the induction of apoptotic cell death in normal tissues, although a therapeutic window has been achieved for venetoclax in humans[32] and for a direct BAX activator in mice[31]. By pharmacologically sensitizing rather than activating BAX, the initial trigger remains

reliant on the expression of BH3-only proteins, which is typically higher in cancer cells, than in normal tissues, potentially providing a therapeutic window.

Our results suggest that the identified BIF-44 binding site, formed by the intersection of the α3–α4 and α5–α6 hairpins, represents a hot spot for sensitizing BAX. Targeting and perturbing the hydrophobic core of the BAX protein in this manner provides both an opportunity to develop novel sensitizers of BAX-mediated apoptosis and a physiologic rationale for direct blockade of this region by BAX-inhibitory motifs such as vMIA and BCL-2 BH4.

REFERENCES

1. Suzuki, M., Youle, R.J. & Tjandra, N. Structure of Bax: coregulation of dimer formation and intracellular localization. *Cell* **103**, 645-54 (2000).

2. Walensky, L.D. & Gavathiotis, E. BAX unleashed: the biochemical transformation of an inactive cytosolic monomer into a toxic mitochondrial pore. *Trends Biochem Sci* **36**, 642-52 (2011).

3. Edwards, A.L. et al. Multimodal interaction with BCL-2 family proteins underlies the proapoptotic activity of PUMA BH3. *Chem Biol* **20**, 888-902 (2013).

4. Gavathiotis, E., Reyna, D.E., Davis, M.L., Bird, G.H. & Walensky, L.D. BH3-triggered structural reorganization drives the activation of proapoptotic BAX. *Mol Cell* **40**, 481-92 (2010).

5. Gavathiotis, E. et al. BAX activation is initiated at a novel interaction site. *Nature* **455**, 1076-81 (2008).

6. Leshchiner, E.S., Braun, C.R., Bird, G.H. & Walensky, L.D. Direct activation of full-length proapoptotic BAK. *Proc Natl Acad Sci U S A* **110**, E986-95 (2013).

7. Gavathiotis, E., Reyna, D.E., Bellairs, J.A., Leshchiner, E.S. & Walensky, L.D. Direct and selective small-molecule activation of proapoptotic BAX. *Nat Chem Biol* **8**, 639-45 (2012).

8. Czabotar, P.E. et al. Bax crystal structures reveal how BH3 domains activate Bax and nucleate its oligomerization to induce apoptosis. *Cell* **152**, 519-31 (2013).

9. Xin, M. et al. Small-molecule Bax agonists for cancer therapy. *Nat Commun* **5**, 4935 (2014).

10. Zhao, G. et al. Activation of the proapoptotic Bcl-2 protein Bax by a small molecule induces tumor cell apoptosis. *Mol Cell Biol* **34**, 1198-207 (2014).

11. Barclay, L.A. et al. Inhibition of Pro-apoptotic BAX by a noncanonical interaction mechanism. *Mol Cell* **57**, 873-86 (2015).

12. Goldmacher, V.S. et al. A cytomegalovirus-encoded mitochondria-localized inhibitor of apoptosis structurally unrelated to Bcl-2. *Proc Natl Acad Sci U S A* **96**, 12536-41 (1999).

13. Arnoult, D. et al. Cytomegalovirus cell death suppressor vMIA blocks Bax- but not Bak-mediated apoptosis by binding and sequestering Bax at mitochondria. *Proc Natl Acad Sci U S A* **101**, 7988-93 (2004).

14. Poncet, D. et al. An anti-apoptotic viral protein that recruits Bax to mitochondria. *J Biol Chem* **279**, 22605-14 (2004).

15. Ma, J. et al. Structural mechanism of Bax inhibition by cytomegalovirus protein vMIA. *Proc Natl Acad Sci U S A* **109**, 20901-6 (2012).

16. Bird, G.H., Crannell, W.C. & Walensky, L.D. Chemical synthesis of hydrocarbon-stapled peptides for protein interaction research and therapeutic targeting. *Curr Protoc Chem Biol* **3**, 99-117 (2011).

17. Lovell, J.F. et al. Membrane binding by tBid initiates an ordered series of events culminating in membrane permeabilization by Bax. *Cell* **135**, 1074-84 (2008).

18. Walensky, L.D. et al. A stapled BID BH3 helix directly binds and activates BAX. *Mol Cell* **24**, 199-210 (2006).

19. Llambi, F. et al. A unified model of mammalian BCL-2 protein family interactions at the mitochondria. *Mol Cell* **44**, 517-31 (2011).

20. Vranken, W.F. et al. The CCPN data model for NMR spectroscopy: development of a software pipeline. *Proteins* **59**, 687-96 (2005).

21. Williamson, M.P. Using chemical shift perturbation to characterise ligand binding. *Prog Nucl Magn Reson Spectrosc* **73**, 1-16 (2013).

22. Kozakov, D. et al. The FTMap family of web servers for determining and characterizing ligand-binding hot spots of proteins. *Nat Protoc* **10**, 733-55 (2015).

23. Pagliari, L.J. et al. The multidomain proapoptotic molecules Bax and Bak are directly activated by heat. *Proc Natl Acad Sci U S A* **102**, 17975-80 (2005).

24. Sarosiek, K.A. et al. BID preferentially activates BAK while BIM preferentially activates BAX, affecting chemotherapy response. *Mol Cell* **51**, 751-65 (2013).

25. Śledź, P., Abell, C. & Ciulli, A. Ligand-Observed NMR in Fragment-Based Approaches. in *NMR of Biomolecules* 264-280 (Wiley-VCH Verlag GmbH & Co. KGaA, 2012).

26. Ngan, C.H. et al. FTSite: high accuracy detection of ligand binding sites on unbound protein structures. *Bioinformatics* **28**, 286-7 (2012).

27. Brahmbhatt, H., Uehling, D., Al-Awar, R., Leber, B. & Andrews, D. Small molecules reveal an alternative mechanism of Bax activation. *Biochem J* **473**, 1073-83 (2016).

28. Hanahan, D. & Weinberg, R.A. The hallmarks of cancer. *Cell* **100**, 57-70 (2000).

29. Hanahan, D. & Weinberg, R.A. Hallmarks of cancer: the next generation. *Cell* **144**, 646-74 (2011).

30. Ashkenazi, A., Fairbrother, W.J., Leverson, J.D. & Souers, A.J. From basic apoptosis discoveries to advanced selective BCL-2 family inhibitors. *Nat Rev Drug Discov* **16**, 273-284 (2017).

31. Reyna, D.E. et al. Direct Activation of BAX by BTSA1 Overcomes Apoptosis Resistance in Acute Myeloid Leukemia. *Cancer Cell* **32**, 490-505 e10 (2017).

32. Roberts, A.W. et al. Targeting BCL2 with Venetoclax in Relapsed Chronic Lymphocytic Leukemia. *N Engl J Med* **374**, 311-22 (2016).

Chapter 4

BIF-44 Sensitizes BAX through an Allosteric Mechanism

Things of this World are in so constant a Flux,
that nothing remains long in the same State.

—John Locke

Second Treatise, 1689

ABSTRACT

In order to form toxic pores in the mitochondrial outer membrane, inactive BAX must undergo a series of conformational changes including the displacement of the α1–α2 loop upon BH3 engagement of the trigger site, the release of α9 to promote mitochondrial translocation and membrane insertion, and the exposure of the BAX BH3 helix to propagate the BAX activation and oligomerization signal. We identified a molecule that sensitizes BAX activation by binding to a region previously linked to BAX inhibition by the BAX-binding domain of the vMIA protein and the BH4 helix of BCL-2 (Chapter 3). Given this intriguing paradox, we sought to mechanistically determine how BIF-44 alters BAX to induce a functional sensitization effect. Computational dynamics experiments with BIF-44 docked into the binding site suggested an allosteric mechanism, whereby BIF-44 induces changes in the α1–α2 loop on the opposite side of the BAX protein. This allosteric model of sensitization was confirmed by a series of hydrogen-deuterium exchange mass spectrometry (HXMS) experiments, in which BIF-44 binding drives deprotection of the α1–α2 loop/BAX BH3 regions and synergized with BIM $SAHB_{A2}$-induced deprotection of the N-terminal α1 helix. By engaging a region of core hydrophobic interactions that otherwise preserve the BAX inactive state, BIF-44 informs fundamental mechanisms for conformational regulation of BAX and provides a new opportunity to reduce the apoptotic threshold for potential therapeutic benefit by allosterically sensitizing BAX.

ATTRIBUTIONS

Portions of this chapter were published in the following manuscript: Pritz, J.R. et al. Allosteric sensitization of proapoptotic BAX. *Nat Chem Biol* **13**, 961-967 (2017).

Contributions to the work described in this chapter were made by Jonathan R. Pritz, Franziska Wachter, Susan Lee, James Luccarelli, Thomas E. Wales, John R. Engen, and Loren D. Walensky

J.R.P., F.W., J.L., S.L., T.E.W., J.R.E., and L.D.W. designed the study; J.R.P. and F.W., generated BAX protein; J.L. performed the docking calculations and molecular dynamics simulations and the data was analyzed with J.R.P.; S.L. and T.E.W. executed the HXMS experiments under the guidance of J.R.E.

INTRODUCTION

The activation of BAX is a dynamic process, transforming from an inactive, cytosolic monomer into a deadly, mitochondrially-embedded oligomeric pore (**Figure 4.1**). The cytosol to mitochondrial translocation is driven by BH3 engagement of the BAX trigger site, which results in a series of conformational changes including the displacement of the α1–α2 loop, exposure of the 6A7 activation epitope, release of the BAX BH3 helix, and mobilization of the α9 transmembrane domain[1,2].

The binding of a BH3 helix to the α1/α6 trigger site directly induces structural rearrangements in the N-terminal region of BAX. In the inactive form of BAX, the trigger site is partially obstructed by the α1–α2 loop, which folds back onto the surface, interacting with residues of the α6 helix[3]. Binding of a BH3 helix such as BIM $SAHB_{A2}$ to the trigger site induces the displacement of this loop, resulting in a switch to an "open" conformation (**Figure 4.1, Step 1**)[1]. The opening of this loop is a key step in BAX activation, as locking the loop into the "closed" conformation by a covalent tether renders BAX incapable of translocating or oligomerizing to form a mitochondrial pore[1]. Furthermore, displacement of the loop is associated with exposure of an established "activation" epitope (amino acids 13–19) recognized by the 6A7 conformation-specific antibody (**Figure 4.1, Step 1**)[4,5]. The 6A7 epitope is occluded in the structure of inactive BAX and only becomes accessible following N-terminal rearrangement during the initiation of BAX activation. Activation of BAX at the trigger site induces exposure of the 6A7 epitope, but covalent tethering of the α1–α2 loop blocks this conformational change[1].

The displacement of the α1–α2 loop is followed by allosteric mobilization of the BAX α9 transmembrane and BH3 helices (**Figure 4.1, Step 2**)[1]. BIM $SAHB_{A2}$ engagement of the trigger site induces NMR chemical shifts in α9 on the opposite side of the protein[1]. Covalent tethering to lock α9 into the canonical groove, where it resides in inactive BAX, abrogates these changes and renders BAX deficient in translocation and mitochondrial outer membrane permeabilization

(MOMP)[1]. Furthermore, HSQC NMR analysis of this α9-tethered BAX revealed chemical shift perturbations in the resonances corresponding to the BAX BH3 following induction by the BIM $SAHB_{A2}$ activator[1]. This trigger site-induced BH3 exposure was further supported by the ability of a BAX BH3-specific antibody to immunoprecipitate BAX only upon transient BAX BH3 exposure following trigger site activation[1]. Exposure of the BAX BH3 is an important step as its hydrophobic surface is believed to mediate BAX oligomerization[6] and it can propagate the death signal by autoactivating additional inactive units of BAX by deploying the BH3 as a trigger site ligand[1,7].

Together, this evidence suggests that trigger site engagement by a BH3 helix represents the initial driving step in BAX activation and without these conformational rearrangements, BAX cannot become physiologically active. Following trigger site activation, BAX translocates to the mitochondria and stably inserts into the mitochondrial outer membrane (**Figure 4.1, Step 3**). At this stage, BAX closely resembles BAK, which is constitutively membrane-inserted. BAX and BAK are believed to require transient BH3 helix engagement at the canonical site to induce the final events that culminate in BAX/BAK homo-oligomerization and poration of the mitochondrial outer membrane.

This model of BAX activation was recently validated using hydrogen-deuterium exchange mass spectrometry (HXMS), a method to measure protein conformational dynamics. HXMS probes protein structure by measuring the deuterium incorporation of backbone amide hydrogens[8]. When diluted into deuterium buffer, backbone hydrogens of flexible and/or exposed protein regions rapidly exchange with deuterium, whereas buried domains and/or those regions that contain hydrogen-bonding involving backbone amide hydrogens (such as in α-helices) demonstrate slowed or suppressed deuterium exchange[9-11]. The amount of deuterium uptake in any given region can be quantified by digesting the protein and measuring the change in mass of the corresponding peptide fragments by mass spectrometry. Therefore, by comparing the relative difference in deuterium uptake between two experimental states, changes in protein conformation

can be detected. By applying HXMS in this manner, BIM $SAHB_{A2}$-triggered changes in BAX conformation were measured in a liposomal membrane environment[12]. In agreement with the biochemical data, the most prominent changes occurred at the N-terminal region, where the trigger site and 6A7 epitope are located[12]. At higher doses of BIM $SAHB_{A2}$, the BAX BH3 became significantly more solvent exposed. Finally, the addition of the BCL-2 BH4 SAHB neutralized all of these activating changes, supporting a model in which the BCL-2 BH4 helix functions by preserving BAX in a stable, inactive conformational state.

We identified BIF-44 as a small molecule sensitizer of BAX (Chapter 2) and determined that it engages the vMIA binding region (Chapter 3). Here, we sought to probe the mechanism of BIF-44-induced sensitization to determine how binding at an “inhibitory” site on BAX can enhance the effect of BH3-mediated activation. Through the combination of computational and experimental protein dynamics studies, including HXMS, we demonstrate that BIF-44 induces allosteric modulation of a region on the opposite face of the protein, specifically the $\alpha1$–$\alpha2$ loop and BAX BH3, to promote the sensitization of BH3-triggered BAX activation.

Figure 4.1 *Direct activation of BAX/BAK.*

Direct activator BH3-only proteins such as BIM, tBID, and PUMA facilitate the activation of BAX/BAK through engagement of the BAX trigger site and/or the BAX/BAK canonical site. BH3 binding at both the trigger and canonical sites are transient, “hit and run” interactions and the activating BH3 is subsequently released. 1. BAX is a cytosolic protein and BH3 binding at the BAX trigger site displaces the α1–α2 loop and exposes the 6A7 epitope. 2. These conformational changes are followed by the release of the BAX BH3 and the α9 transmembrane domain from the body of the protein. 3. Following conformational activation, BAX translocates to the mitochondrial outer membrane. Translocation exposes the canonical site, which is normally occluded by the α9 helix. Mitochondrial BAX resembles BAK, which is constitutively localized to the mitochondria. The homo-oligomerization of BAX/BAK is believed to involve transient engagement by the BAX/BAK BH3 helix at the canonical site. This event leads to homo-oligomerization and poration of the mitochondrial outer membrane, releasing cytochrome *c* and other apoptogenic factors into the cytosol.

Figure 4.1 (Continued)

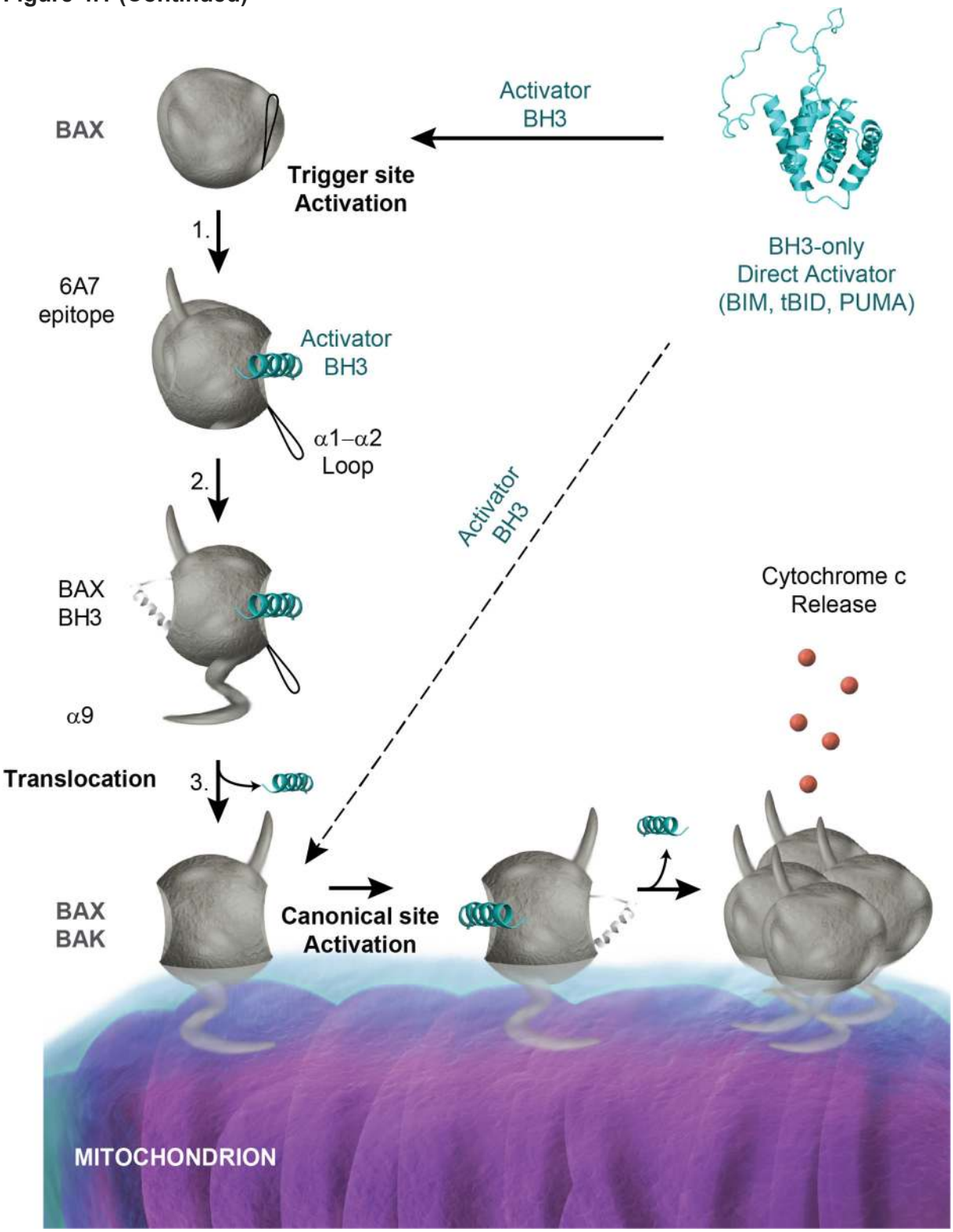

METHODS

Peptide Synthesis

Solid-state peptide synthesis using Fmoc chemistry was performed as previously described[13]. BIM $SAHB_{A2}$ (^{145}EIWIAQELRXIGDXFNAYYA^{164}-$CONH_2$)[2] peptides (X, stapling amino acid (*S*)-*N*-2-(4′-pentenyl)alanine) was N-terminally derivatized with an acetyl group. BIM $SAHB_{A2}$ was purified by LC-MS to >95% purity and quantified by amino acid analysis. Lyophilized peptide was reconstituted in 100% DMSO and diluted into the indicated aqueous buffer for experimental use.

Expression and Purification of Full-length BAX

Recombinant, full-length BAX was expressed in BL21 (DE3) *E. coli* using the pTYB1 vector[2,3]. Cell pellets were resuspended in 20 mM Tris, 250 mM NaCl, pH 7.2 and lysed by two passes through a microfluidizer (Microfluidics) chilled to 4°C. The lysate was clarified by centrifugation at 20,000 rpm. BAX was purified by batch affinity binding at 4°C using chitin resin (New England Biolabs), followed by loading onto gravity flow columns for washing and elution. The intein-chitin binding domain tag was cleaved by 36 hour incubation in 50 mM dithiothreitol at 4°C. Pure protein was isolated by size exclusion chromatography (Superdex 75 10/300; 20 mM HEPES, 150 mM KCl, pH 7.2 or 20 mM potassium phosphate, pH 6.2) using an FPLC system (GE Healthcare Life Sciences).

Molecular Docking

The Schrodinger software suite (Version 2016-2) was used for docking calculations. Conformations of molecule BIF-44 were generated in MacroModel using the OPLS3 forcefield[14]. Each of the 20 NMR conformations of BAX (PDB:1F16) was separately prepared using the default parameters in the PrepWiz wizard in Maestro. The docking receptor grid (radius 1 nm) was defined at the center of Ala124, the amino acid with the greatest HSQC shift. BIF-44 was then docked onto all 20 structures using Glide Extra Precision (XP) mode[15]. The top-scoring poses

were then manually inspected for consistency with experimentally-determined HSQC shifts for the complex.

Molecular Dynamics Simulation

Starting structures for MD calculations included the first NMR structure of BAX from PDB ID 1F16 and the BIF-44/BAX complex generated by molecular docking. The protein was prepared using the default parameters of the Protein Preparation Workflow in Maestro[16]. Protonation states were those predicted to occur at pH 7.0 using the Epik module[17]. Protein was pre-soaked in a cubic box of TIP3P water molecules using the System Builder workflow in Desmond[18]. The box was sized such that all peptide atoms were at least 1 nm from the boundaries. All overlapping solvent molecules were removed, the system was charge neutralized with appropriate counterions, and 150 mM NaCl was added to simulate buffer conditions. All MD simulations were performed using the Desmond package, with the OPLS3 forcefield applied to model all interactions. Periodic boundary conditions were maintained throughout. Long-range electrostatic interactions were calculated using the particle-mesh Ewald method[19], and van der Waals and short-range electrostatic interactions were smoothly truncated at 0.9 nm. Constant system temperature of 300 K was maintained using Nose-Hoover thermostats[20], and system pressure was maintained at 1 atm using the Martina-Tobias-Klein method[21]. The equations of motion were integrated using the RESPA integrator[22], with a 2.0 fs timestep for bonded and short-range interactions and a 6.0 fs timestep for non-bonded interactions beyond the 0.9 nm cutoff. The default parameters in Desmond were used to relax the system prior to simulation[23]. Following this procedure, a 100 ns production simulation was run and configurations saved at 4 ps intervals. All simulations were judged to have converged on the basis of radius of gyration calculations and RMSD. Principal component analysis was conducted using the Bio3D package[24,25]. All-atom elastic network model normal mode analysis (aaNMA) was performed using the Bio3D package[24,26] and the aaenm2

forcefield. The first three non-trivial normal modes were analyzed as both trajectories and per-residue fluctuations.

Liposome Preparation

Large unilamellar vesicles (LUVs) with a lipid composition similar to the outer mitochondrial membrane were formed by liposome extrusion as previously described[27]. Briefly, a lipid mixture containing a 48:28:10:10:4 molar ratio of phosphatidylcholine, phosphatidylethanolamine, phosphatidylinositol, dioleoyl phosphatidylserine, and tetraoleolyl cardiolipin (Avanti Polar Lipids) was generated in chloroform. Lipid films were formed by evaporation of solvent, initially under nitrogen gas and then by overnight vacuum, followed by storage at –80 °C under nitrogen. Lipid films were hydrated in 1 mL assay buffer (10 mM HEPES, 200 mM KCl, 1 mM $MgCl_2$, pH 7.0). Liposomes were formed by 5 freeze/thaw cycles followed by extrusion through a 100 nm polycarbonate membrane and purified using a Sepharose CL-2B size-exclusion column.

Hydrogen-Deuterium Exchange Mass Spectrometry (HXMS)

HXMS experiments were performed as described[12,28]. Deuterium labeling was initiated with an 18-fold dilution into D_2O buffer (10 mM HEPES, 200 mM KCl, 1 mM $MgCl_2$, pD 6.6) of a pre-equilibrated (15 min, room temperature) aliquot of each BAX protein (30 μM), BIF-44 (Alfa-Aesar, 99% purity), peptide, and/or antibody (BAX BH3, Abgent AP1302a; BAX 6A7, Santa Cruz Biotechnology sc-23959) mixture. At the indicated time points, the labeling reaction was quenched with the addition of an equal volume of quench buffer (0.8 M guanidinium chloride, 0.8% formic acid [v/v]). Each deuterium labeling experiment was performed in at least duplicate. Proteolysis was performed by incubation on ice with 40 μg pepsin and 20 μg factor XIII (both at 10 mg/mL in water) for 5 min. Digested samples were then processed and analyzed as described previously[12]. Briefly, the peptides were trapped and desalted on a VanGuard Pre-Column trap (2.1 x 5 mm,

ACQUITY UPLC BEH C18, 1.7 μm) for 3 min, eluted from the trap using a 5–35% gradient of acetonitrile over 6 min at a flow rate of 65 μL/min, and then separated using an ACQUITY UPLC HSS T3, 1.8 μm, 1.0 x 50 mm column. Peptides from an unlabeled protein were identified using ProteinLynx Global Server (PLGS) searches of a protein database including analyte protein. All mass spectra were acquired using a Waters SYNAPT G2 or G2Si mass spectrometer. The relative deuterium levels of identified peptides common to all evaluated conditions are shown. The error of determining the average deuterium incorporation for each peptide was at or below ± 0.25 Da. Relative deuterium levels for each peptide were calculated by subtracting the average mass of the undeuterated control sample from that of the deuterium-labeled sample. All mass spectra were processed using DynamX 3.0 (Waters Corporation). Deuterium levels were not corrected for back exchange and thus reported as relative.

RESULTS

Molecular Dynamics Predict a BIF-44 Allosteric Effect on BAX Conformation

To develop a mechanistic hypothesis for the sensitization activity of BIF-44, we used the HSQC NMR results (Chapter 3) to calculate docked structures of the BIF-44/BAX complex. Centering the receptor grid on the amino acid with the greatest HSQC shift (alanine 124), BIF-44 was docked to all 20 NMR solution structures of BAX using an ensemble docking protocol in Glide[3] (PDB ID 1F16). Eighteen of twenty dockings position BIF-44 at a deep pocket formed by the core hydrophobic α5 and α6 helices and the loop between α3 and α4 (**Figure 4.2**), in full agreement with the previous HSQC experimental data (Chapter 3).

Applying the computational docking results, we then performed molecular dynamics (MD) simulations that assessed the movement of BAX in the presence or absence of BIF-44 at the docked site. The MD trajectories were first analyzed by calculating the root-mean-square fluctuations (RMSF) for each residue over the course of the 100 ns simulation (**Figure 4.3a**). Predictably, the labile N- and C-terminal residues, display the greatest RMSF and were excluded from further analyses. When the difference in RMSF values between the two conditions were calculated, a clear increase in the conformational flexibility of the α1–α2 region of BAX (aa 36–53) was observed (**Figure 4.3a–b)**. As this location is distant from the BIF-44 docking site, the MD data suggested that BIF-44 may induce allosteric changes in this region. The predicted allosteric increase in α1–α2 loop flexibility was further supported by principal component analysis (PCA), a second method of MD trajectory analysis. PCA revealed that BIF-44 binding increased the contribution of the principle component that corresponded to motion of the α1–α2 loop (**Figure 4.3c–d**).

An independent computational method to calculate protein flexibility is normal mode analysis (NMA). NMA calculations were performed to evaluate and compare the large-scale motions of the BAX protein in the presence and absence of BIF-44 interaction. Consistent with

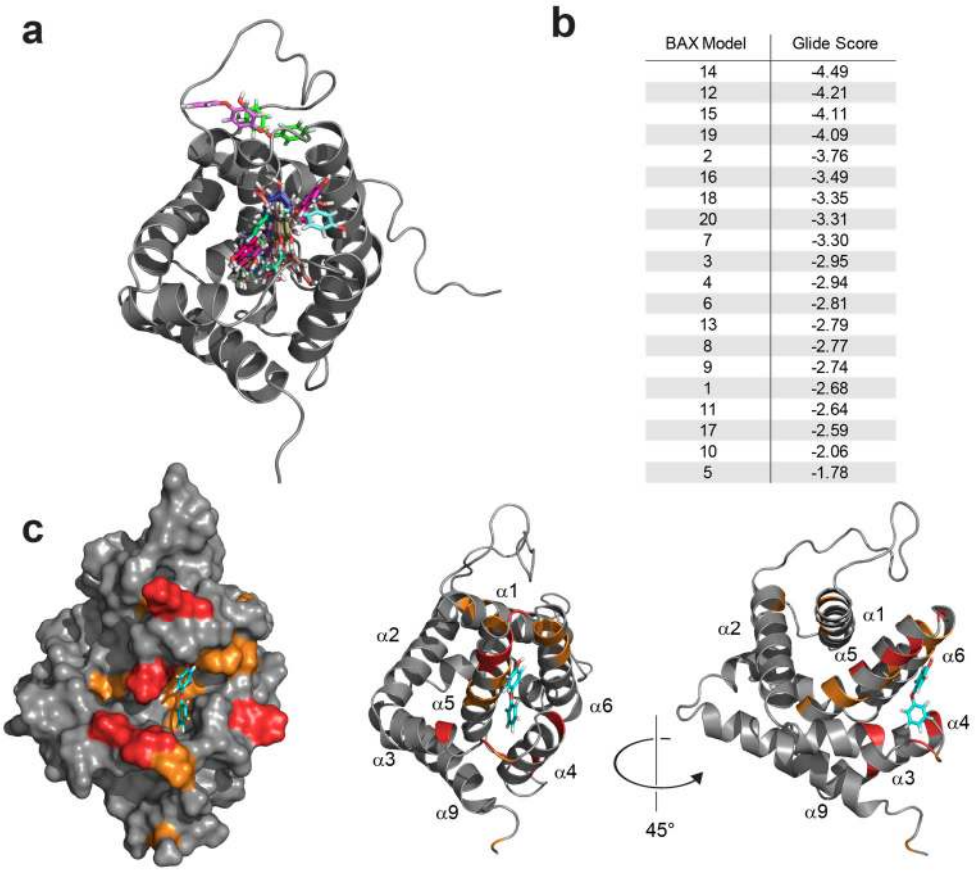

BAX Model	Glide Score
14	-4.49
12	-4.21
15	-4.11
19	-4.09
2	-3.76
16	-3.49
18	-3.35
20	-3.31
7	-3.30
3	-2.95
4	-2.94
6	-2.81
13	-2.79
8	-2.77
9	-2.74
1	-2.68
11	-2.64
17	-2.59
10	-2.06
5	-1.78

Figure 4.2 *Molecular docking of BIF-44 coincides with a ligand binding "hot spot" on BAX.* (**a–b**) Guided by the HSQC NMR results, docked structures of the BIF-44/BAX complex were calculated using an ensemble docking protocol incorporating all 20 NMR solution structures (PDB ID 1F16). Eighteen of twenty dockings position BIF-44 at a deep pocket formed by the core hydrophobic α5 and α6 helices and the loop between α3 and α4 (**a**). The pose corresponding to the top Glide score for each model (**b**) is shown superimposed on the first NMR solution structure (**a**). (**c**) The top scoring pose for BIF-44 docked into the pocket, with observed chemical shift changes colored orange (1 SD) and red (2 SD) on surface (left) and ribbon (middle, right) views of BAX.

Figure 4.3 *Molecular dynamics simulations of the BIF-44/BAX interaction.*

(**a**) RMSF values for the C_α of each BAX residue over the course of the 100 ns molecular dynamics simulation for BAX in the presence (red) or absence (black) of BIF-44. (**b**) The difference in RMSF (ΔRMSF) between unliganded and liganded forms of BAX. Residues above one SD threshold are shown in red, indicate increased mobility upon BIF-44 binding, and localize to the α1–α2 region of BAX. Residues from the unstructured portions at the N- and C-termini (residues 1–15 and 188–192, respectively) are excluded from the plot. (**c–d**) Principal component analysis (PCA) of the MD trajectory in the absence (**c**) or presence (**d**) of BIF-44 indicated an increased contribution of the principle component corresponding to motion of the α1–α2 loop upon BIF-44 binding. (**e–f**) Normal mode analysis was performed to compare the large-scale motions of BAX in the absence (**e**) or presence (**f**) of BIF-44 interaction and likewise indicated greater flexibility of the α1–α2 region for the BIF-44/BAX complex compared to BAX alone.

Figure 4.3 (Continued)

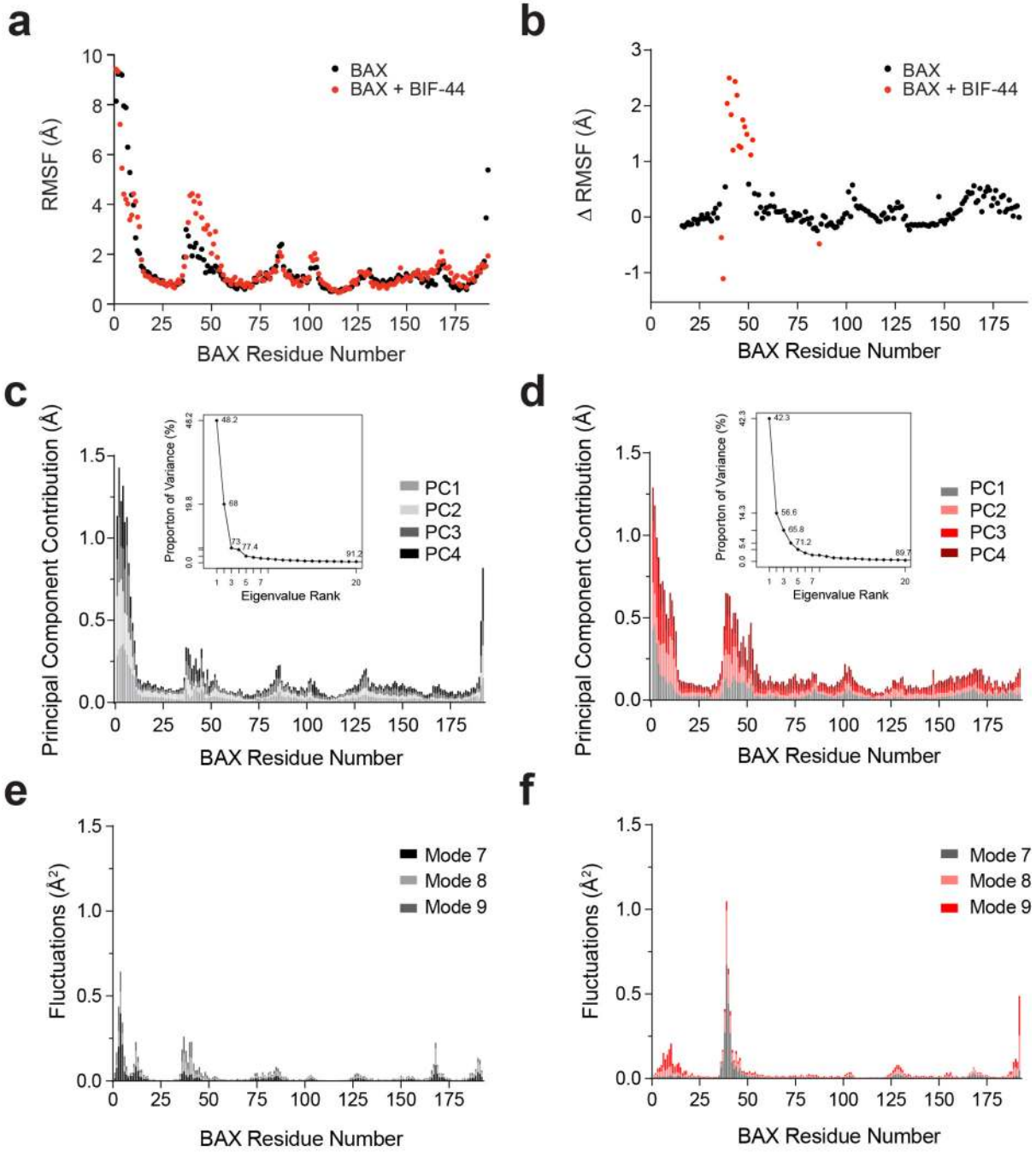

the difference in root mean square fluctuation (ΔRMSF) and PCA results (**Figure 4.3a–d**), the NMA also indicates greater flexibility of the α1–α2 region for the BIF-44/BAX complex compared to BAX alone (**Figure 4.3e–f**). The results of these calculations led us to hypothesize that BIF-44 engagement at the vMIA binding region could sensitize BH3-mediated BAX activation through allosteric mobilization of the distinct α1–α2 region, which has been implicated in the initiation of BAX activation[1].

HXMS Reveals BAX Sensitization by an Allosteric Mechanism

To evaluate whether the BIF-44 sensitization mechanism indeed derives from allosteric mobilization of the α1–α2 region, which is implicated in BH3-mediated initiation of BAX activation via an N-terminal trigger site, we performed comparative HXMS analyses. To capture the specific BIF-44-induced conformational changes in BAX, we measured hydrogen-deuterium exchange in a mixture of BAX and liposomes in the presence or absence of BIF-44. Here, we use our liposomal system to explicitly correlate functional activation of BAX, as measured by BAX-mediated liposomal release assay, with conformational modulation in a membrane environment that simulates the physiologic context for regulated BAX activation and poration.

First, we demonstrated that the deuterium exchange profile of our recombinant, full-length, monomeric BAX preparation is consistent with the NMR structure (PDB ID 1F16), such that exposed regions are progressively labeled and buried regions are shielded from exchange, and remains similarly stable over time (10 sec, 1 min, 100 min) in the presence or absence of liposomes (**Figure 4.4**). Upon incubating BAX with BIF-44 in the liposomal context that supports functional activation of BAX, we reproducibly observe focal deprotection of peptide fragments corresponding to amino acids 46–62, the very region that encompasses the distal portion of the α1–α2 loop and proximal half of the α2 BH3 helix (**Figure 4.5a–b**). To further validate the specificity of this finding, we tested the influence of two antibodies, which bind to discrete regions

Figure 4.4 *Deuterium exchange profiles of recombinant, full-length BAX over time in the absence and presence of liposomes.*

(**a–b**) The relative fractional deuterium uptake for BAX (30 μM) in the absence (**a**) or presence (**b**) of liposomes at 10 sec, 1 min, and 100 min demonstrates a range of deuterium uptake across the protein sequence, reflecting the differences in flexibility and solvent exposure of the discrete regions of BAX. As evidenced by the consistent contour and stability of the plots, the conformational disposition of inactive monomeric BAX is similar among the two conditions. (**c**) The spectral envelopes of representative BAX peptides demonstrate the deuterium exchange at 10 sec, 1 min, and 100 min in the presence of liposomes, highlighting the purity and stability of these species over time.

Figure 4.4 (Continued)

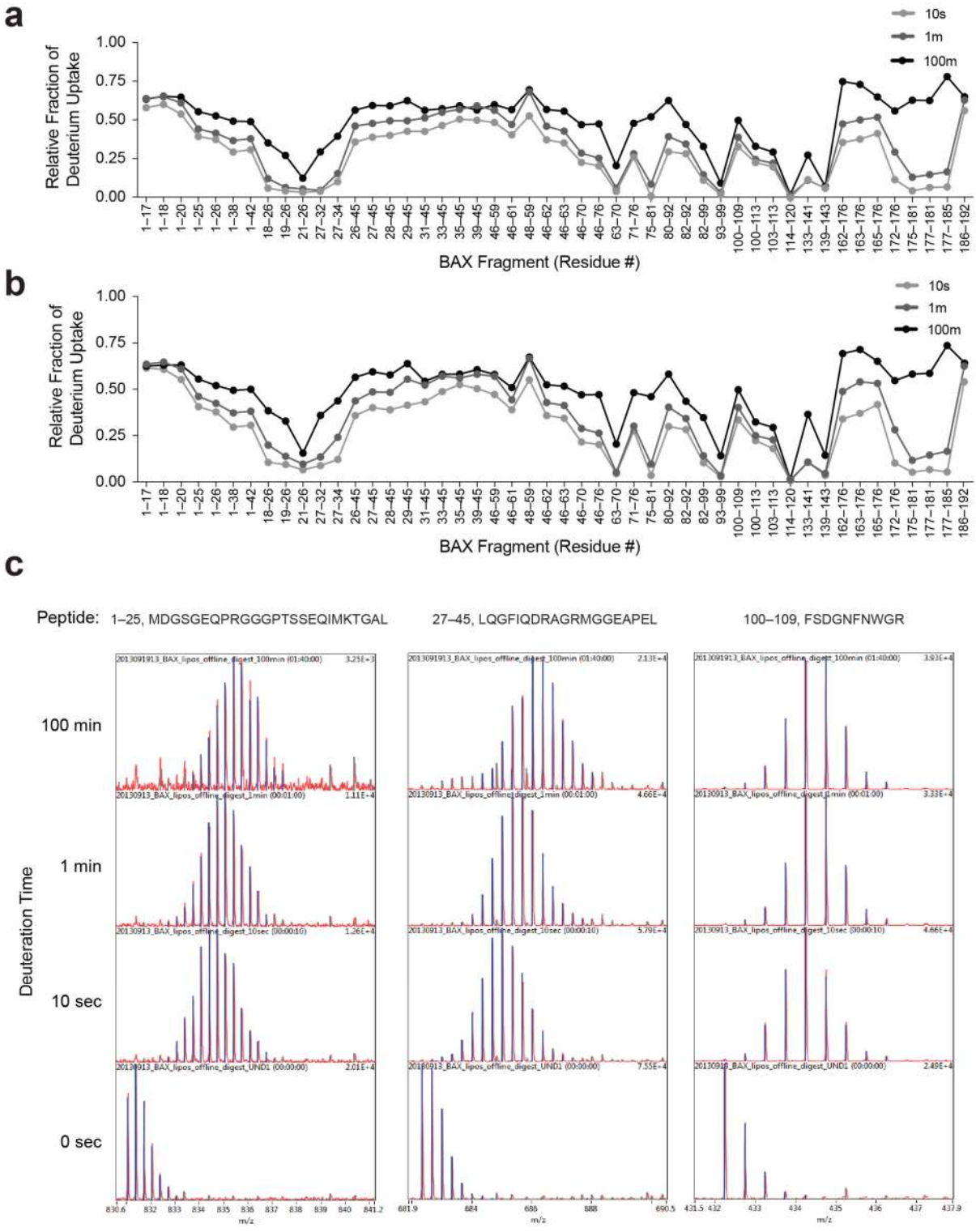

Figure 4.5 *Allosteric deprotection of the α1–α2 loop and BAX BH3 domain upon BIF-44 binding*. (**a**,**b**) The addition of BIF-44 to BAX (30 μM, 10:1 BIF:BAX, 15 min incubation/10 sec deuteration) in a liposomal environment triggered a regiospecific increase in deuterium incorporation compared to unliganded BAX, as measured by HXMS (**a**). The difference in deuterium uptake plot reflects the relative deuterium incorporation of BIF-44/BAX minus the relative deuterium incorporation of BAX. Dark gray shading, changes below significance threshold of 0.5 Da; light gray shading and white region, changes above significance thresholds of 0.5 Da and 0.8 Da, respectively. Data are representative of two independent experiments. (**b**) The region of BIF-44-induced deprotection encompasses peptide fragments corresponding to amino acids 46–62, which are highlighted in red on the ribbon diagram (left, PDB ID 1F16) and amino acid sequence (right), and map to the critical α1–α2 loop and BH3 regions of BAX. (**c**, **d**) The deprotection induced by BIF-44 is suppressed by co-incubation with an anti-BAX BH3 antibody (30 μM BAX, 1:10:0.5 BAX:BIF-44:antibody) (**c**), but not the BAX 6A7 antibody (**d**), which binds to N-terminal residues of conformationally-activated BAX. The BAX amino acid sequences recognized by the BAX BH3 and 6A7 antibodies are underlined in tan and brown, respectively (**b**). The difference in deuterium uptake plots reflect the relative deuterium incorporation of BIF-44/BAX/BH3 Ab (**c**) and BIF-44/BAX/6A7 Ab (**d**) minus the relative deuterium incorporation of BAX, as measured at 10 sec. Data are representative of two independent experiments.

Figure 4.5 (Continued)

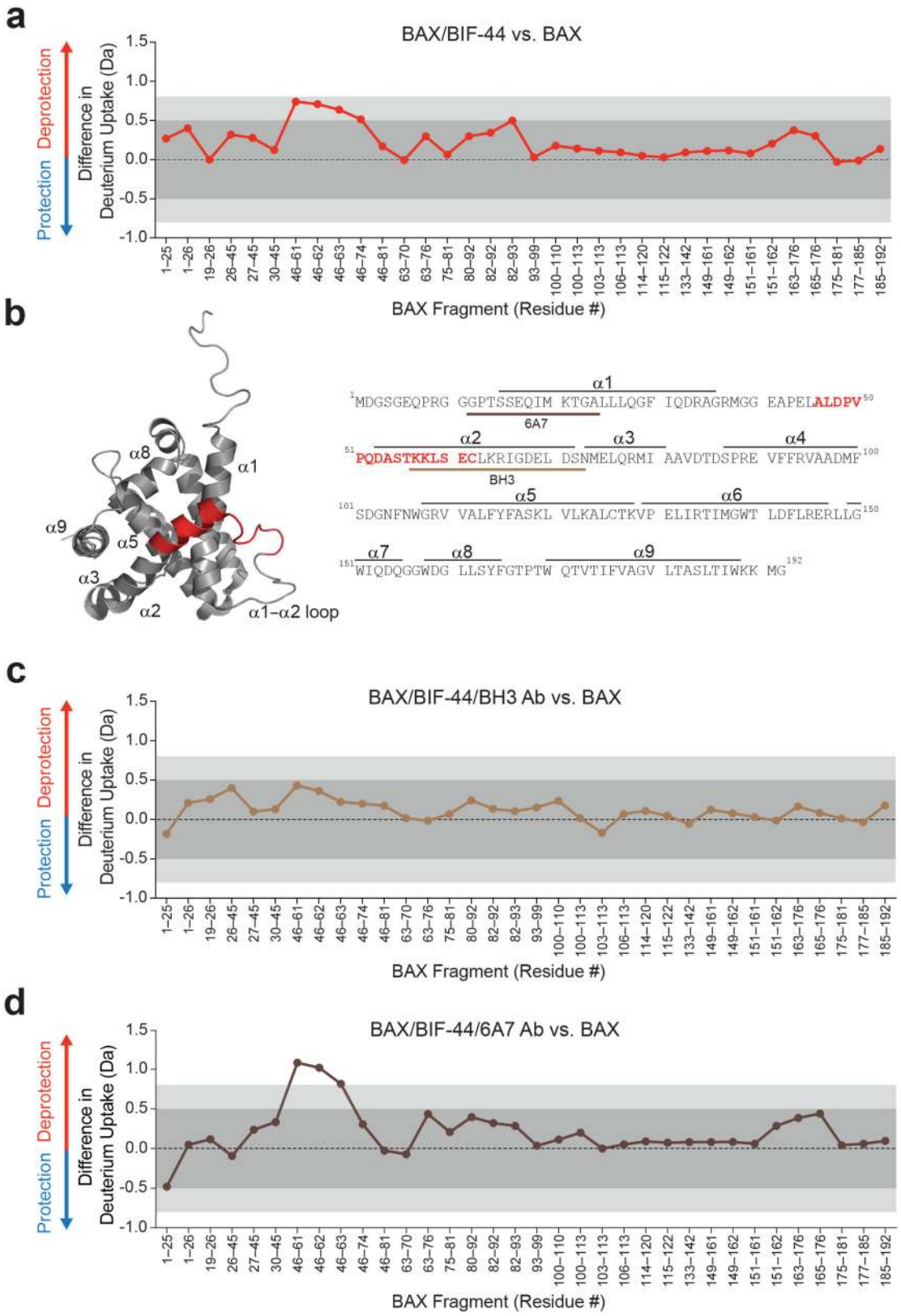

of BAX, on the observed BIF-44-induced deprotection. We reasoned that if BIF-44 was specifically mobilizing or exposing the BH3 region of BAX, a BAX-BH3-specific antibody would promptly bind and suppress access of this region to deuterium exchange. Conversely, an antibody such as 6A7 that binds to an alternate region of the protein, which becomes exposed upon BH3-triggered BAX activation (aa 12–24)[2,4], would serve as a negative control. Indeed, we found that the BH3 antibody selectively suppressed the observed deuterium exchange promoted by BIF-44 in the BAX BH3 region (**Figure 4.5c**), whereas the 6A7 antibody had no inhibitory effect on BIF-44 mediated-deprotection (**Figure 4.5d**). Taken together, the NMR, computational, and HXMS results, are consistent in linking BIF-44 binding at a noncanonical interaction site to allosteric mobilization of the α1–α2 region, where BH3-induced conformational changes initiate BAX activation.

To examine how BIF-44 and BIM SAHB$_{A2}$ engagement at distinct sites synergize to trigger BAX activation, we performed HXMS analyses of BAX in the presence of BIF-44, BIM SAHB$_{A2}$, or the combination. The hydrogen-deuterium exchange profiles of BIM SAHB$_{A2}$ and BIF-44 are notably distinct, consistent with their different sites of engagement and distinct mechanisms of action. BIM SAHB$_{A2}$ directly binds to the N- terminal trigger site formed by surface residues of α-helices 1 and 6 and displaces the α1–α2 loop leading to 6A7 epitope exposure[1,12]. These conformational changes are observed as significant deprotection in the N-terminal and distal α1–α2 loop region (**Figure 4.6a, blue**). In contrast, BIF-44 engages a distant site, causing focal allosteric changes localized to the distal α1–α2 loop and proximal α2 BH3 helix, as reflected by a significant deprotection peak (**Figure 4.6a, red**). Combined treatment amplified deprotection of both the N-terminal and the α1–loop–α2 regions (**Figure 4.6, green**), with a deuterium exchange profile that is stable over time (**Figure 4.7**). These results are consistent with the ability of BIF-44 to effectively sensitize BIM SAHB$_{A2}$-mediated conformational activation of BAX and enhance the potency of this activating peptide. Thus, the BAX sensitizer molecule BIF-44 facilitates the

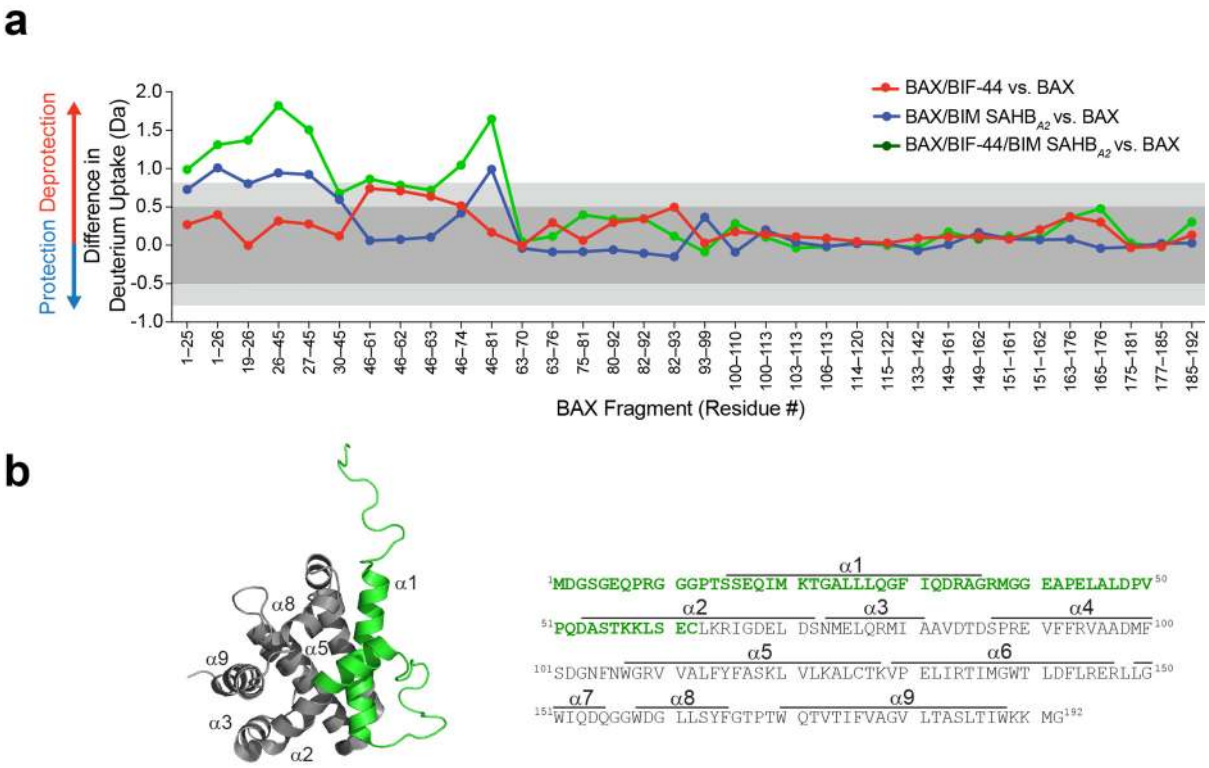

Figure 4.6 *BIF-44 sensitizes BH3-triggered conformational activation of BAX.*

(**a**) Comparative HXMS profiles of BAX in the presence of liposomes upon exposure to BIF-44 (red), BIM SAHB$_{A2}$ (blue), or both ligands (green). The difference in deuterium uptake plots reflect the relative deuterium incorporation of BIF-44/BAX (red), BIM SAHB$_{A2}$/BAX (blue), and BIF-44/BIM SAHB$_{A2}$/BAX (green) minus the relative deuterium incorporation of BAX, as measured at 10 sec (BAX 30 μM, 10x BIF-44, 1x peptide). Dark gray shading represents changes in the plot that are below the significance threshold of 0.5 Da, whereas light gray shading and the white region highlight changes above the baseline significance threshold of 0.5 Da and the more stringent threshold of 0.8 Da, respectively. (**b**) Region of significant deprotection from (**a**) is mapped the structure and sequence of BAX. PDB:1F16. Data are representative of two independent experiments.

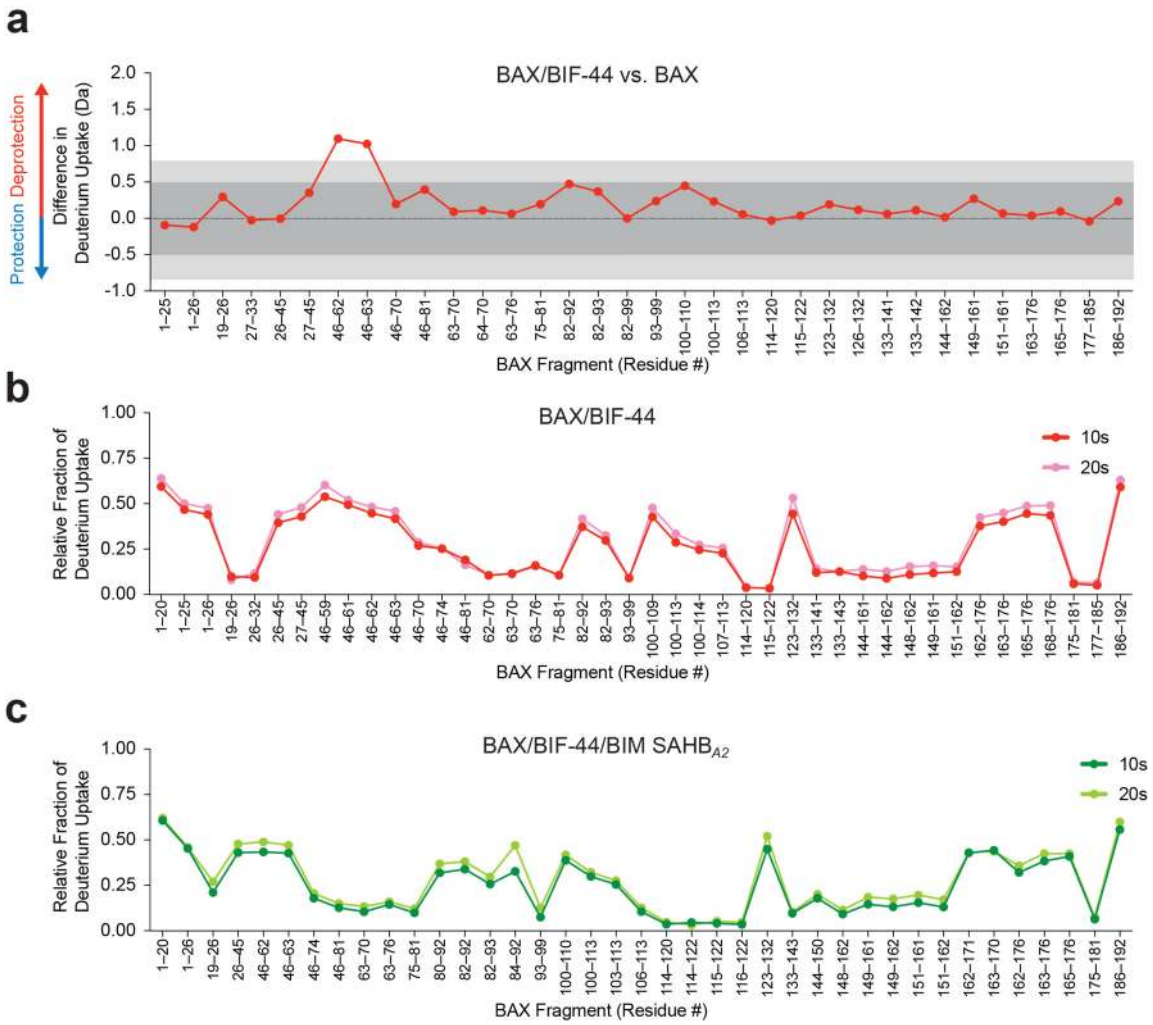

Figure 4.7 *HXMS analysis of BAX in the presence of BIF-44 and the BIF-44/BIM SAHB$_{A2}$ combination.*

(**a**) The addition of BIF-44 to BAX (30 μM, 10:1 BIF:BAX, 10 sec) in a liposomal environment reproducibly triggers a regiospecific increase in deuterium incorporation compared to unliganded BAX, in the region of the α1–α2 loop and BH3 domain (α2). (**b–c**) The relative fractional deuterium uptake for BAX in the presence of BIF-44 (**b**) or the BIF-44/BIM SAHB$_{A2}$ combination (**c**) demonstrates the consistency of deuterium exchange across the protein sequence at exemplary 10 and 20 sec time points.

initiation of BH3-mediated direct BAX activation by engagement of the vMIA region, which produces a novel allosteric mobilization of the α1–α2 loop/α2 BH3 helix. These allosteric changes enhance the efficacy of BH3-mediated conformational changes in BAX, sensitizing the protein to functional activation.

DISCUSSION

Allostery has emerged as a key feature of BCL-2 family protein regulation, influencing both the apoptotic response and opportunities to pharmacologically manipulate the apoptotic mediators. For example, BH3-only triggering of BAX at the α1/α6 interaction site on the N-terminal face of the protein drives release of α9 at the C-terminal face for mitochondrial translocation[1,29], BCL-2 BH4 and vMIA engagement restricts the conformational activation of BAX[12,30], PUMA induces partial unfolding of BCL-X_L to release sequestered p53 from a distal site[31], and covalent modification or mutagenesis of an α6 cysteine of MCL-1 influences the functional activity of its canonical anti-apoptotic binding pocket at the opposite face of the protein[28]. Indeed, one of the cardinal features and mechanistic requirements for activation and homo-oligomerization of the essential executioner proteins of mitochondrial apoptosis, BAX and BAK, involves exposure of their respective BH3 helices, which can either be trapped by the canonical pockets of anti-apoptotic members[32] or remain free to mediate formation of toxic mitochondrial pores[6]. Thus, pharmacologic approaches that induce the release or sequestration of the BAX and BAK BH3 domains stand to directly influence cell fate in a host of diseases.

An allosteric mechanism of BIF-44 sensitization was suggested by RMSF analysis of computational MD simulations, which pointed to enhanced conformational flexibility of the α1–α2 region upon BIF-44 binding. This initial observation was further supported by PCA of MD trajectories and by NMA analyses, which identified a similar increase in the mobility of this region in the presence of BIF-44. Indeed, HXMS experimental studies confirmed that BIF-44 induces

deprotection of a portion of the α1–α2 loop and the BAX BH3 helix. This focal increase in deuterium exchange was selectively blocked by a BH3-specific antibody, but not by the 6A7 antibody, which neutralized the BIF-44-induced BAX conformational changes. Finally, in agreement with a sensitizing effect, BIF-44 increased the deprotection of the N-terminal region. Overall, the allosteric consequences of BIF-44 interaction, namely the synergistic mobilization of the α1–α2 loop and BH3 domain of BAX, underscores the mechanistic importance of the N-terminal conformational change to BH3-mediated initiation of BAX activation.

Compounds that bind to the BIF-44 site and induce this subset of BAX-sensitizing changes, could provide a novel pharmacologic approach for lowering the threshold for BH3-triggered BAX activation. A BAX sensitizer, delivered in combination with an anti-apoptotic inhibitor or standard chemotherapy, has the potential to robustly induce cancer cell apoptosis and thus serve as a highly effective therapeutic strategy across many diverse tumor types.

REFERENCES

1. Gavathiotis, E., Reyna, D.E., Davis, M.L., Bird, G.H. & Walensky, L.D. BH3-triggered structural reorganization drives the activation of proapoptotic BAX. *Mol Cell* **40**, 481-92 (2010).

2. Gavathiotis, E. et al. BAX activation is initiated at a novel interaction site. *Nature* **455**, 1076-81 (2008).

3. Suzuki, M., Youle, R.J. & Tjandra, N. Structure of Bax: coregulation of dimer formation and intracellular localization. *Cell* **103**, 645-54 (2000).

4. Hsu, Y.T. & Youle, R.J. Nonionic detergents induce dimerization among members of the Bcl-2 family. *J Biol Chem* **272**, 13829-34 (1997).

5. Hsu, Y.T. & Youle, R.J. Bax in murine thymus is a soluble monomeric protein that displays differential detergent-induced conformations. *J Biol Chem* **273**, 10777-83 (1998).

6. Wang, K., Gross, A., Waksman, G. & Korsmeyer, S.J. Mutagenesis of the BH3 domain of BAX identifies residues critical for dimerization and killing. *Mol Cell Biol* **18**, 6083-9 (1998).

7. Tan, C. et al. Auto-activation of the apoptosis protein Bax increases mitochondrial membrane permeability and is inhibited by Bcl-2. *J Biol Chem* **281**, 14764-75 (2006).

8. Engen, J.R. Analysis of protein conformation and dynamics by hydrogen/deuterium exchange MS. *Anal Chem* **81**, 7870-5 (2009).

9. Laiken, S.L., Printz, M.P. & Craig, L.C. Tritium-hydrogen exchange studies of protein models. I. Gramicidin S-A. *Biochemistry* **8**, 519-26 (1969).

10. Printz, M.P., Williams, H.P. & Craig, L.C. Evidence for the presence of hydrogen-bonded secondary structure in angiotensin II in aqueous solution. *Proc Natl Acad Sci U S A* **69**, 378-82 (1972).

11. Shi, X.E. et al. Hydrogen exchange-mass spectrometry measures stapled peptide conformational dynamics and predicts pharmacokinetic properties. *Anal Chem* **85**, 11185-8 (2013).

12. Barclay, L.A. et al. Inhibition of Pro-apoptotic BAX by a noncanonical interaction mechanism. *Mol Cell* **57**, 873-86 (2015).

13. Bird, G.H., Crannell, W.C. & Walensky, L.D. Chemical synthesis of hydrocarbon-stapled peptides for protein interaction research and therapeutic targeting. *Curr Protoc Chem Biol* **3**, 99-117 (2011).

14. Harder, E. et al. OPLS3: A Force Field Providing Broad Coverage of Drug-like Small Molecules and Proteins. *J Chem Theory Comput* **12**, 281-96 (2016).

15. Friesner, R.A. et al. Extra precision glide: docking and scoring incorporating a model of hydrophobic enclosure for protein-ligand complexes. *J Med Chem* **49**, 6177-96 (2006).

16. Sastry, G.M., Adzhigirey, M., Day, T., Annabhimoju, R. & Sherman, W. Protein and ligand preparation: parameters, protocols, and influence on virtual screening enrichments. *J Comput Aided Mol Des* **27**, 221-34 (2013).

17. Shelley, J.C. et al. Epik: a software program for pK(a) prediction and protonation state generation for drug-like molecules. *J Comput Aided Mol Des* **21**, 681-91 (2007).

18. Jorgensen, W.L., Chandrasekhar, J., Madura, J.D., Impey, R.W. & Klein, M.L. Comparison of simple potential functions for simulating liquid water. *The Journal of Chemical Physics* **79**, 926-935 (1983).

19. Essmann, U. et al. A smooth particle mesh Ewald method. *The Journal of Chemical Physics* **103**, 8577-8593 (1995).

20. Hoover, W.G. Canonical dynamics: Equilibrium phase-space distributions. *Phys Rev A Gen Phys* **31**, 1695-1697 (1985).

21. Martyna, G.J., Tobias, D.J. & Klein, M.L. Constant pressure molecular dynamics algorithms. *The Journal of Chemical Physics* **101**, 4177-4189 (1994).

22. Humphreys, D.D., Friesner, R.A. & Berne, B.J. A Multiple-Time-Step Molecular Dynamics Algorithm for Macromolecules. *The Journal of Physical Chemistry* **98**, 6885-6892 (1994).

23. Guo, Z. et al. Probing the alpha-helical structural stability of stapled p53 peptides: molecular dynamics simulations and analysis. *Chem Biol Drug Des* **75**, 348-59 (2010).

24. Grant, B.J., Rodrigues, A.P., ElSawy, K.M., McCammon, J.A. & Caves, L.S. Bio3d: an R package for the comparative analysis of protein structures. *Bioinformatics* **22**, 2695-6 (2006).

25. Skjaerven, L., Yao, X.Q., Scarabelli, G. & Grant, B.J. Integrating protein structural dynamics and evolutionary analysis with Bio3D. *BMC Bioinformatics* **15**, 399 (2014).

26. Yao, X.Q., Skjaerven, L. & Grant, B.J. Rapid Characterization of Allosteric Networks with Ensemble Normal Mode Analysis. *J Phys Chem B* **120**, 8276-88 (2016).

27. Pitter, K., Bernal, F., Labelle, J. & Walensky, L.D. Dissection of the BCL-2 family signaling network with stabilized alpha-helices of BCL-2 domains. *Methods Enzymol* **446**, 387-408 (2008).

28. Lee, S. et al. Allosteric inhibition of antiapoptotic MCL-1. *Nat Struct Mol Biol* **23**, 600-7 (2016).

29. Goping, I.S. et al. Regulated targeting of BAX to mitochondria. *J Cell Biol* **143**, 207-15 (1998).

30. Ma, J. et al. Structural mechanism of Bax inhibition by cytomegalovirus protein vMIA. *Proc Natl Acad Sci U S A* **109**, 20901-6 (2012).

31. Follis, A.V. et al. PUMA binding induces partial unfolding within BCL-xL to disrupt p53 binding and promote apoptosis. *Nat Chem Biol* **9**, 163-8 (2013).

32. Sattler, M. et al. Structure of Bcl-xL-Bak peptide complex: recognition between regulators of apoptosis. *Science* **275**, 983-6 (1997).

Chapter 5

Conclusions and Future Directions

DISCUSSION OF RESULTS

Rationale for Targeting BAX

In order to maintain tissue homeostasis within an organism, the rate of mitotic cellular division is balanced by a predetermined proportion of apoptotic cell death. The proper regulation of apoptosis is essential to maintain this balance and prevent diseases of pathologic cell survival or cell death. As the regulators of mitochondrial apoptosis, BCL-2 family proteins are responsible for sensing cellular stress and transmitting the death signal to apoptotic effectors at the mitochondria. Cellular stress leads to the upregulation of the BH3-only proteins, which, in turn, influence the anti-apoptotic reserve and the activation of BAX and BAK. Conformational activation of BAX/BAK and subsequent oligomerization produces large pores in the mitochondrial outer membrane, releasing cytochrome *c* and other factors that activate the caspase cascade, driving apoptosis to completion.

The BCL-2 family proteins represent prime drugs targets for the pharmacologic manipulation of cell fate. To avoid apoptotic death, cancer cells frequently upregulate the expression of anti-apoptotic proteins, which inactivate BAX and the BH3-only proteins through sequestration[1-3]. By “inhibiting the inhibitors” of apoptosis, compounds targeting the anti-apoptotic proteins BCL-2, BCL-X_L, BCL-w, and/or MCL-1 have shown promising anti-tumor potential[4-9]. However, a distinct, but complementary approach to reactivating apoptosis is to directly target the pro-apoptotic proteins that serve as effectors of the death pathway. Pharmacologic mechanisms to directly activate BAX would overwhelm the anti-apoptotic reserve and effectively bypass the inhibitory regulatory network allowing for efficient induction of cell death in tumor cells. Unlike the anti-apoptotic proteins that display tissue-specific expression, BAX is expressed across all tissue types, including normal tissue[10] (proteinatlas.org) and cancer cells[11] (portals.broadinstitute.org /ccle). Additionally, BAX is rarely mutated in human cancers, with only 65 out of 10,188 specimens (0.6%) in the Genomic Data Commons database with a reported non-synonymous mutation in the BAX locus (release 9.0; portal.gdc.cancer.gov). Given the prevalence of wild type BAX

expression across human cancers, pharmacologic strategies that can activate this protein have the potential to lower the apoptotic threshold in cancer and thus serve as a novel anti-cancer therapy.

Rationale for Fragment-based Screening

Fragment-based screening is an efficient method for identifying compounds that bind to a target protein of interest. In contrast to traditional high-throughput screening of drug-like molecules, fragment-based screening leverages the power of small, relatively simple compounds (<300 Da) to identify binders from a relatively small library of compounds. The affinity of these fragments for the target is typically low, but can be readily detected using a variety of sensitive NMR techniques. Given the ability of fragments to bind to proteins that are difficult to screen by conventional methods, fragment-based screening is often used to identify chemical starting points for drug development. There are dozens of molecules currently in clinical development that are derived from a fragment screening hit[12]. Vemurafenib, a BRAF V600E inhibitor, was the first fragment-derived molecule to become FDA approved[13]. Another notable success story is ABT-737, a potent inhibitor of BCL-2/BCL-x_L/BCL-w[4]. In an effort to develop an inhibitor of BCL-X_L, scientists at Abbott laboratories employed the SAR by NMR fragment-based screening approach to identify and elaborate on chemical matter that bound to the target[14]. Subsequent optimization of the screening hits, led to the development of ABT-737 and, eventually, the BCL-2 specific inhibitor venetoclax[4,14,15].

Due to the challenge of producing recombinant BAX in sufficient quantities, purity, and stability for direct screening, *in vitro* screening methods have not been previously implemented. Instead, *in silico* screening approaches have been applied to identify molecules that could bind to either the canonical groove or the trigger site on BAX[16-18]. However, the regulation of BAX activity is complex and, by implementing a biased screening strategy, novel modes of interaction and protein modulation could be missed. In order to discover novel BAX-binding compounds to inform

drug discovery and probe BAX's complex biology, we overcame these hurdles and performed an NMR-based fragment screen against full length BAX. Indeed, by applying this unbiased screening approach, we identified a molecule, BIF-44 (Chapter 2), which bound to an unexpected site on BAX (Chapter 3) and functioned to modulate BAX activity by a novel, allosteric, sensitization mechanism (Chapter 4) (**Figure 5.1**).

Allosteric Mechanism of BAX Sensitization

Given its importance in controlling cell fate, the regulation of BAX activation is biologically complex and remains an active area of scientific research. The transition of BAX from an inactive monomer to a membrane-embedded pore is achieved through sequential engagement of two BH3-binding sites. Initial binding at the trigger site induces a series of conformational changes, including opening of the $\alpha1$–$\alpha2$ loop, exposure of the 6A7 epitope, mobilization of the BAX BH3 helix, and release of the $\alpha9$ transmembrane domain[19,20]. These changes facilitate the translocation of BAX to the mitochondria, where subsequent canonical site engagement drives BAX oligomerization and mitochondrial outer membrane permeabilization. These activating conformational changes can be inhibited by anti-apoptotic binding and sequestration of the BAX BH3 or by the binding of an anti-apoptotic BH4 helix to stabilize the inactive BAX conformation[1,21]. In addition, the BAX-binding domain of the cytomegalovirus vMIA protein binds to BAX and induces its translocation to the mitochondria, thereby preventing subsequent BAX activation[22,23].

Using a ligand-detected STD NMR screening approach, we successfully screened a 940-compound fragment library against pure, recombinant, monomeric, full-length BAX. We identified 53 BAX-interacting fragments (BIFs) and functionally characterized these hits using a BAX-mediated liposomal release assay. This revealed a novel BAX sensitization effect, which was best exemplified by BIF-44. Intriguingly, in both competitive STD NMR and fluorescence polarization approaches, BIF-44 was not competed by BIM $SAHB_{A2,}$ a stapled BH3 peptide that binds to the

activating sites on BAX. Instead, a peptide corresponding to the BAX-binding domain of vMIA competed with BIF-44 in these assays. This curious observation of BIF-44 engagement at an "inhibitory" site was confirmed by HSQC NMR chemical shift mapping, which localized the BIF-44 binding site to the region of vMIA interaction.

These results presented an intriguing paradox: how could a molecular fragment that sensitizes BH3-triggered BAX activation do so by engaging BAX in a region that mediates BAX inhibition? A series of BIF-44-induced HSQC chemical shifts localized to the core of BAX, hinting at the possibility of an allosteric conformational change. To further probe the mechanism of action, we undertook a series of experiments to monitor for the BIF-44-induced changes in BAX conformational dynamics. Computational molecular dynamics calculations suggested that BIF-44 engagement resulted in increased mobility of the $\alpha1$–$\alpha2$ loop on the opposite side of BAX from the BIF-44 binding site. This allosteric effect was subsequently detected experimentally by hydrogen-deuterium exchange mass spectrometry (HXMS). In the presence of BIF-44, the $\alpha1$–$\alpha2$ loop and the BH3 motif of BAX ($\alpha2$) showed increased solvent exposure (deprotection). Furthermore, in agreement with the observed sensitization of BAX to BIM $SAHB_{A2}$ activation in the liposomal and mitochondrial release assays, BIF-44 increased the magnitude of BIM $SAHB_{A2}$-induced conformational changes as measured by HXMS. Together, these results support an allosteric model of sensitization through the engagement of the vMIA binding region, an apparent site of structural vulnerability (**Figure 5.1**). The development of compounds that engage this site and sensitize BAX to activation represents a novel strategy to lower the threshold for apoptosis in cancer.

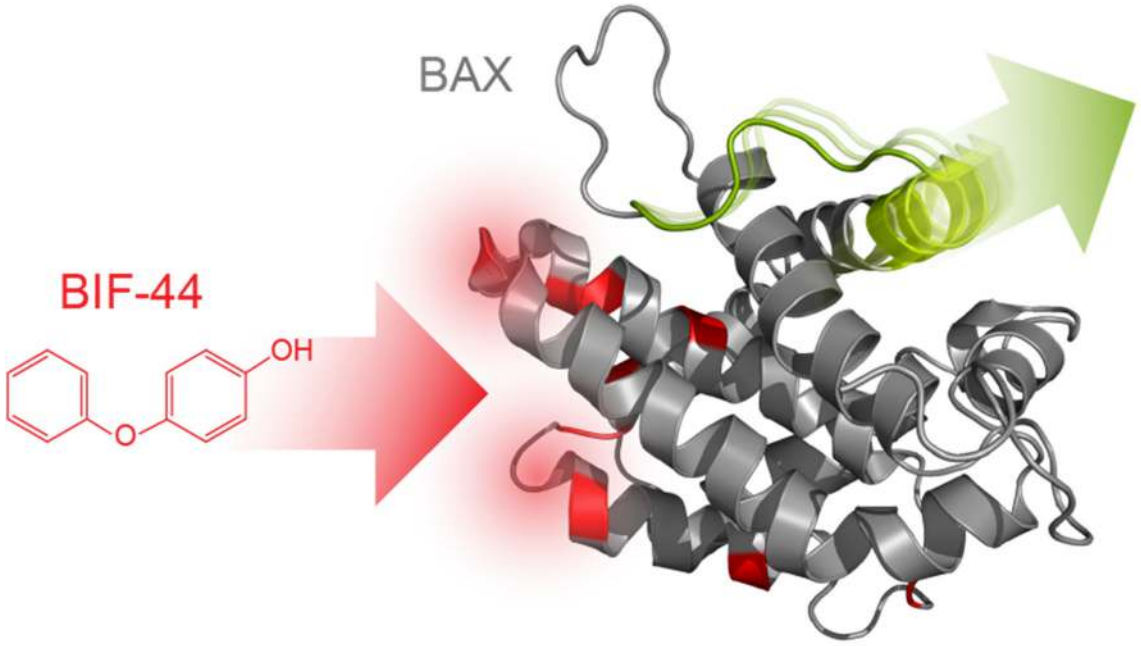

Figure 5.1 *Model of BIF-44-induced allosteric sensitization of pro-apoptotic BAX.*

Binding of BIF-44 to BAX (red) initiates allosteric mobilization of the $\alpha1$–$\alpha2$ loop and BH3 region on the opposite side of the BAX protein (green), sensitizing BAX to direct activation by BH3 activators, such as BIM $SAHB_{A2}$

FUTURE DIRECTIONS

BIF-44 provides a molecular prototype for allosterically sensitizing BAX to pro-apoptotic stimuli. However, since BIF-44 emerged as a relatively small BAX-binding fragment with a micromolar K_D, BIF-44 is presumed to lack the necessary potency and specificity to validate on-target efficacy of this novel mechanism in a cellular context. Thus, the goal of the future directions proposed below is to develop a potent and selective sensitizer of BAX activation for cellular and, ultimately, translational studies. Such studies would necessarily begin with a robust medicinal chemistry effort designed to generate and test an expansive library of BIF-44 like compounds.

While a purpose of small molecule optimization efforts is to improve binding potency, in the case of BAX, the affinity required may not be especially high due to the mechanism of BAX activation. Anti-apoptotic inhibitors, such as venetoclax, function by stably engaging the canonical groove of anti-apoptotic proteins and competing with native BH3-only and BAX BH3 helices for binding at the same groove[8]. In order to disrupt these critical protein-protein interactions and effectively reactivate apoptosis *in vivo*, anti-apoptotic inhibitors require picomolar target affinity and, in some cases, stoichiometric binding to induce apoptosis[4-6,9]. In contrast, the activation of BAX occurs through a transient, “hit-and-run” mechanism, whereby activating BH3 helices bind to BAX, induce conformational changes, and then are released from BAX[24,25]. Importantly, activated BAX can then activate another BAX unit, resulting in an auto-catalytic increase in BAX activity[19,26]. Given this important mechanistic distinction between anti- and pro-apoptotic targeting, BAX-activating compounds are not expected to require an exquisite level of affinity to induce a potent biological effect. In support of this hypothesis, the BAX trigger site activator molecule (BTSA1) induces apoptosis in cancer cells and in xenograft animal models, with an *in vitro* IC_{50} of 250 nM[27]. Therefore, the development of BIF-44 into a drug-like BAX sensitizer may be quite tractable.

Optimization through SAR by NMR

An effective approach to fragment optimization is SAR by NMR[14,28] (**Figure 5.2a**). In this method, the potency of the fragment initially identified by ^{1}H-^{15}N HSQC NMR is improved by SAR studies of a focused library of chemically-expanded molecules, followed by "joining" hits from sequential screening. A second fragment screen searches for other ligands that can to bind an adjacent site from the first binding location by HSQC. Following optimization of this second fragment hit, the two fragments are linked together and optimized a third time to maximize potency. Given the requirement of a large quantity of ^{15}N-labeled BAX to conduct SAR by NMR optimization, this particular approach is not especially compatible with the development of BAX modulators.

Nevertheless, there are several aspects of SAR by NMR that can be leveraged for BIF-44 optimization. First, a larger SAR panel of BIF-44 homologs can be synthesized and tested for improved BAX-binding potency. While we tested some BIF-44 homologs to ensure specificity of the BIF-44-BAX interaction (Chapter 2), a more expansive medicinal chemistry effort would be required to maximize the opportunity to identify more potent binders. By altering the chemical substituents of the BIF-44 core, including the location and composition of the functional groups, as well as, the aryl linker length and composition, a large panel of homologous compounds could be assembled. Initial screening of the library would be accomplished using Glide to computationally dock the compounds into the BIF-44 site, as accomplished for BIF-44 (Chapter 4)[29]. By comparing binding scores of the BIF-44 derivatives to that of BIF-44, this *in silico* approach could enrich the library for those compounds most likely to have improved binding activity. The panel could then be tested in the liposomal release assay to determine if any of the compounds enhance the potency of the BIM $SAHB_{A2}$-induced BAX sensitization effect. The binding site of the most potent derivatives would be validated by ^{15}N-BAX HSQC NMR.

With the optimized BIF fragment (opti-BIF) in hand, the same STD NMR screening approach as implemented in Chapter 2 could be used to rescreen the library for a fragment that can bind in the presence of opti-BIF (**Figure 5.2**). This method allows for the identification of BAX-

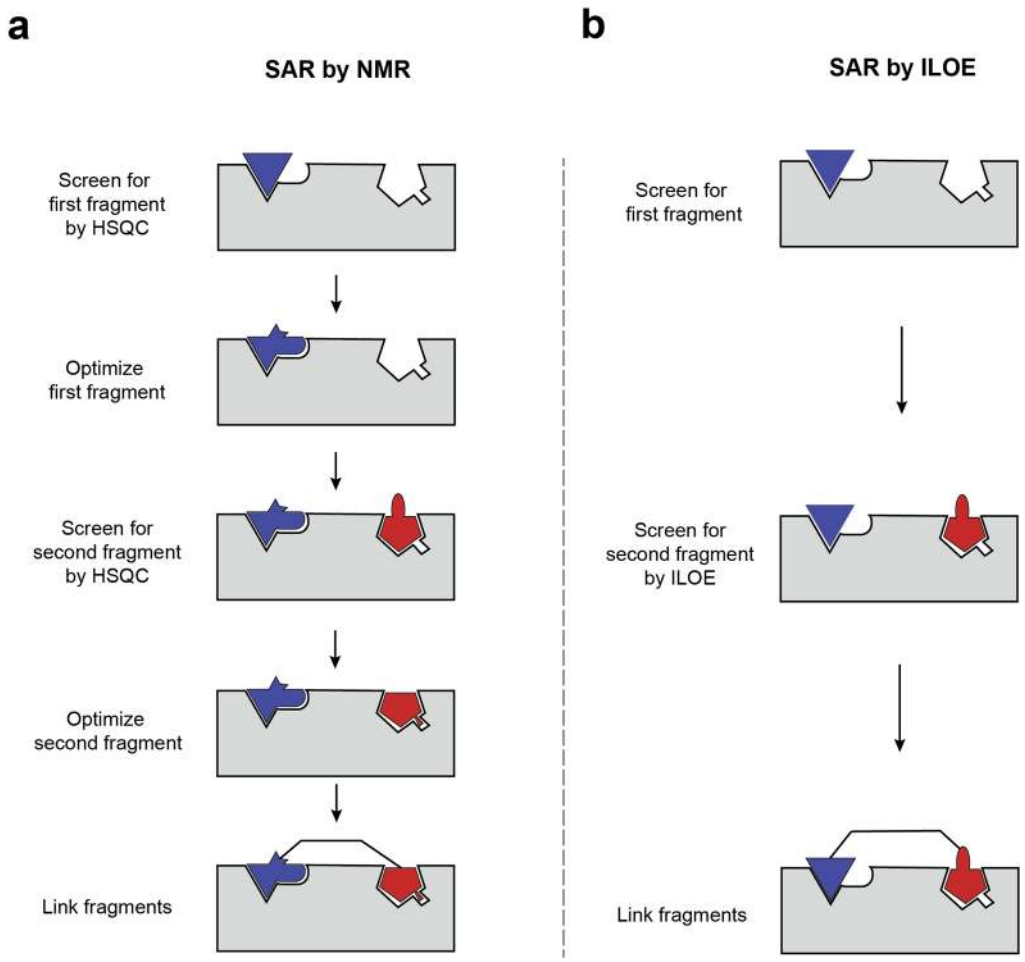

Figure 5.2 *Overview of fragment optimization strategies.*

The goal of these two strategies is to identify fragments with low binding affinity that bind next to each other at a site of interest. Chemical linkage of these fragments results in a molecule that is significantly more potent than the starting fragments. (**a**) SAR by NMR involves two rounds of screening by ^{1}H-^{15}N HSQC NMR to identify fragments that bind proximal to one another. These fragments are individually optimized to maximize their potency. Co-structures of the fragments bound to the protein of interest are used to inform the chemical linkage process. (**b**) SAR by ILOE uses interligand NOE measurements (trNOE) to identify two fragments that bind to adjacent surfaces. As this technique reveals the relative orientation of the two fragments, additional structural information is not required to link the fragments together.

sensitizing fragments that engage BAX, but at distinct sites. The hits from this screen would be tested in the liposomal release assay in the presence of opti-BIF. This assay would determine if any of the newly identified fragments further increase the potency of opti-BIF-induced BAX sensitization. Fragments that display improved potency in combination with BIF-44 would then be tested by HSQC to determine if they bind proximally to the BIF-44 binding site.

The next phase of development is to covalently link the two hits together to produce an even more potent BAX-sensitizing molecule. Since the dissociation constant of the linked small molecule, is approximately the product of dissociations constants of the two individual fragment components, combining two adjacent fragments can lead to a significant enhancement of binding potency[30]. This process, however, is a challenging task that is usually informed by a structure of the fragment/protein interaction. Fortunately, an X-ray crystal structure of full-length, dimeric BAX was recently reported by making one of two inactivating point mutations to prevent BAX oligomerization in solution[27]. Applying these methods, BAX-fragment co-crystal structures could be generated by soaking the fragments into the BAX dimer crystals. Indeed, the inhibitory interactions within the dimer may serve to be beneficial, effectively stabilizing the BAX-fragment interaction and preventing conformational rearrangements from occurring.

Alternative Methods of Optimization

In the absence of structural data, additional NMR experiments can be used to gather information about the binding mode of a fragment. Since proteins tumble more slowly in solution than small molecules, the interaction of a ligand with a protein can be measured in a standard nuclear Overhauser effect (NOE) spectroscopy experiment (NOESY)[29,31]. The transferred NOE (trNOE) between the protein and ligand results in the appearance of strong negative NOE peaks in the presence of the protein. This approach can be used to identify ligands that bind to proteins and more accurately determine the orientation of the ligand within the binding site. Therefore, trNOE

data can be used to accurately dock BIF-44 into the binding site and determine which atoms within BIF-44 may be amenable to modification.

Furthermore, an extension of the trNOE experiment can be used to detect two fragments that bind simultaneously at proximal sites on a protein through the formation of an inter-ligand NOE (ILOE) (**Figure 5.2b**). The formation of ILOEs only occurs when two ligands bind sufficiently close to one another to allow for ligand-ligand magnetization transfer[32]. As the ILOE occurs between specific protons on the ligands, this approach can determine the relative orientation of these two fragments to each other. This information is useful for determining strategies to link the fragments together, independently of a solved structure of the complex[29,30]. This so-called SAR by ILOE method has been implemented successfully to develop inhibitors of BID and MCL-1/BCL-X_L [33,34].

Our NMR-based fragment screen identified 53 BAX-interacting fragments (BIFs), 12 of which exerted a functional effect (Chapter 2). Therefore, the first step in implementing an SAR by ILOE approach would be to test whether any of these fragments can interact with BAX at an adjacent site to that of BIF-44. This could be accomplished by collecting NOESY spectra with pairs of BIF-44 and each of the other BIFs in the presence of BAX and looking for the appearance of ILOEs. The functional activity of potential hits can be verified by (1) adding vMIA as a competitor to the NOESY experiment and (2) determining the binding site of the second BIF by ^{1}H-^{15}N HSQC NMR. Similarly, the 53 previously characterized BIFs can be added alongside BIF-44 in the liposomal release assay to screen for compounds that enhance the sensitization activity beyond that of BIF-44 alone. If none of the characterized BIFs form ILOEs with BIF-44, this technique could be used to rescreen a fragment library specifically looking for fragments that bind proximally to BIF-44.

If a promising fragment pair emerges, *in silico* methods could be used to design a library of linked compounds. To enrich for molecules with optimal binding activities, libraries of molecules bearing multiple linkers lengths and chemistries can be docked into the BIF-44 site using the Glide

program. The top scoring compounds would be synthesized and tested by liposomal release assay and HSQC NMR to detect potent BAX sensitization activity through engagement of the BIF-44 binding region.

BAX Sensitization as a Therapeutic Approach

In 2001, the approval of imatinib, an inhibitor of the ABL kinase, ushered in a new era of targeted anti-cancer therapies[35]. As opposed to the classic cytotoxic chemotherapeutic agents, such therapies target the specific vulnerabilities of cancer cells. As a result, targeted therapies can potentially broaden the therapeutic window and reduce off-target side effects[36]. Over the years, dozens of other targeted anti-cancer agents have emerged. However, the use of these targeted therapies as a single agent often leads to the development of resistance either through the upregulation of compensatory pathways or through the selection of cells containing specific mutations that render the drug ineffective[37,38]. A potential solution to this problem is the combination of multiple therapies, a strategy that has proven effective for the pharmacologic control of human immunodeficiency virus (HIV) and hepatitis c virus (HCV) infections[39]. By targeting multiple essential targets and pathways, the opportunity for cancer cells to survive and generate escape mutations is diminished[37,38].

To effectively treat cancer using combination therapies, it is critical to understand the molecular drivers of a given tumor subtype. To achieve this goal, large scale efforts, such as The Cancer Genome Atlas, have been underway to sequence tumors across cancer subtypes[40]. As a result, it has become apparent that an incredible diversity of molecular lesions contributes to the pathogenesis of cancer. Instead of treating patients based on their tumor's tissue of origin, current and future cancer treatments focus on the development of drug regimens tailored to disrupt the specific oncogenic drivers of each individual disease[41]. Given the large number of cancer drivers, creating specific therapies against each target may not be achievable. Instead, combination therapies targeting the most essential cancer pathways is likely to have the greatest impact.

The modulation of apoptosis will be a critical part of almost any combination therapy regimen. As all tumors must shut down cell death pathways to survive and proliferate, mechanisms that push a cancer cell toward apoptotic death have the potential for broad efficacy across cancer types. Therefore, the pharmacologic reactivation of apoptosis by inhibiting the anti-apoptotic proteins and/or directly activating pro-apoptotic BAX represents a central goal for anti-cancer drug development.

The first and only FDA-approved drug to target BCL-2 family regulated apoptosis in human cancer is the selective BCL-2 inhibitor, venetoclax. This therapy is currently bring used to treat chronic lymphocytic leukemia (CLL) with a 17p deletion[15] and is undergoing testing in other malignances such as multiple myeloma, acute myeloid leukemia (AML), and mantle cell lymphoma[3]. Combinations of venetoclax with rituximab, an anti-CD20 antibody, or ibrutinib, a Bruton's tyrosine kinase (BTK) inhibitor, are showing increased efficacy in refractory CLL[42,43]. Not surprisingly, a potential mechanism of resistance to single agent venetoclax is upregulation of alternate anti-apoptotic proteins, such as BCL-X_L, MCL-1, and BFL-1/A1, which lie outside the binding spectrum of venetoclax[44,45]. Inhibitors of MCL-1, for example, are currently in development to expand the arsenal of anti-apoptotic inhibitors for treating a broader range of cancer subtypes and potentially addressing the development of venetoclax resistance[8,9,46].

A second strategy for activating apoptosis in cancer involves directly activating BAX itself. The BAX activator molecule, BAM7, binds to the BAX trigger site and thereby mimics the function of an activating BH3 helix. Thus, BAM7 induces the conformational activation of BAX, leading to oligomerization and mitochondrial poration[16]. BTSA1, a more potent drug-like derivative of BAM7, was recently reported to induce on-target killing of a variety of AML cancer cell lines and primary patient-derived AML cells. Additionally, BTSA1 produced an anti-tumor response in xenograft mouse models of AML, while sparing normal tissue[27]. Together, these studies suggest that direct induction of BAX activity is a viable strategy for the treatment of cancer. Interestingly, BTSA1

strongly synergized with venetoclax, suggesting that simultaneous targeting of direct and indirect mechanism of BAX activation can maximize anti-tumor activity.

The sensitization of BAX activation represents a novel and promising therapeutic strategy to lower the threshold of apoptosis activation for the treatment of cancer. While the efficacy of this mechanism remains to be tested *in vivo*, the success of other BAX-activating molecules suggests this alternative and complementary mode of BAX modulation could be a viable anti-cancer strategy[16-18,27,47]. As a BAX sensitizer, BIF-44-like compounds would be expected to have to little no effect as a single agent. Instead, the benefit of a BAX sensitizer would derive from its ability to synergize with therapies that activate BAX. Pairing a BAX sensitizer with any chemotherapeutic agent that induces BH3-only expression is likely to enhance the potency of that drug. This could allow for the dose of chemotherapy to be reduced, potentially decreasing chemotherapy-associated side effects. The therapeutic window for such an approach would be determined by the expression level and BH3-occupancy of anti-apoptotic proteins to counterbalance pharmacologic BAX activation. That is, as tumor cells use their anti-apoptotic reserve to bind and sequester BAX and BH3-only proteins, these primed cells are much more sensitive to changes in the balance of activated BAX[48]. In contrast, unstressed normal cells maintain an anti-apoptotic reserve that can bind and trap activated BAX, and thereby prevent terminal activation and apoptosis induction.

Combining a BAX sensitizer molecule with a second drug that targets the apoptotic pathway may achieve the most robust anti-cancer effect. For example, administering a BAX sensitizer in combination with an anti-apoptotic inhibitor, such as venetoclax, is likely to be more effective at killing cancer cells than venetoclax alone, as suggested by the synergy observed for the BTSA1-venetoclax combination described above[27]. In fact, the most exciting results may result from combining a BAX sensitizer molecule with a direct BAX activator molecule like BTSA1. Since both molecules target BAX in distinct ways, simultaneous delivery is predicted to produce a strong synergistic effect, as observed in this study when BIF-44 was combined with BIM

$SAHB_{A2}$. The level of inhibitory BAX dimer, in the cytosol has been reported as a biomarker for resistance to BTSA1[27,49]. However, it is plausible that by combining BTSA1 with a BAX sensitizer molecule, this inhibitory mechanism may be overcome, resulting in apoptosis activation in these otherwise resistant cancer cell populations

Overall, strategies designed to reactivate BAX-mediated apoptosis, whether by “inhibiting the inhibitors”, “activating the activators”, or sensitizing BAX activation, represent a new-generation of pharmacologic opportunities to modulate the mitochondrial apoptosis pathway for therapeutic benefit in cancer. Indeed, the combination of these distinct targeting strategies could be highly synergistic and, when paired with agents that target other key control components of oncogenesis and chemoresistance, new and more effective anti-cancer drug cocktails may emerge.

All things must pass
All things must pass away

All things must pass
None of life's strings can last
So, I must be on my way
And face another day

Now the darkness only stays at nighttime,
In the morning, it will fade away
Daylight is good at arriving at the right time
It's not always going to be this grey

All things must pass
All things must pass away

George Harrison
“All Things Must Pass", 1970

REFERENCES

1. Czabotar, P.E., Lessene, G., Strasser, A. & Adams, J.M. Control of apoptosis by the BCL-2 protein family: implications for physiology and therapy. *Nat Rev Mol Cell Biol* **15**, 49-63 (2014).

2. Beroukhim, R. et al. The landscape of somatic copy-number alteration across human cancers. *Nature* **463**, 899-905 (2010).

3. Delbridge, A.R., Grabow, S., Strasser, A. & Vaux, D.L. Thirty years of BCL-2: translating cell death discoveries into novel cancer therapies. *Nat Rev Cancer* **16**, 99-109 (2016).

4. Oltersdorf, T. et al. An inhibitor of Bcl-2 family proteins induces regression of solid tumours. *Nature* **435**, 677-81 (2005).

5. Souers, A.J. et al. ABT-199, a potent and selective BCL-2 inhibitor, achieves antitumor activity while sparing platelets. *Nat Med* **19**, 202-8 (2013).

6. Tse, C. et al. ABT-263: a potent and orally bioavailable Bcl-2 family inhibitor. *Cancer Res* **68**, 3421-8 (2008).

7. Tao, Z.F. et al. Discovery of a Potent and Selective BCL-XL Inhibitor with in Vivo Activity. *ACS Med Chem Lett* **5**, 1088-93 (2014).

8. Ashkenazi, A., Fairbrother, W.J., Leverson, J.D. & Souers, A.J. From basic apoptosis discoveries to advanced selective BCL-2 family inhibitors. *Nat Rev Drug Discov* **16**, 273-284 (2017).

9. Kotschy, A. et al. The MCL1 inhibitor S63845 is tolerable and effective in diverse cancer models. *Nature* **538**, 477-482 (2016).

10. Uhlen, M. et al. Proteomics. Tissue-based map of the human proteome. *Science* **347**, 1260419 (2015).

11. Barretina, J. et al. The Cancer Cell Line Encyclopedia enables predictive modelling of anticancer drug sensitivity. *Nature* **483**, 603-7 (2012).

12. Erlanson, D.A., Fesik, S.W., Hubbard, R.E., Jahnke, W. & Jhoti, H. Twenty years on: the impact of fragments on drug discovery. *Nat Rev Drug Discov* **15**, 605-19 (2016).

13. Tsai, J. et al. Discovery of a selective inhibitor of oncogenic B-Raf kinase with potent antimelanoma activity. *Proc Natl Acad Sci U S A* **105**, 3041-6 (2008).

14. Petros, A.M. et al. Discovery of a potent inhibitor of the antiapoptotic protein Bcl-xL from NMR and parallel synthesis. *J Med Chem* **49**, 656-63 (2006).

15. Roberts, A.W. et al. Targeting BCL2 with Venetoclax in Relapsed Chronic Lymphocytic Leukemia. *N Engl J Med* **374**, 311-22 (2016).

16. Gavathiotis, E., Reyna, D.E., Bellairs, J.A., Leshchiner, E.S. & Walensky, L.D. Direct and selective small-molecule activation of proapoptotic BAX. *Nat Chem Biol* **8**, 639-45 (2012).

17. Xin, M. et al. Small-molecule Bax agonists for cancer therapy. *Nat Commun* **5**, 4935 (2014).

18. Zhao, G. et al. Activation of the proapoptotic Bcl-2 protein Bax by a small molecule induces tumor cell apoptosis. *Mol Cell Biol* **34**, 1198-207 (2014).

19. Gavathiotis, E., Reyna, D.E., Davis, M.L., Bird, G.H. & Walensky, L.D. BH3-triggered structural reorganization drives the activation of proapoptotic BAX. *Mol Cell* **40**, 481-92 (2010).

20. Gavathiotis, E. et al. BAX activation is initiated at a novel interaction site. *Nature* **455**, 1076-81 (2008).

21. Barclay, L.A. et al. Inhibition of Pro-apoptotic BAX by a noncanonical interaction mechanism. *Mol Cell* **57**, 873-86 (2015).

22. Arnoult, D. et al. Cytomegalovirus cell death suppressor vMIA blocks Bax- but not Bak-mediated apoptosis by binding and sequestering Bax at mitochondria. *Proc Natl Acad Sci U S A* **101**, 7988-93 (2004).

23. Ma, J. et al. Structural mechanism of Bax inhibition by cytomegalovirus protein vMIA. *Proc Natl Acad Sci U S A* **109**, 20901-6 (2012).

24. Wei, M.C. et al. tBID, a membrane-targeted death ligand, oligomerizes BAK to release cytochrome c. *Genes Dev* **14**, 2060-71 (2000).

25. Walensky, L.D. & Gavathiotis, E. BAX unleashed: the biochemical transformation of an inactive cytosolic monomer into a toxic mitochondrial pore. *Trends Biochem Sci* **36**, 642-52 (2011).

26. Tan, C. et al. Auto-activation of the apoptosis protein Bax increases mitochondrial membrane permeability and is inhibited by Bcl-2. *J Biol Chem* **281**, 14764-75 (2006).

27. Reyna, D.E. et al. Direct Activation of BAX by BTSA1 Overcomes Apoptosis Resistance in Acute Myeloid Leukemia. *Cancer Cell* **32**, 490-505 e10 (2017).

28. Shuker, S.B., Hajduk, P.J., Meadows, R.P. & Fesik, S.W. Discovering high-affinity ligands for proteins: SAR by NMR. *Science* **274**, 1531-4 (1996).

29. Pellecchia, M. et al. NMR-based techniques in the hit identification and optimisation processes. *Expert Opin Ther Targets* **8**, 597-611 (2004).

30. Becattini, B. & Pellecchia, M. SAR by ILOEs: an NMR-based approach to reverse chemical genetics. *Chemistry* **12**, 2658-62 (2006).

31. Śledź, P., Abell, C. & Ciulli, A. Ligand-Observed NMR in Fragment-Based Approaches. in *NMR of Biomolecules* 264-280 (Wiley-VCH Verlag GmbH & Co. KGaA, 2012).

32. Li, D., DeRose, E.F. & London, R.E. The inter-ligand Overhauser effect: a powerful new NMR approach for mapping structural relationships of macromolecular ligands. *J Biomol NMR* **15**, 71-6 (1999).

33. Becattini, B. et al. Targeting apoptosis via chemical design: inhibition of bid-induced cell death by small organic molecules. *Chem Biol* **11**, 1107-17 (2004).

34. Rega, M.F. et al. SAR by interligand nuclear overhauser effects (ILOEs) based discovery of acylsulfonamide compounds active against Bcl-x(L) and Mcl-1. *J Med Chem* **54**, 6000-13 (2011).

35. Capdeville, R., Buchdunger, E., Zimmermann, J. & Matter, A. Glivec (STI571, imatinib), a rationally developed, targeted anticancer drug. *Nat Rev Drug Discov* **1**, 493-502 (2002).

36. Huang, M., Shen, A., Ding, J. & Geng, M. Molecularly targeted cancer therapy: some lessons from the past decade. *Trends Pharmacol Sci* **35**, 41-50 (2014).

37. Lopez, J.S. & Banerji, U. Combine and conquer: challenges for targeted therapy combinations in early phase trials. *Nat Rev Clin Oncol* **14**, 57-66 (2017).

38. Holohan, C., Van Schaeybroeck, S., Longley, D.B. & Johnston, P.G. Cancer drug resistance: an evolving paradigm. *Nat Rev Cancer* **13**, 714-26 (2013).

39. De Clercq, E. The design of drugs for HIV and HCV. *Nat Rev Drug Discov* **6**, 1001-18 (2007).

40. Cancer Genome Atlas Research, N. et al. The Cancer Genome Atlas Pan-Cancer analysis project. *Nat Genet* **45**, 1113-20 (2013).

41. Schilsky, R.L. Personalized medicine in oncology: the future is now. *Nat Rev Drug Discov* **9**, 363-6 (2010).

42. Deng, J. et al. Bruton's tyrosine kinase inhibition increases BCL-2 dependence and enhances sensitivity to venetoclax in chronic lymphocytic leukemia. *Leukemia* **31**, 2075-2084 (2017).

43. Seymour, J.F. et al. Venetoclax plus rituximab in relapsed or refractory chronic lymphocytic leukaemia: a phase 1b study. *Lancet Oncol* **18**, 230-240 (2017).

44. Zhang. Mechanisms of Acquired Resistance to Venetoclax in Preclinical AML Models. *Blood* **126**, 328 (2015).

45. Tahir, S.K. et al. Potential mechanisms of resistance to venetoclax and strategies to circumvent it. *BMC Cancer* **17**, 399 (2017).

46. Leverson, J.D. et al. Potent and selective small-molecule MCL-1 inhibitors demonstrate on-target cancer cell killing activity as single agents and in combination with ABT-263 (navitoclax). *Cell Death Dis* **6**, e1590 (2015).

47. Li, R. et al. Modulation of Bax and mTOR for Cancer Therapeutics. *Cancer Res* **77**, 3001-3012 (2017).

48. Letai, A. et al. Distinct BH3 domains either sensitize or activate mitochondrial apoptosis, serving as prototype cancer therapeutics. *Cancer Cell* **2**, 183-92 (2002).

49. Garner, T.P. et al. An Autoinhibited Dimeric Form of BAX Regulates the BAX Activation Pathway. *Mol Cell* **63**, 485-97 (2016).

Appendix

Supplementary Data

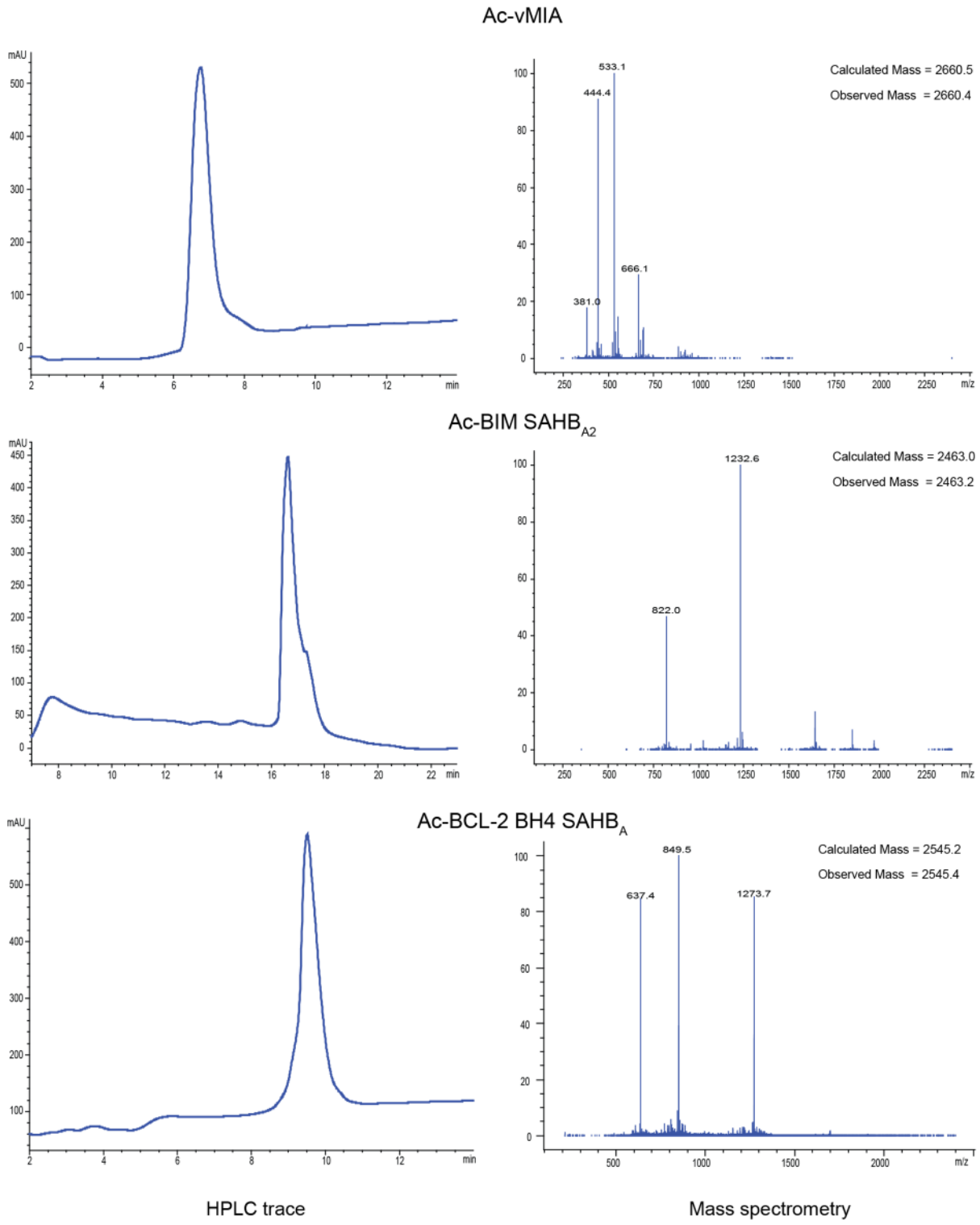

Figure S.1 *Analysis of peptide purity*. HPLC traces (left) and mass spectrometry analysis (right) for to document the purity of vMIA, BIM SAHB$_{A2}$, and BCL-2 BH4 SAHB$_{A}$ peptides.

Table S.1 *Biochemical Activities of BIFs*

		STD-NMR Competition Fragment/Peptide		Liposomal Release Assay	
Name	STD-Binder	vMIA	BIM SAHB$_{A2}$	Sensitizer	Activator
BIF-1	+	+	-	-	-
BIF-2	+	-	+	-	-
BIF-3	+	-	-	-	-
BIF-4	+	-	-	-	-
BIF-5	+	-	-	-	-
BIF-6	+	+	-	-	-
BIF-7	+	-	-	-	-
BIF-8	+	-	-	-	-
BIF-9	+	-	-	-	-
BIF-10	+	-	-	-	-
BIF-11	+	-	-	-	-
BIF-12	+	-	-	-	-
BIF-13	+	+	-	-	-
BIF-14	+	-	-	-	-
BIF-15	+	-	-	-	+
BIF-16	+	-	-	-	-
BIF-17	+	-	-	-	-
BIF-18	+	-	-	-	-
BIF-19	+	-	-	+	-
BIF-20	+	-	+	-	-
BIF-21	+	-	-	-	-
BIF-22	+	-	-	-	-
BIF-23	+	-	+	-	+
BIF-24	+	-	-	-	-
BIF-25	+	+	-	+	-
BIF-26	+	+	-	-	-
BIF-27	+	+	-	+	-
BIF-28	+	-	-	-	+
BIF-29	+	-	-	-	-
BIF-30	+	-	-	-	-
BIF-31	+	+	-	-	-
BIF-32	+	-	-	-	-
BIF-33	+	+	-	-	-
BIF-34	+	-	-	-	-
BIF-35	+	-	-	-	-
BIF-36	+	-	-	-	-
BIF-37	+	-	-	-	-
BIF-38	+	-	-	-	-
BIF-39	+	-	-	-	-
BIF-40	+	-	-	-	-
BIF-41	+	-	-	+	-
BIF-42	+	-	-	-	-
BIF-43	+	-	-	-	-
BIF-44	+	+	-	+	-
BIF-45	+	-	+	+	-
BIF-46	+	-	+	+	-
BIF-47	+	-	-	-	-
BIF-48	+	-	-	-	-
BIF-49	+	+	-	-	+
BIF-50	+	+	-	-	-
BIF-51	+	-	-	+	-
BIF-52	+	-	-	-	-
BIF-53	+	-	-	-	-
ANA-BIF-1	+	N.D.	N.D.	+	+
ANA-BIF-2	+	N.D.	N.D.	+	+
ANA-BIF-3	+	N.D.	N.D.	+	-
ANA-BIF-4	+	N.D.	N.D.	-	-
ANA-BIF-5	+	N.D.	N.D.	-	-

Table S.2 *Molecular structures of BAX-interacting fragments (BIFs)*

BIF-1	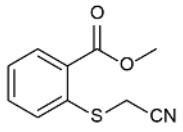	BIF-10	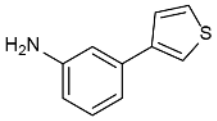	BIF-19	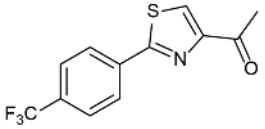
BIF-2	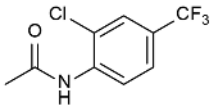	BIF-11	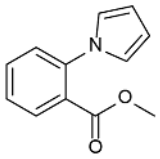	BIF-20	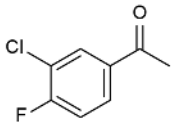
BIF-3	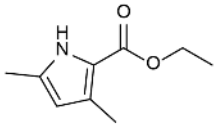	BIF-12	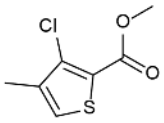	BIF-21	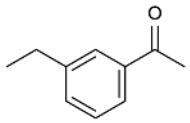
BIF-4	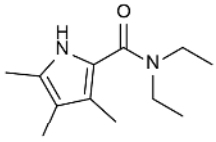	BIF-13	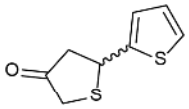	BIF-22	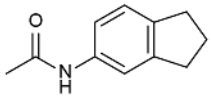
BIF-5	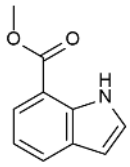	BIF-14	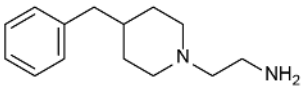	BIF-23	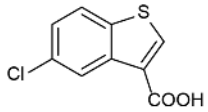
BIF-6	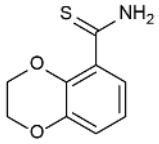	BIF-15	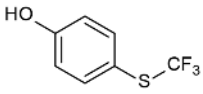	BIF-24	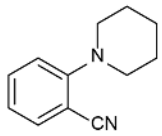
BIF-7	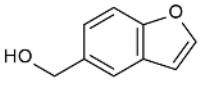	BIF-16	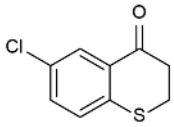	BIF-25	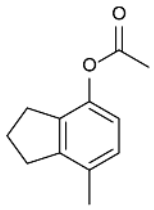
BIF-8	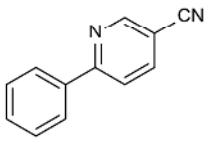	BIF-17	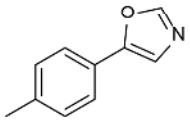	BIF-26	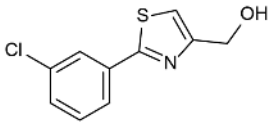
BIF-9	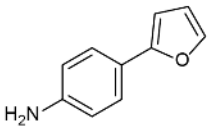	BIF-18	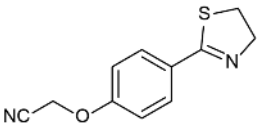	BIF-27	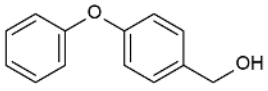

Table S.2 (Continued)

BIF-28	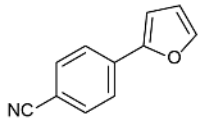	BIF-37	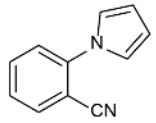	BIF-46	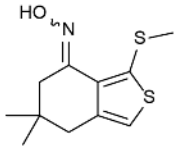
BIF-29	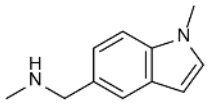	BIF-38	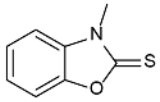	BIF-47	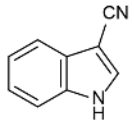
BIF-30	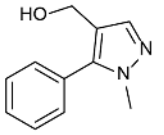	BIF-39	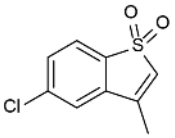	BIF-48	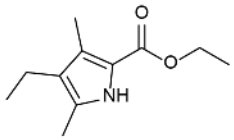
BIF-31	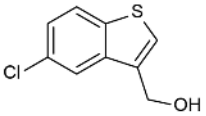	BIF-40	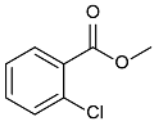	BIF-49	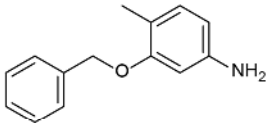
BIF-32	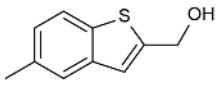	BIF-41	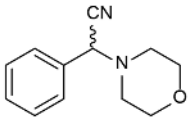	BIF-50	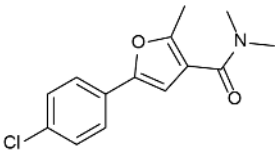
BIF-33	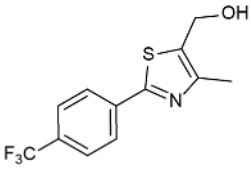	BIF-42	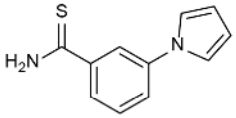	BIF-51	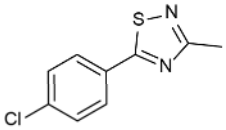
BIF-34	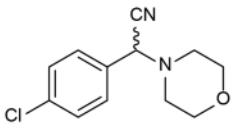	BIF-43	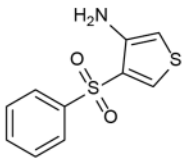	BIF-52	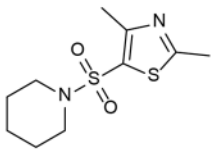
BIF-35	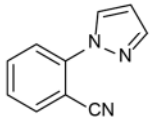	BIF-44	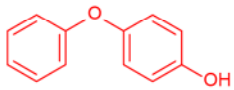	BIF-53	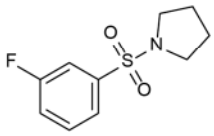
BIF-36	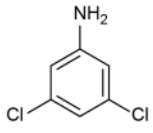	BIF-45	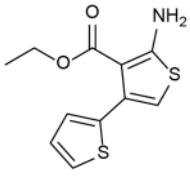		

Table S.3 *Maximal values of BAX-mediated liposomal release by condition*

	Sample	Average (%)	SD (%)
Figure 2.2	BAX	10.9	1.8
	BAX, 150x BIF-44	20.3	0.5
	BAX, BIM $SAHB_{A2}$, Vehicle	55.4	1.1
	BAX, BIM $SAHB_{A2}$, 150x BIF-44	77.8	0.3
Figure 2.4	BAX	-1.7	4.0
	BAX, BIM $SAHB_{A2}$	64.2	2.1
	BAX, 150x ANA-BIF-1	31.3	2.0
	BAX, BIM $SAHB_{A2}$, 150x ANA-BIF-1	102.6	1.6
	BAX, 150x ANA-BIF-2	19.9	5.5
	BAX, BIM $SAHB_{A2}$, 150x ANA-BIF-2	105.5	7.9
	BAX, 150x ANA-BIF-3	10.3	1.4
	BAX, BIM $SAHB_{A2}$, 150x ANA-BIF-3	85.3	1.1
	BAX, 150x ANA-BIF-4	-16.1	2.7
	BAX, BIM $SAHB_{A2}$, 150x ANA-BIF-4	59.8	3.1
	BAX, 150x ANA-BIF-5	-10.5	3.3
	BAX, BIM $SAHB_{A2}$, 150x ANA-BIF-5	59.9	8.2
Figure 3.2	Liposomes	0.4	1.0
	BAX	19.3	1.8
	175x BIF-44	-1.9	2.0
	BAX, 10x BIF-44	13.4	1.1
	BAX, 50x BIF-44	16.6	0.7
	BAX, 75x BIF-44	18.1	1.1
	BAX, 100x BIF-44	18.9	2.6
	BAX, 150x BIF-44	22.4	0.4
	BAX, 175x BIF-44	28.0	1.5
	BAX, BIM $SAHB_{A2}$	48.7	1.2
	BAX, BIM $SAHB_{A2}$, 10x BIF-44	59.7	2.3
	BAX, BIM $SAHB_{A2}$, 50x BIF-44	62.9	6.2
	BAX, BIM $SAHB_{A2}$, 75x BIF-44	67.1	5.4
	BAX, BIM $SAHB_{A2}$, 100x BIF-44	75.5	2.0
	BAX, BIM $SAHB_{A2}$, 150x BIF-44	76.3	6.3
	BAX, BIM $SAHB_{A2}$, 175x BIF-44	80.0	0.7
Figure 3.3	Liposomes	-19.6	1.9
	150x BIF-44	-15.6	3.9
	150x BIF-44, BIM $SAHB_{A2}$	-10.7	1.0
	BAX	14.2	2.0
	BAX, 150x BIF-44	20.7	1.8
	BAX, BIM $SAHB_{A2}$	46.2	2.8
	BAX, BIM $SAHB_{A2}$, 150x BIF-44 (co-treatment)	94.0	2.0
	BAX, 150x BIF-44, then BIM $SAHB_{A2}$	97.7	5.5
	BAX, BIM $SAHB_{A2}$, then 150x BIF-44	92.9	2.1
Figure 3.4	BAX	22.0	0.9
	BAX, 150x BIF-44	27.3	2.6
	BAX, BAX SAHB	34.5	1.5
	BAX, BAX SAHB, 150x BIF-44	51.4	2.5
	BAX, PUMA SAHB	42.8	0.7
	BAX, PUMA SAHB, 150x BIF-44	62.8	2.6
	BAX (heat)	43.6	1.5
	BAX, 150x BIF-44 (heat)	83.4	4.8
	BAX	3.3	5.0
	BIM_L, 150x BIF-44	-3.0	2.3
	BAX, 150x BIF-44	3.0	1.0
	BAX, BIM_L	44.5	3.6
	BAX, BIM_L, 150x BIF-44	65.7	3.2